

SSC-118

**STUDIES OF THE STRAIN DISTRIBUTION IN WIDE PLATES  
DURING BRITTLE FRACTURE PROPAGATION**

by  
S. T. Rolfe  
T. M. Lynam  
and  
W. J. Hall

SHIP STRUCTURE COMMITTEE

# SHIP STRUCTURE COMMITTEE

## MEMBER AGENCIES:

BUREAU OF SHIPS, DEPT. OF NAVY  
MILITARY SEA TRANSPORTATION SERVICE, DEPT. OF NAVY  
UNITED STATES COAST GUARD, TREASURY DEPT.  
MARITIME ADMINISTRATION, DEPT. OF COMMERCE  
AMERICAN BUREAU OF SHIPPING

## ADDRESS CORRESPONDENCE TO:

SECRETARY  
SHIP STRUCTURE COMMITTEE  
U. S. COAST GUARD HEADQUARTERS  
WASHINGTON 25, D. C.

December 30, 1959

Dear Sir:

As part of its research program related to the improvement of hull structures of ships, the Ship Structure Committee is sponsoring an investigation of Brittle Fracture Mechanics at the University of Illinois. Herewith is a copy of the Fourth Progress Report, SSC-118, Studies of the Strain Distribution in Wide Plates During Brittle Fracture Propagation by S. T. Rolfe, T. M. Lynam, and W. J. Hall.

This project is being conducted under the advisory guidance of the Committee on Ship Structural Design of the National Academy of Sciences-National Research Council.

This report is being distributed to individuals and groups associated with or interested in the work of the Ship Structure Committee. Comments concerning this report are solicited.

Sincerely yours,



E. H. Thiele  
Rear Admiral, U. S. Coast Guard  
Chairman, Ship Structure Committee

Serial No. SSC-118

Fourth Progress Report  
of  
Project SR-137

to the

SHIP STRUCTURE COMMITTEE

on

STUDIES OF THE STRAIN DISTRIBUTION IN WIDE PLATES  
DURING BRITTLE FRACTURE PROPAGATION

by

S. T. Rolfe, T. M. Lynam and W. J. Hall

University of Illinois  
Urbana, Illinois

under

Department of the Navy  
Bureau of Ships Contract NObs-65790  
BuShips Index No. NS-731-034

transmitted through

Committee on Ship Structural Design  
Division of Engineering and Industrial Research  
National Academy of Sciences-National Research Council

under

Department of the Navy  
Bureau of Ships Contract NObs-72046  
BuShips Index No. NS-731-036

Washington, D. C.  
National Academy of Sciences-National Research Council  
December 30, 1959

## ABSTRACT

This report summarizes the results of a series of tests made as a part of the study of the propagation of brittle fractures in 6-ft wide steel plates. All plates were tested at an average net applied stress of 19,000 psi, a temperature of about -10 F, and an impact energy of about 1000 ft-lb, which made it possible to superimpose the test data and obtain contours of strain on the surface of the plate for a propagating fracture. Contours of both the maximum principal strain and strain measured with vertically oriented gages for various lengths of crack are presented in this report. A study of all the applicable data from earlier tests made as a part of this program indicates that the strain contour data presented here are also representative of the data from these earlier tests. The studies indicate that for the particular specimen geometry and associated test conditions, the strain field associated with the tip of the advancing fracture remains essentially unchanged after traversing about one-third of the plate width and extends only about 8--10 in. ahead of the crack tip.

## CONTENTS

	<u>Page</u>
INTRODUCTION . . . . .	1
General . . . . .	1
Object and Scope . . . . .	1
Acknowledgment . . . . .	2
Nomenclature . . . . .	3
DESCRIPTION OF SPECIMENS AND INSTRUMENTATION . .	3
Specimens and Material Properties . . . . .	3
Instrumentation . . . . .	6
Data Reduction . . . . .	17
Apparatus and Test Procedure . . . . .	17
ANALYSIS OF TEST RESULTS . . . . .	18
General . . . . .	18
Recorded Test Data . . . . .	20
Computed Principal Strains . . . . .	39
Discussion of Strain Traces . . . . .	41
Maximum Principal and Vertical Strain Contours . .	45
Crack Path and Surface Texture . . . . .	60
SUMMARY . . . . .	62
REFERENCES . . . . .	64

BRITTLE FRACTURE MECHANICS ADVISORY COMMITTEE

for the

COMMITTEE ON SHIP STRUCTURAL DESIGN  
Division of Engineering & Industrial Research  
National Academy of Sciences-National Research Council

Chairman:

N. J. Hoff  
Head of Department of Aeronautical Engineering  
Stanford University

Members:

D. S. Clark  
Professor of Mechanical Engineering  
California Institute of Technology

Morris Cohen  
Department of Metallurgy  
Massachusetts Institute of Technology

F. J. Feely, Jr.  
Esso Research & Engineering Company

Martin Goland  
Vice President  
Southwest Research Institute

G. R. Irwin  
Head, Mechanics Division  
Naval Research Laboratory

Egon Orowan  
Department of Mechanical Engineering  
Massachusetts Institute of Technology

W. R. Osgood  
Department of Mechanics  
Rensselaer Polytechnic Institute

M. P. White  
Head, Civil Engineering Department  
University of Massachusetts

## INTRODUCTION

### General

Brittle fractures in riveted and welded steel structures have been reported in the engineering literature for many years. These fractures generally are characterized 1) by a lack of the ductility usually associated with failures of structural steel and 2) by a sudden occurrence with little or no previous warning.

The significance of the brittle fracture problem was not fully appreciated until World War II, when a large number of welded merchant vessels failed in this manner. Fortunately, through the use of improved geometrical layout, crack arrestors, and improved materials and fabrication procedures, it was possible to reduce greatly the number of major ship failures. In many cases, provisions have been made to incorporate similar improvements or changes in the design of structures other than ships in order to minimize the possibility of the occurrence of brittle fractures. Nevertheless, in spite of these improvements in design which have resulted from the large amount of research completed during and since World War II, brittle fractures still occur, and further studies are required if a better understanding of the brittle fracture problem is to be obtained.

### Object and Scope

The brittle fracture phenomenon is extremely complicated in that it involves a consideration of materials and their behavior in various environments. This particular program is concerned with a study of the propagation of brittle fractures in wide steel plates. The experimental approach followed in this investigation has consisted of measuring surface strains and crack speed as the fracture traverses a wide steel plate to obtain fundamental data.

The primary purpose of these tests and studies was to obtain sufficient data to establish representative strain contours on the plate surface during the time a brittle fracture is propagating. Thus far, six major fracture tests of 6-ft wide, semikilled steel plates have been completed in which 34 channels of cathode ray oscilloscope recording instrumentation have been utilized; in each test, 33 channels were used for 11 rectangular strain rosettes and one channel was used for speed

detectors. The plates were tested at an average net applied stress of 19,000 psi and at a temperature of about -10 F. The fractures were initiated from one edge of the plate with the notch-wedge-impact method of fracture initiation. In conjunction with the crack arrestor program (Project SR-134), one additional set of records has been obtained for a plate tested at a higher stress level (28,000 psi) and at a lower temperature (-15 F). The results presented in this report are based on the tests that are reported here for the first time, as well as on all of the previous applicable data obtained as part of this program.<sup>1-4</sup>

Among the more important items presented in this report are the following:

- (1) strain gage traces from the component gages of the strain rosettes
- (2) principal strain curves computed from the component gage strain traces
- (3) discussion of the factors affecting the computed principal strain magnitudes and strain rates
- (4) representative vertical and maximum principal strain contours for various crack lengths during the time the fracture is propagating, and
- (5) typical sets of maximum principal strain contours and vertical strain contours associated with a crack in the central portion of the plate.

The strain contours should be of considerable value in correlating the test results and associated significant parameters with other experimental and analytical results.

#### Acknowledgment

The work described in this report was conducted in the Structural Research Laboratory of the Department of Civil Engineering, University of Illinois. The project is under the general direction of N. M. Newmark, Professor and Head of the Department of Civil Engineering. The program is sponsored by the Ship Structure Committee, and the members of the Brittle Fracture Mechanics Advisory Committee under the Committee on Ship Structural Design of the National Academy of Sciences-National Research Council have acted in an advisory capacity in the planning of the program.

V. J. McDonald, Associate Professor of Civil Engineering, supervised the instrumentation and reduction of the test data from the photographic records. M. P. Gaus, Research Associate in Civil Engineering, prepared the computer code for

the strain rosette computations, and F. W. Barton, Research Assistant in Civil Engineering, helped with the tests and preparation of the figures for the report.

### Nomenclature

The following terms are used repeatedly throughout the text:

Dynamic strain gage--SR-4 Type A7 (1/4-in. gage length) strain gage whose signal is monitored with respect to time on an oscilloscope during the fracture test.

Static strain gage--SR-4 Type A7 (1/4-in. gage length) strain gage used to monitor the static strain level.

Component strain gage--One of the three individual strain gages of a rectangular strain rosette.

Crack detector--A single-wire SR-4 Type A9 (6-in. gage length) strain gage located on the plate surface perpendicular to the expected fracture path. A rough measure of the fracture speed may be obtained from a knowledge of the distance between the detectors and the time interval corresponding to the breaking of adjacent detectors.

Initiation edge--The edge of the specimen at which the brittle fracture is initiated.

Notch line--An imaginary straight line connecting the fracture initiation notches on opposite edges of the plate specimen.

Test load strain--At any gage point, the strain corresponding to the applied test load.

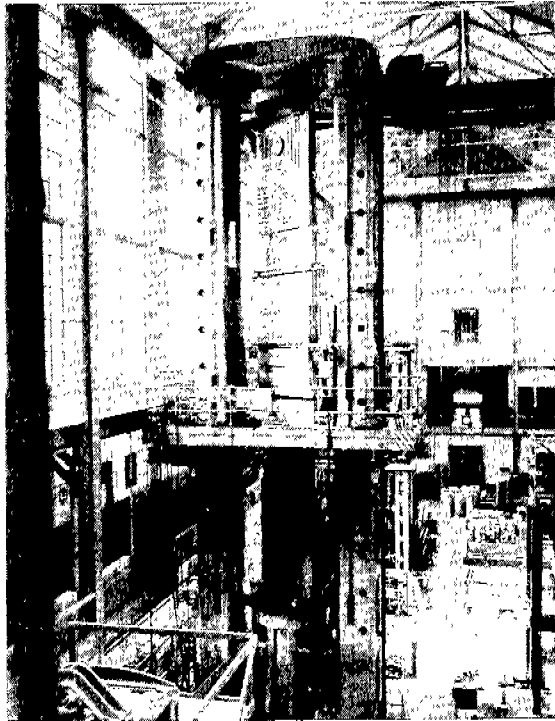
## DESCRIPTION OF SPECIMENS AND INSTRUMENTATION

### Specimens and Material Properties

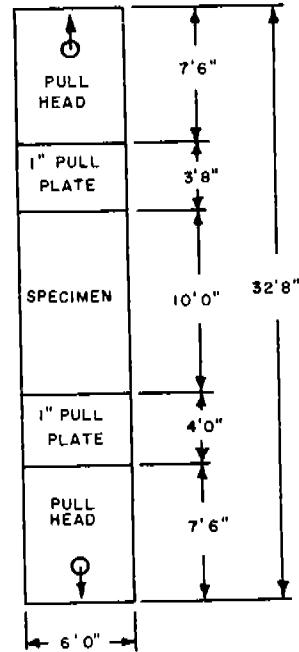
The plate material for the six major fracture tests outlined in Table 1 (Tests 33, 34 and 36 through 39) was a semikilled steel, USS heat No. 64M487, and was tested in the as-rolled condition. The steel was from the same stock that was used in the earlier tests made as a part of this program and its properties, typical of A-7 structural steels, are in agreement with those reported earlier.<sup>1, 2, 5</sup> The specimens were 3/4 in. thick, 72 in. wide, and 20 in. long;

TABLE 1. OUTLINE OF TESTS

Test No. (Plate No.)	Initial Load (kips)	Avg. Stress on Net Section (ksi)	Avg. Temp. (F)	Remarks
<p>With the exception of Test 35, all tests were conducted on 3/4-in. by 72-in. by 120-in. semi-killed steel plate specimens welded with E7016 electrodes to 1-in. thick pull-plates in the 3,000,000-lb Baldwin hydraulic testing machine. The brittle fractures were initiated by the notch-wedge-impact method with a nominal lateral impact of 1200 ft-lb.</p>				
<p>The notch was 1-1/8 in. long and consisted of a slot four hacksaw blades wide (~0.141 in.) for the first 1 in., one blade wide (~0.034 in.) for the next 1/16 in., and ended with a jeweler's saw-cut (~0.012 in.) 1/16 in. long.</p>				
33 (XC-1)	1000	19.0	0	Complete fracture--good strain records obtained from 7 rosettes.
34 (XF-1)	1000	19.0	0	Complete fracture--good strain records obtained from 10 rosettes.
35 (RTRT-4)	1475	28.0	-15	Plate specimen composed of 36-in. starter strake of rimmed steel, 4-in. strake of T-1, 20-in. strake of rimmed steel, and a 12-in. strake of T-1 steel. Specimen was 27 in. long. Fracture arrested at leading edge of final T-1 strake. Final load--85 kips. Good strain records obtained from 4 rosettes.
(Tested in conjunction with Project SR-134)				
36 (X2B)	997	19.0	-10	Complete fracture--fair strain records obtained from 11 rosettes. Double fracture last two-thirds of plate width.
37 (X2F)	997	19.0	-8	Complete fracture--good strain records obtained from 11 rosettes.
38 (X1B)	997	19.0	-9	Complete fracture--good strain records obtained from 11 rosettes.
39 (X2E)	997	19.0	-6	Complete fracture--good strain records obtained from 11 rosettes.



Specimen Ready for Testing



Line Diagram of Specimen

Fig. 1. Typical Test Setup

the net width at the notch line was approximately 2-1/4 in. less than the gross width because of the notches on each edge. Both ends of the specimen were welded with double-V butt welds made with E7016 electrodes to 1-in. thick pull-plates mounted in the testing machine; in welding the specimen to the pull-plates, care was taken to keep the warping and residual stresses to a minimum. A line diagram of the specimen and pull-plates and a view of a typical test setup in the 3,000,000-lb hydraulic testing machine are shown in Fig. 1.

The composite plate specimen for the arrestor test (Test 35) was fabricated from, in order, 1) a 36-in. fracture starter strake of rimmed steel (the plate on which the strain rosette gages were mounted), 2) a 4-in. strake of T-1 steel, 3) a 20-in. strake of rimmed steel, and 4) a 12-in. strake of T-1 steel. Over all, the specimen was 3/4 in. thick, 72 in. wide, and 27 in. long.

Mechanical property tests were made on material taken from the central portion of the plates after the plates had been fractured. The check ana-

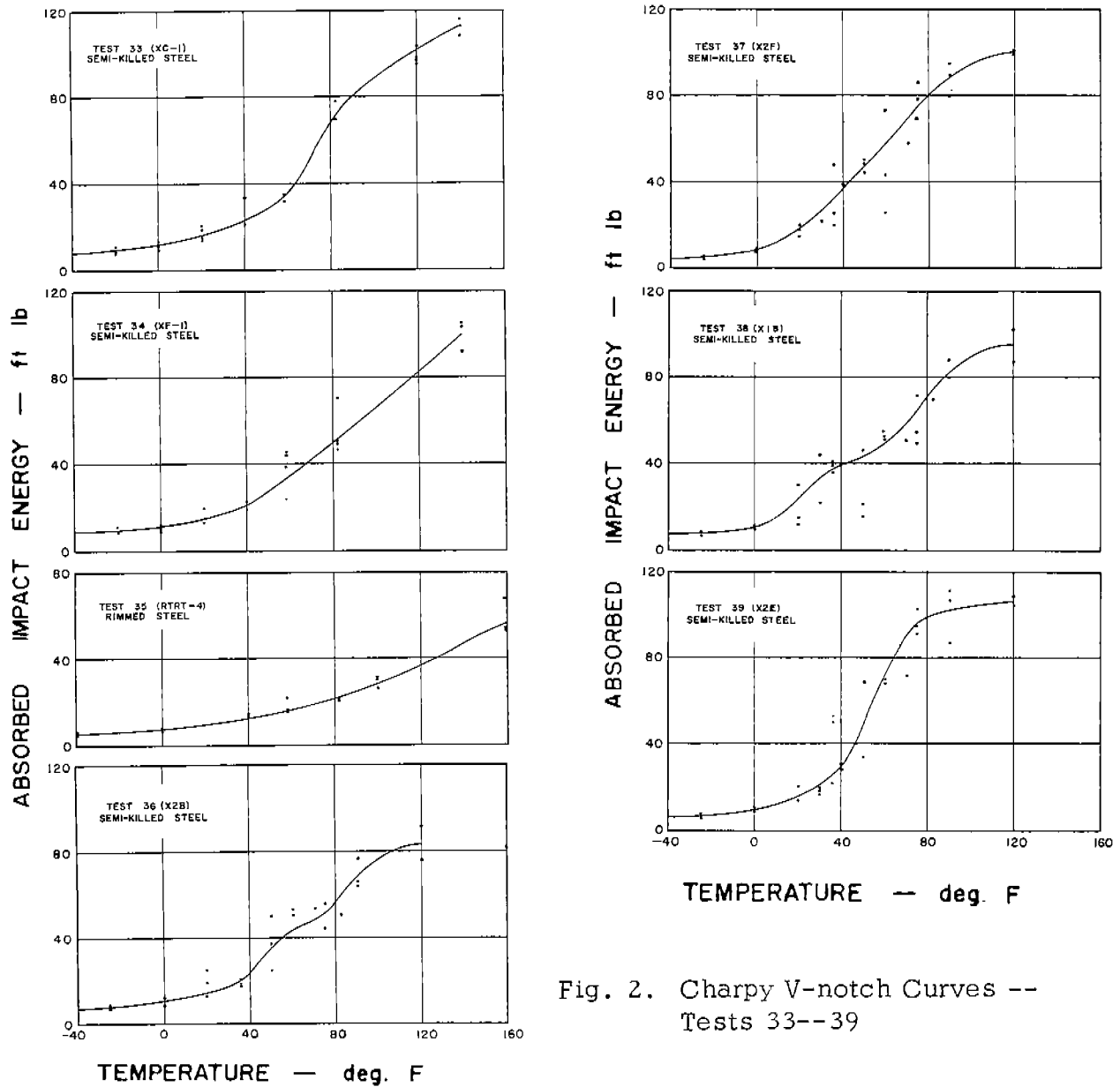


Fig. 2. Charpy V-notch Curves -- Tests 33--39

lyses and the tensile test data for each of the rimmed and semikilled steel plates are presented in Tables 2 and 3. Charpy V-notch data are presented in Fig. 2.

### Instrumentation

Until recently, it had been possible to obtain only a limited amount of data from any one test because a maximum of only nine channels of cathode-ray oscilloscope recording equipment had been available. Nevertheless, earlier work on this program with both 2-ft wide and 6-ft wide plates produced much valuable information concerning expected fracture speed and the strain distribu-

TABLE 2. CHECK ANALYSES OF STEEL PLATE MATERIAL

Test No.	Material	Chemical Composition in Per Cent							
		C	Mn	P	S	Si	Cu	Ni	Al
33	Semikilled	0.17	0.71	0.019	0.028	0.058	0.02	0.0	0.03
34, 37	Semikilled	0.20	0.76	0.019	0.028	0.052	0.02	Trace	0.03
35	Rimmed	0.18	0.42	0.013	0.031	0.02	0.23	0.14	0.003
36, 38	Semikilled	0.21	0.82	0.018	0.030	0.058	0.02	0.0	0.03
39	Semikilled	0.20	0.76	0.019	0.040	0.03	0.04	0.16	0.002

TABLE 3. TENSILE TEST DATA FOR STEEL PLATE MATERIAL  
(Standard ASTM 0.505-in. diam specimens)

Test No.	Material (Plate No.)	Heat No.	Lower Yield Strength (ksi)	Maximum Strength (ksi)	Elongation in 2-in. %	Reduction of Area %
33	Semikilled (XC-1)	64M487	(L)* 32.9	59.3	40.5	66.5
			(T)**32.6	58.8	41.0	59.5
34	Semikilled (XF-1)	64M487	(L) 32.9	61.8	40.7	66.3
			(T) 34.5	62.4	40.0	61.7
35	Rimmed (Z1A)	16445	(L) 34.7	68.1	36.5	57.6
			(T) 35.2	68.7	31.2	51.6
36	Semikilled (X2B)	64M487	(L) 36.5	67.2	36.0	63.5
			(T) 35.2	67.8	34.5	58.8
37	Semikilled (X2F)	64M487	(L) 35.5	64.4	41.0	67.8
			(T) 35.0	64.2	36.3	61.8
38	Semikilled (X1B)	64M487	(L) 35.5	66.8	36.5	64.3
			(T) 35.6	66.4	36.8	59.8
39	Semikilled (X2E)	64M487	(L) 34.3	61.6	39.5	65.3
			(T) 35.2	62.1	36.8	57.5

\*(L) Average of two specimens taken parallel to the direction of rolling.  
 \*\*(T) Average of two specimens taken transverse to the direction of rolling.

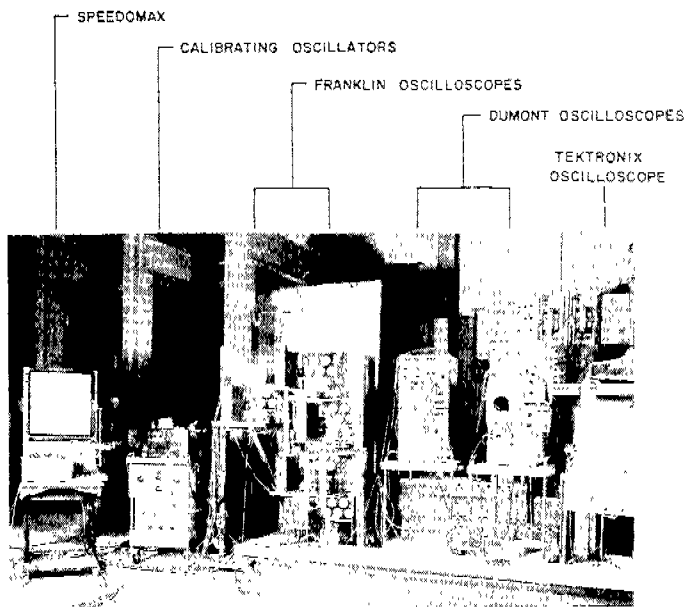
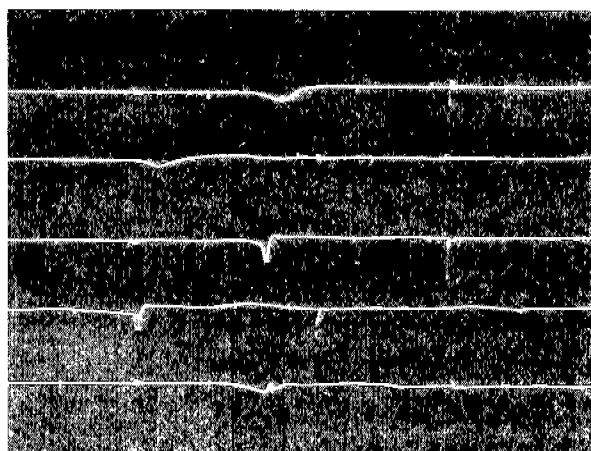


Fig. 3. Recording Equipment

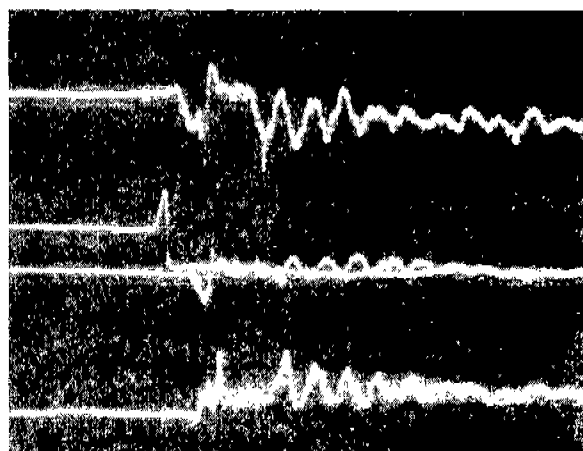
tion at various points on the plate surface as recorded by single strain gages. The results of the work through the end of 1956 have been reported in a paper<sup>5</sup> and, in more detail, in two technical reports.<sup>1, 2</sup> In 1957, an additional 25 channels of cathode-ray oscilloscope recording equipment were made available to the program by the Naval Research Laboratory.

The latest 25 channels of the cathode-ray oscilloscope equipment were five-channel units manufactured by Franklin Electronics. The nine earlier channels consisted of two DuMont Type 333 and two DuMont Type 322 dual-beam cathode-ray oscilloscopes, and a Tektronix Type 512 single beam unit. The recording equipment, along with the calibrating oscillator that supplied the time signals, is shown in Fig. 3; the cameras for the DuMont equipment are not shown.

Six of the DuMont oscilloscope channels are sufficiently sensitive to allow at least 1-1/2 in. of trace deflection for 0.001 in./in. of strain. However, the deflection scale used to record the test data on these DuMont scopes was limited by the size of the scope face and the maximum value of expected strain. The other 28 channels only allowed about 1/2 in. of trace deflection for the same strain. In planning the recording of the test data, the equipment was arranged so that the strain gages that were expected to produce signals of lowest electrical magnitude were connected to the six DuMont oscilloscopes as they had the highest sensitivity. The frequency response of all oscilloscopes was flat up to at least 50 kc and therefore, they were considered to be adequate to record the strain signals. Portions of two typical strain records are presented in Fig. 4. The oscilloscope channels used to measure and record strain were



Franklin Oscilloscope Record



DuMont Oscilloscope Record

Fig. 4. Typical Strain Records

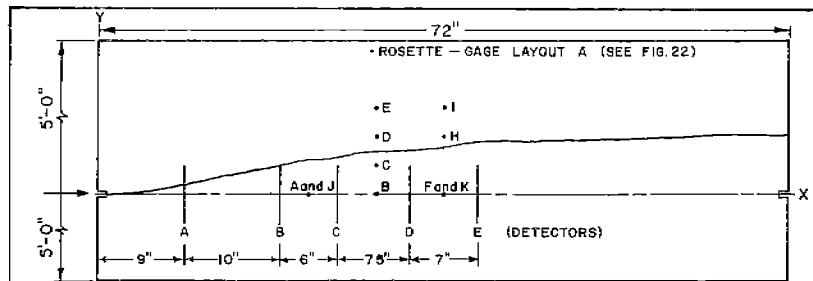
calibrated by shunting gages with a resistance whose equivalent strain value was known.

The time base for the records obtained from the DuMont and Franklin oscilloscopes was supplied by continuously moving 35-mm film. Timing marks on the traces from the Franklin units were energized by the oscillator and recorded as part of the strain traces; the DuMont units employed intensity modulation of the electron spot to define the time base. On all of the strain traces a simultaneous "blip" was produced by a synchronizing signal supplied from the Tektronix oscilloscope circuit, immediately before and after the test. This signal made it possible to synchronize accurately with each other all the strain traces from a particular test. The synchronizing "blip" is visible on the records shown in Fig. 4.

The crack detector trace on the Tektronix oscilloscope was recorded on a single frame of 35-mm film. The time axis was calibrated by putting a time signal of known frequency on the channel and photographing one sweep. This was done immediately after the test was completed.

Since only 34 channels of strain recording equipment were available (33 channels for 11 rectangular strain rosettes and one channel for crack speed detectors) and the exact location of the fracture path was unknown prior to each





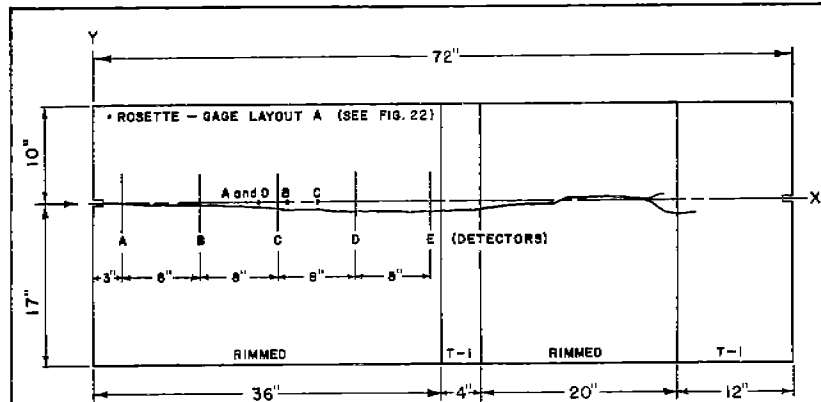
DYNAMIC STRAIN GAGES

Rosette No.	Strain Gage No.	Orien- tation	X (in.)	Y (in.)	Test Load Strain (in./in.)	Distance to Fracture (in.)
A	1	V	22.0	0	.00068	+3.6
	2	H	22.3	0	-.00018	+3.6
	3	D	22.3	+0.3	.00029	+3.3
B	4	V	29.0	0	.00066	+4.4
	5	H	29.3	0	-.00018	+4.4
	6	D	29.3	+0.3	.00026	+4.1
C	7	V	29.0	+3.0	.00065	+1.4
	8	H	29.3	+3.0	-.00018	+1.4
	9	D	29.3	+3.3	.00019	+1.1
D	10	V	29.0	+6.0	.00068	-1.6
	11	H	29.3	+6.0	-.00018	-1.6
	12	D	29.3	+6.3	.00024	-1.9
E	13	V	29.0	+9.0	.00067	-4.6
	14	H	29.3	+9.0	-.00018	-4.6
	15	D	29.3	+9.3	.00023	-4.9
F	16	V	36.0	0	.00066	+4.8
	17	H	36.3	0	-.00018	+4.8
	18	D	36.3	+0.3	.00021	+4.5
H	22	V	36.0	+6.0	.00066	-1.2
	23	H	36.3	+6.0	-.00018	-1.2
	24	D	36.3	+6.3	.00015	-1.5
I	25	V	36.0	+9.0	.00067	-4.2
	26	H	36.3	+9.0	-.00019	-4.2
	27	D	36.3	+9.3	.00019	-4.5
J	28	V	22.0	0	.00057	+3.6
	29	H	22.3	0	-.00017	+3.6
	30	D	22.3	+0.3	.00021	+3.3
K	31	V	36.0	0	.00057	+4.8
	32	H	36.3	0	-.00017	+4.8
	33	D	36.3	+0.3	.00021	+4.5

CRACK PATH

X (in.)	Y (in.)
1.1	0
4	.2
6	.4
12	1.5
16.5	2.5
18	2.6
22	3.6
24	3.8
29	4.4
36	4.8
42	5.5
48	5.6
54	5.8
60	6.0
66	6.1
72	6.1

FIG. 6 INSTRUMENTATION LAYOUT AND CRACK PATH - TEST 34



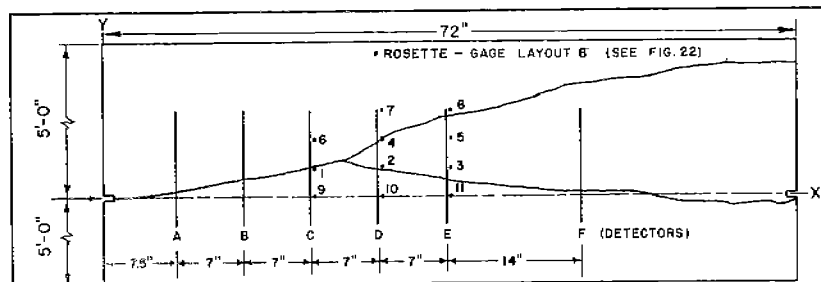
DYNAMIC STRAIN GAGES

Rosette No.	Strain Gage No.	Orien- tation	X (in.)	Y (in.)	Test Load Strain (in./in.)	Distance to Fracture (in.)
A	1	V	17.0	0	.00092	-0.5
	2	H	17.3	0	-.00024	-0.5
	3	D	17.3	+0.3	.00035	-0.8
B	4	V	20.0	0	.00093	-0.6
	5	H	20.3	0	-.00022	-0.6
	6	D	20.3	+0.3	.00036	-0.9
C	7	V	23.0	0	.00092	-0.8
	8	H	23.3	0	-.00022	-0.8
	9	D	23.3	+0.3	.00038	-1.1
D	10	V	17.0	0	.00094	-0.5
	11	H	17.3	0	-.00026	-0.5
	12	D	17.3	+0.3	.00029	-0.8

CRACK PATH

X (in.)	Y (in.)
1.1	0
11	-.2
14.5	-.3
17	-.5
20	-.6
23	-.8
30	-1.1
35	-1.1
40.4	-.9
44	-.3
48.5	0
53	+0.3
57	0
60	-1.4
62	Fracture arrested in T-1

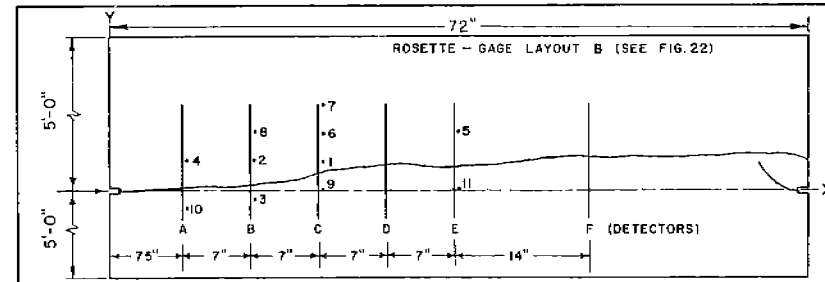
FIG. 7 INSTRUMENTATION LAYOUT AND CRACK PATH - TEST 35



DYNAMIC STRAIN GAGES							CRACK PATH	
Rosette No.	Strain Gage No.	Orien- tation	X (in.)	Y (in.)	Test Load Strain (in./in.)	Distance to Fracture (in.)	X (in.)	Y (in.)
1	1	H	22.0	3.0	-.00016	0.0 (Lower)	1.1	0
	2	D	22.3	3.3	.00022	0.0 "	5	.2
	3	V	22.0	3.3	.00070	0.15 "	10	.9
2	6	H	29.0	3.0	-.00017	0.15 "	15	1.9
	7	D	29.3	3.3	.00026	0.50 "	20	2.6
	8	V	29.0	3.3	.00074	0.55 "	22	3.2
3	11	H	36.0	3.0	-.00017	1.35 "	25.0*	3.8
	12	D	36.3	3.3	.00027	1.80 "		
	13	V	36.0	3.3	.00070	1.70 "		
4	16	H	29.0	6.0	-.00016	0.0 (Upper)	26	4.2 3.4
	17	D	29.3	6.3	.00020	0.10 "	27	4.6 3.1
	18	V	29.0	6.3	.00071	0.10 "	29	5.9 2.8
5	21	H	36.0	6.0	-.00017	2.60 "	30	6.5 2.7
	22	D	36.3	6.3	.00026	2.15 "	35	8.1 1.9
	23	V	36.0	6.3	.00069	2.20 "	38	8.7 1.2
6	4	D	22.3	6.3	.00017	-3.00 (Lower)	45	10.3 0.7
	5	V	22.0	6.3	.00070	-3.10 "	48	11.3 0.3
	24	H	22.0	6.0	-.00016	-2.80 "	52	11.0 0.3
7	26	H	29.0	9.0	-.00015	-3.00 (Upper)	55	12.1 0.3
	27	D	29.3	9.3	.00026	-3.10 "	57	12.3 0
	28	V	29.0	9.3	.00072	-3.30 "	59	12.9 -0.4
8	29	H	36.0	9.0	-.00017	-0.45 "	65	13.5 -0.9
	32	D	36.3	9.3	.00027	-0.80 "	66.5	13.5 -1.0
	31	V	36.0	9.3	.00071	-0.75 "	69.5	13.5 -0.8
9	9	D	22.3	0.3	.00021	3.05 (Lower)	70	13.5 -1.0
	10	V	22.0	0.3	.00068	2.90 "	72	13.6 -0.7
	25	H	22.0	0.0	-.00017	3.25 "		
10	14	D	29.3	0.3	.00030	2.55 "		
	15	V	29.0	0.3	.00069	2.55 "		
	30	H	29.0	0.0	-.00017	2.85 "		
11	19	D	36.3	0.3	.00027	1.15 "		
	20	V	36.0	0.3	.00070	1.15 "		
	33	H	36.0	0.0	-.00017	1.65 "		

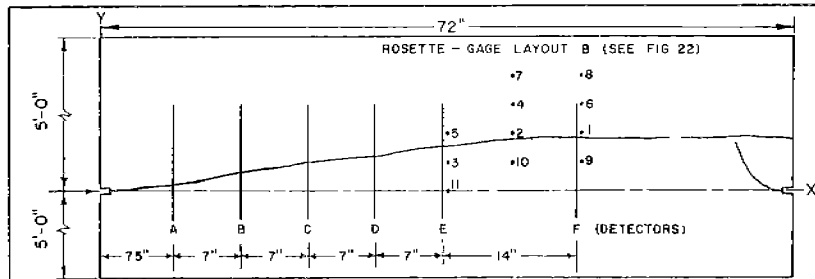
\*Crack Branched  
(U)= Upper Crack  
(L)= Lower Crack

FIG. 8 INSTRUMENTATION LAYOUT AND CRACK PATH - TEST 36



DYNAMIC STRAIN GAGES							CRACK PATH	
Rosette No.	Strain Gage No.	Orien- tation	X (in.)	Y (in.)	Test Load Strain (in./in.)	Distance to Fracture (in.)	X (in.)	Y (in.)
1	1	H	22	3	-.00018	-1.70	1.1	0
	2	D	22.3	3.3	.00022	-2.10	3	0
	3	V	22	3.3	.00063	-2.10	8	.2
2	6	H	15	3	-.00018	-2.40	15	.6
	7	D	15.3	3.3	.00022	-2.70	20	1.1
	8	V	15	3.3	.00066	-2.70	22	1.6
3	11	H	15	-3	-.00018	+1.65	25	1.8
	12	D	15.3	-2.7	.00023	+1.35	29	2.2
	13	V	15	-2.7	.00065	+1.35	32.5	2.6
4	16	H	8	3	-.00019	-2.80	35.5	2.6
	17	D	8.3	3.3	.00023	-3.10	36	2.4
	18	V	8	3.3	.00067	-3.10	39	2.4
5	21	H	36	6	-.00017	-3.65	49	3.5
	22	D	36.3	6.3	.00024	-4.00	55	3.6
	23	V	36	6.3	.00067	-4.00	64	3.6
6	24	H	22	6	-.00017	-4.70	69	3.7
	4	D	22.3	6.3	.00021	-5.10	70	3.6
	5	V	22	6.3	.00067	-5.10	72	3.2
7	26	H	22	9	-.00017	-7.70		
	27	D	22.3	9.3	.00027	-8.10		
	28	V	22	9.3	.00066	-8.10		
8	29	H	15	6	-.00018	-5.40		
	32	D	15.3	6.3	.00026	-5.70		
	31	V	15	6.3	.00068	-5.70		
9	25	H	22	0	-.00016	+1.35		
	9	D	22.3	.3	.00027	+1.00		
	10	V	22	.3	.00060	+1.00		
10	30	H	8	-3	-.00017	+2.20		
	14	D	8.3	-2.7	.00018	+1.90		
	15	V	8	-2.7	.00061	+1.90		
11	33	H	36	0	-.00017	+2.35		
	19	D	36.3	.3	.00023	+2.00		
	20	V	36	.3	.00066	+2.00		

FIG. 9 INSTRUMENTATION LAYOUT AND CRACK PATH - TEST 37



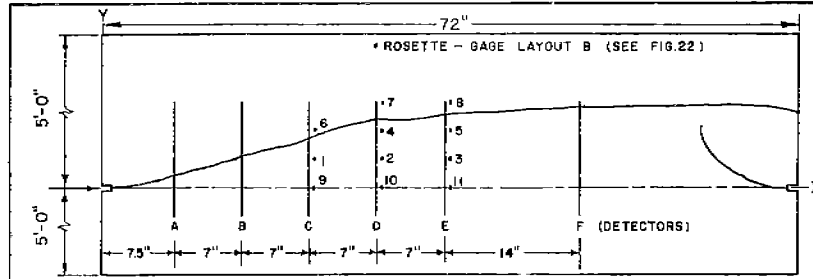
DYNAMIC STRAIN GAGES

Rosette No.	Strain Gage No.	Orien- tation	X (in.)	Y (in.)	Test Load Strain (in./in.)	Distance to Fracture (in.)
1	1	H	50	6	-.00017	-0.70
	2	D	50.3	6.3	.00018	-1.05
	3	V	50	6.3	.00046	-1.05
2	6	H	43	6	-.00018	-1.05
	7	D	43.3	6.3	.00019	-1.30
	8	V	43	6.3	.00056	-1.40
3	11	H	36	3	-.00017	+1.65
	12	D	36.3	3.3	.00018	+1.25
	13	V	36	3.3	.00050	+1.25
4	16	H	43	9	-.00019	-4.05
	17	D	43.3	9.3	.00021	-4.30
	18	V	43	9.3	.00056	-4.40
5	21	H	36	6	-.00017	-1.30
	22	D	36.3	6.3	.00014	-1.73
	23	V	36	6.3	.00060	-1.73
6	4	H	50	9	-.00017	-5.70
	5	D	50.3	9.3	.00015	-4.05
	5	V	50	9.3	.00056	-4.05
7	26	H	43	12	-.00018	-7.05
	27	D	43.3	12.3	.00018	-7.30
	28	V	43	12.3	.00044	-7.40
8	29	H	50	12	-.00018	-6.70
	32	D	50.3	12.3	.00023	-7.05
	31	V	50	12.3	.00057	-7.05
9	9	H	50	3	-.00017	+2.35
	9	D	50.3	3.3	.00021	+2.10
	10	V	50	3.3	.00056	+2.00
10	30	H	43	3	-.00017	+1.95
	14	D	43.3	3.3	.00028	+1.70
	15	V	43	3.3	.00056	+1.65
11	33	H	36	0	-.00018	+4.65
	19	D	36.3	.3	.00009	+4.30
	20	V	36	.3	.00054	+4.30

CRACK PATH

X (in.)	Y (in.)
1.1	0
5.0	.2
6.0	.3
10	.8
22	2.9
24	3.2
27	3.5
30	3.8
35	4.6
40	4.9
45	5.1
50	5.4
54	5.4
56	5.3
60	5.4
65	5.5
70	5.5
72	5.4

FIG. 10 INSTRUMENTATION LAYOUT AND CRACK PATH - TEST 38



DYNAMIC STRAIN GAGES

Rosette No.	Strain Gage No.	Orien- tation	X (in.)	Y (in.)	Test Load Strain (in./in.)	Distance to Fracture (in.)
1	1	H	22	3	-.00017	+2.29
	2	D	22.3	3.3	.00021	+2.10
	3	V	22	3.3	.00062	+1.96
2	6	H	29	3	-.00017	+4.14
	7	D	29.3	3.3	.00019	+3.90
	8	V	29	3.3	.00061	+3.85
3	11	H	36	3	-.00017	+4.50
	12	D	36.3	3.3	.00019	+4.22
	13	V	36	3.3	.00058	+4.12
4	16	H	29	6	-.00016	+1.09
	17	D	29.3	6.3	.00022	+0.88
	18	V	29	6.3	.00060	+0.85
5	21	H	36	6	-.00017	+1.55
	22	D	36.3	6.3	.00023	+1.14
	23	V	36	6.3	.00062	+1.12
6	4	H	22	6	-.00017	-0.73
	4	D	22.3	6.3	.00025	-0.90
	5	V	22	6.3	.00056	-1.08
7	26	H	29	9	-.00018	-1.76
	27	D	29.3	9.3	.00020	-2.07
	28	V	29	9.3	.00061	-2.12
8	29	H	36	9	-.00018	-1.47
	32	D	36.3	9.3	.00023	-1.80
	31	V	36	9.3	.00062	-1.85
9	25	H	22	0	-.00017	+5.27
	9	D	22.3	0.3	.00022	+5.10
	10	V	22	0.3	.00059	+4.98
10	30	H	29	0	-.00019	+7.17
	14	D	29.3	0.3	.00019	+6.85
	15	V	29	0.3	.00059	+6.89
11	33	H	36	0	-.00017	+7.50
	19	D	36.3	0.3	.00026	+7.20
	20	V	36	0.3	.00060	+7.14

CRACK PATH

X (in.)	Y (in.)
1.1	0
6	0.7
10	1.8
15	3.3
20	4.6
21	4.8
25	6.3
28	7.1
32	7.0
35	7.4
40	7.9
45	8.2
50	8.4
55	8.5
60	8.5
65	8.6
69	8.4
72	7.9

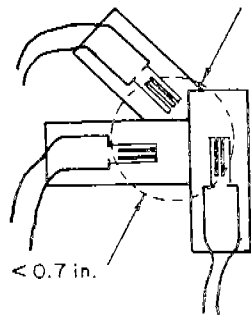
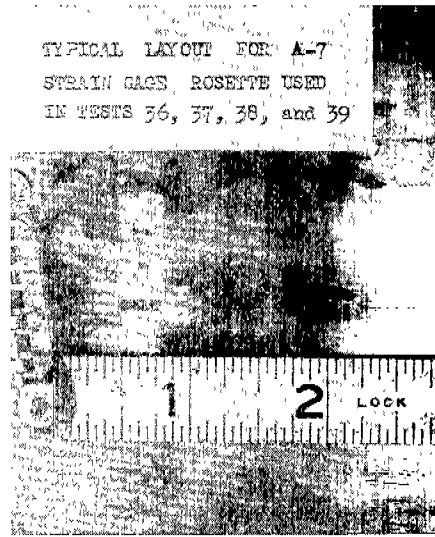
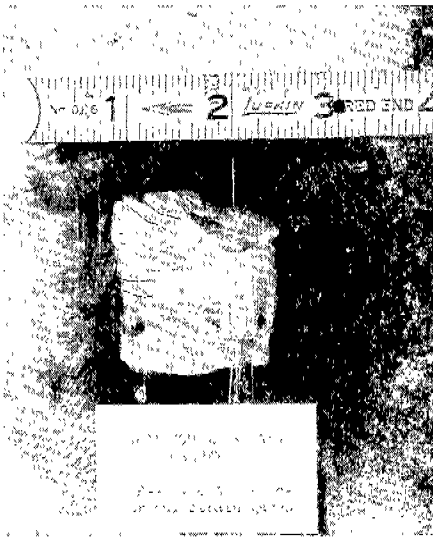
FIG. 11 INSTRUMENTATION LAYOUT AND CRACK PATH - TEST 39

intervals across the plate in order to obtain strain values at intervals of one-tenth the net plate width. Since a double fracture occurred in Test 36, a duplicate test (Test 39) was conducted.

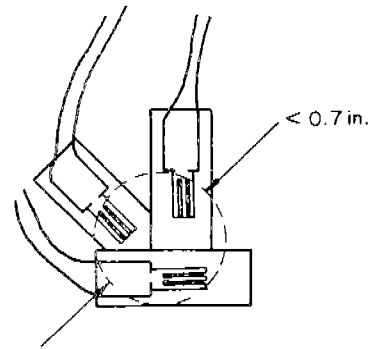
Rectangular strain rosettes consisting of three SR-4 Type A-7 strain gages were used to determine the principal strains at various locations on the surface of each specimen. Since the component gages were of a finite size, it was obviously not possible to measure the strain in three directions precisely at a point; however, since the three component strain gages of the rosettes had a 1/4-in. gage length, it was possible to mount the three gage elements within a 0.7-in. diameter circle, and this was considered to be satisfactory under the circumstances. In the tests reported here, two rosette layouts of the component gages were used. Photographs and drawings of both gage layouts are presented in Fig. 12. In layout A (Tests 33, 34, and 35), the diagonal gage was centered directly above the horizontal gage, and the vertical gage was mounted on the side near the initiation edge; in layout B (Tests 36 through 39), the vertical gage was centered directly above the horizontal gage, and the diagonal gage was mounted on the side away from the initiation edge.

The gages for dynamic measurements were connected in the customary Wheatstone bridge circuit. Three similar electrical strain gages, which were isolated from the specimen, were used as resistances to complete the bridge circuit. These bridges were excited by direct current and their outputs fed to the recording oscilloscope channels. A diagram of typical circuits is shown in Fig. 13.

The crack speed was measured with a system of six surface crack detectors which broke as the fracture traversed the plate; at each detector location in Tests 36 through 39, two 6-in. detectors (Baldwin SR-4 Type A-9 strain gages) were wired in series to give a 12-in. detector. The breaking of a crack detector opened an electrical circuit and caused a stepped change in voltage. A diagram of a typical crack detector circuit is shown in Fig. 14. From a knowledge of the spacing between detectors and the elapsed time between successive interruptions of the circuit, the speed of the fracture could be computed. This system gives an average surface speed of the fracture since the crack front location is not known precisely at the time the detector breaks. Thus, all calculated speeds were rounded off to the nearest 50 fps. Crack detector calibration was obtained



Gage Layout A



Gage Layout B

Fig. 12. Component Gage Layouts A and B

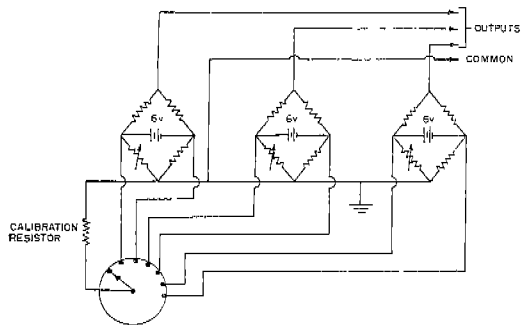


Fig. 13. Strain Gage Circuits

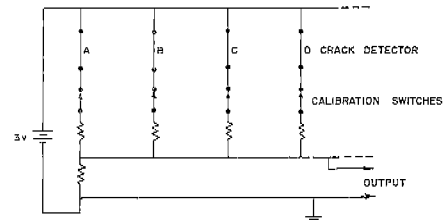


Fig. 14. Crack Detector Circuits

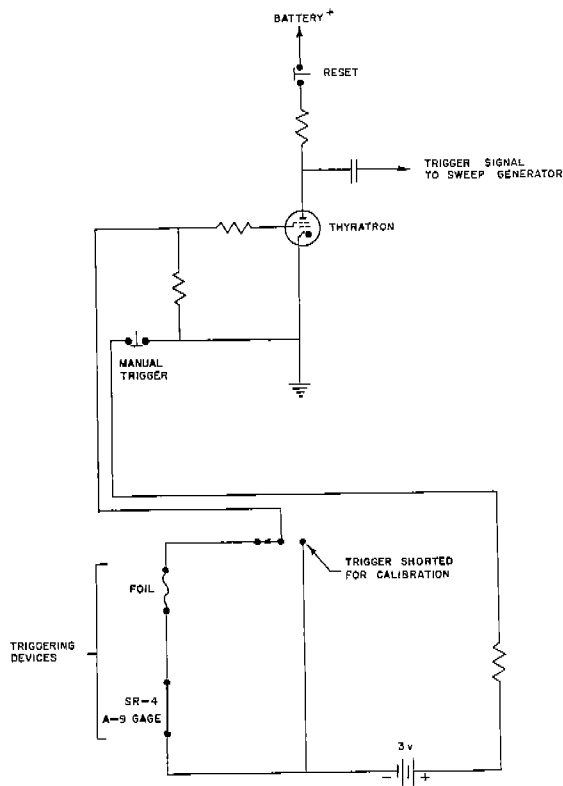


Fig. 15. Trigger Circuit

by successively opening switches arranged in series with the various detectors and recording the trace steps. The switch locations are indicated in the circuit shown in Fig. 14.

A triggering device, referred to as an external trigger because of its location, was utilized in these tests to activate the sweep and spot intensifying circuits in the recording equipment. This trigger consisted of a strip of aluminum foil which was broken as the piston device drove the wedge into the notch; thus, the circuits in the recording devices were energized just before the fracture was initiated. To insure that

the circuits would be energized in the event of failure of the external trigger, a plate surface trigger (A-9 strain gage) was connected in series with the external trigger. The trigger circuit is shown in Fig. 15.

Static strain gages also were located every 7 in. along the notch line on both faces of the plate and three sets of back-to-back gages were placed 18 in. above the notch line. However, to simplify the instrumentation drawings presented in Figs. 5--11, the positions of the static strain gages are not shown. Strain readings showed that in each test there was a fairly uniform static strain distribution across the plate during application of the test load; in addition, bending strains were noted to be less than 0.0002 in./in. in all tests.

The temperature of the specimen was continuously recorded during cooling by means of a Leeds and Northrup Type G "Speedomax" recorder and copper-constantan thermocouples located in 1/4-in. deep holes at various points across the specimen.

A more complete description of the instrumentation may be found in reports and papers previously issued as a part of this program.<sup>1, 2, 5</sup>

### Data Reduction

Reduction of the strain data recorded on 35-mm strip film was facilitated with a decimal converter and the University of Illinois high-speed digital computer, the ILLIAC.

A brief summary of the data reduction procedure is presented below. The 35-mm film strips were enlarged and the calibration and timing marks scaled on the enlargements. With the aid of the decimal converter, values of component gage strain versus time were simultaneously punched on IBM cards, plotted on an X-Y plotter, and typed in tabular form. The strain-time values were then transferred from IBM cards to punched paper tape and processed through the ILLIAC which computed values of the principal strains. The ILLIAC results consisted of tabulated principal strain data, as well as scaled oscilloscope displays of component gage and principal strain traces. The scaled oscilloscope displays were photographed for later enlargement and processing.

### Apparatus and Test Procedure

In most respects, the apparatus and test procedure used for these tests was similar to that used in earlier tests made as a part of this program.

The notch-wedge-impact method of fracture initiation was used in these tests. A closeup view of the 1-1/8 in. deep notch and the wedge is shown in Fig. 16. A view of the gas-operated piston device that provides the external impact is shown in Fig. 17. The theoretical output energy of the piston device was 1200 ft-lb, but calibration tests indicate that the device actually delivered about 1000 ft-lb.

Crushed dry ice was used to cool the plate specimen. Photographs of the dry ice containers, as well as a diagram showing the thermocouple locations for the specimens, are presented in Fig. 18. Typical cooling curves for Tests 33--39 are presented in Fig. 19.

After the instrumentation was mounted on the plate and the plate specimen had been welded to the pull-heads, the specimen was stressed at room

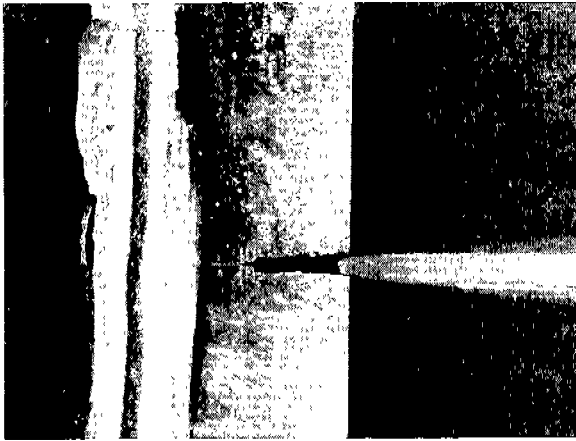


Fig. 16. Closeup of Notch and Tip of Wedge.

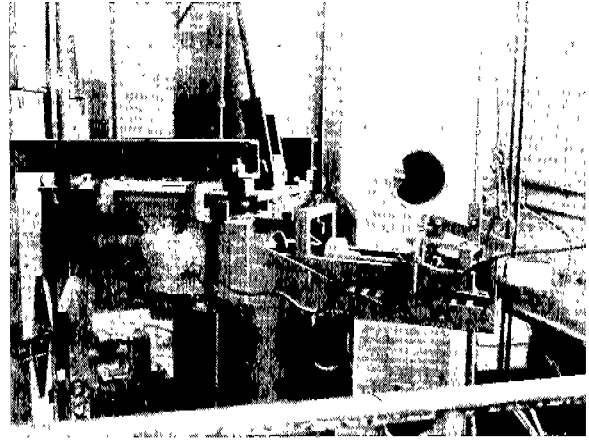


Fig. 17. Piston Device Used for Fracture Initiation.

temperature to the test load to check the behavior of the strain gages; at the same time, it was possible to ascertain the static strain distribution in the specimen and to obtain the test load strain values for each dynamic gage. Any gages that displayed faulty or questionable response were replaced and the newly installed gages were checked by another test load cycle.

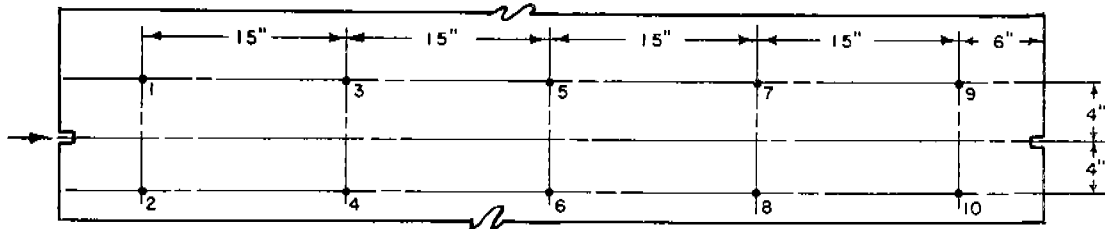
In Tests 36--39, wiring between gages and oscilloscopes was double checked by shunting each gage with a resistor and noting the direction of trace movement on the face of its respective oscilloscope. This gave a positive identification of the scope trace corresponding to each gage and the direction of the compression calibration for each gage.

At the time of test, the cooling tanks were filled with crushed dry ice; when the test temperature was approached, the plate was stressed to the test load. After loading, the recording equipment was calibrated, and the gas operated piston device pressurized. When the desired specimen temperature was obtained, the recording cameras were started, and the gas-operated piston device was fired to drive the wedge into the edge notch to initiate the brittle fracture.

## ANALYSIS OF TEST RESULTS

### General

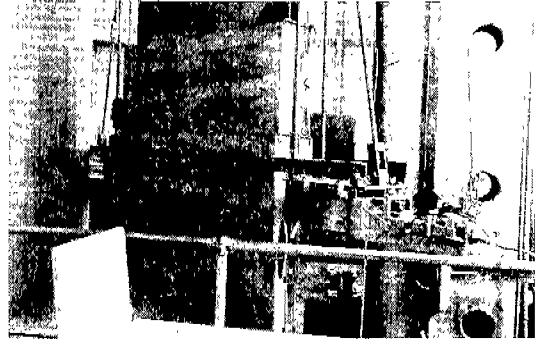
The results presented here are based on all of the applicable data ob-



Thermocouple Locations



Individual Cooling Tank



Cooling Tanks Mounted Prior to Testing

Fig. 18. Thermocouple Locations and Cooling Apparatus

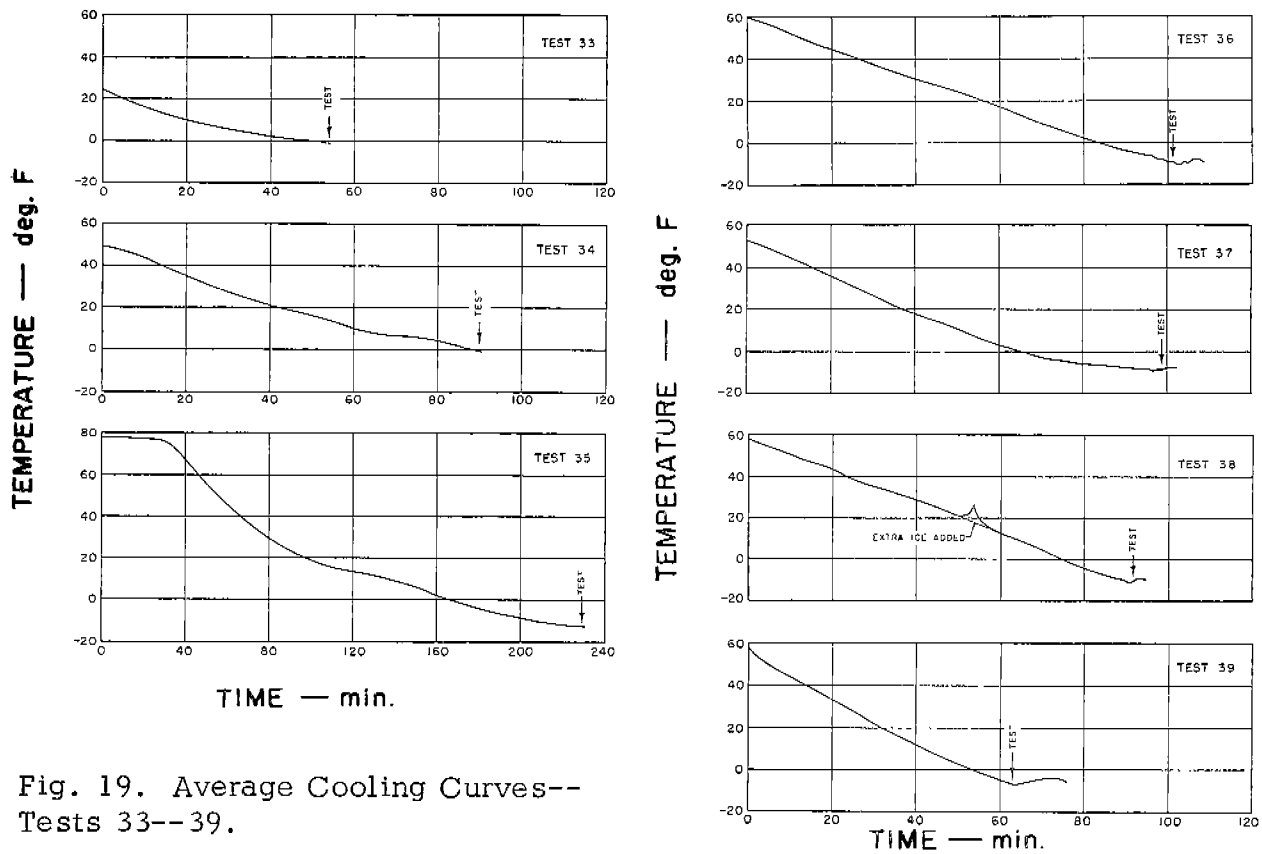
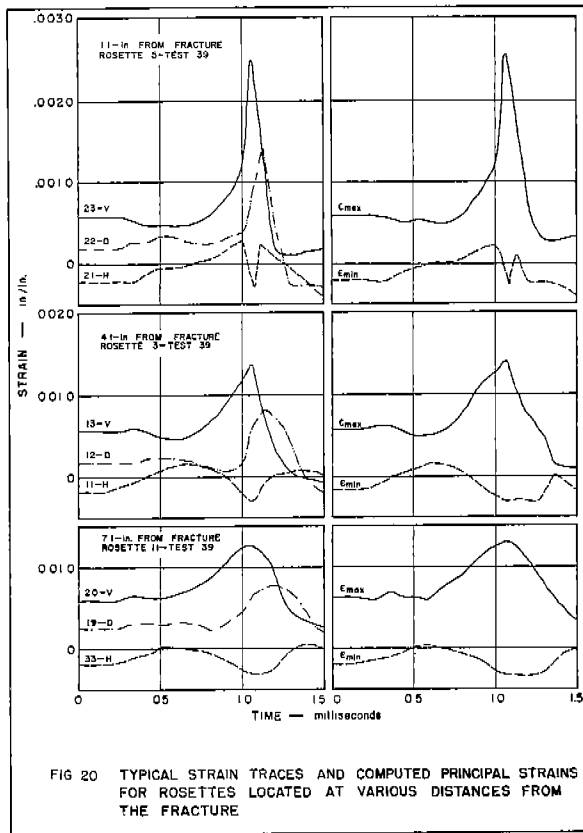


Fig. 19. Average Cooling Curves-- Tests 33--39.



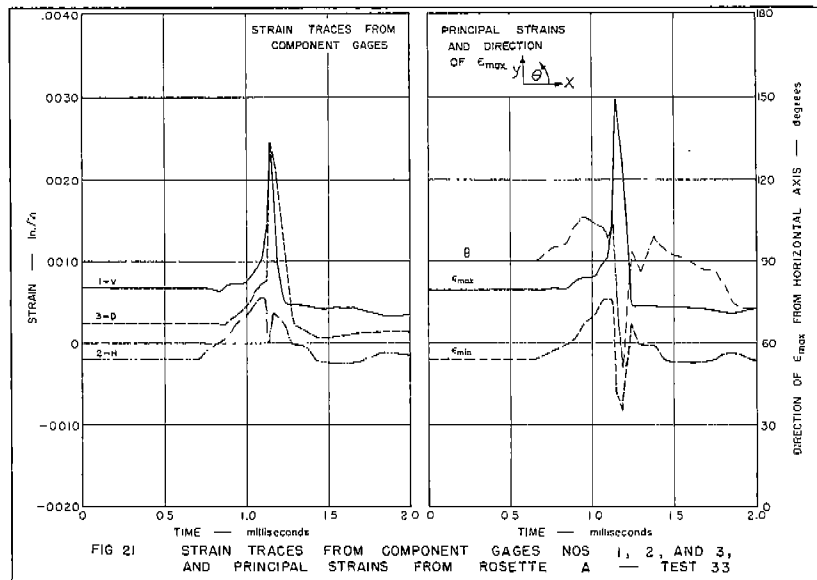
tained as a part of this program. The extensive strain data obtained in Tests 33--39 are presented in this report for the first time. The use of strain rosettes in the latter tests permits the plotting of contours of maximum principal strain, as well as contours of vertical strain, on the surface of the plate as the fracture propagates across the plate. The data obtained in earlier tests<sup>1, 2</sup> support the results of the more recent tests which are presented here.

#### Recorded Test Data

Typical strain traces for component gages located at various distances from the fracture may be seen in

Fig. 20; the three rosettes are from one plate and are mounted directly above one another at distances of 1.1 in., 4.1 in., and 7.1 in. from the fracture. The strain traces shown are representative of the strain-time curves obtained from all tests conducted as a part of this program. The decrease in maximum strain magnitude and the change in pulse shape as the distance between the gage and fracture changes may be clearly noted.

The vertical and diagonal gage traces exhibit a general shape characterized by a fairly steady and rapid increase in strain to a maximum (peak) strain value as the fracture propagates past the gage; the peak strain is followed by a decrease to a strain level associated with the removal of external load. For gages located close to the fracture, the peak is very sharp; for gages located away from the fracture, the peak is of a lower magnitude and the pulse extends over a longer time.



The horizontal gage traces are characterized by three major changes in strain. The strain trace first exhibits an initial relaxation of compressive strain, and this is followed by a compression pulse corresponding to the tension peak of the vertical gage. Finally, the trace exhibits another relaxation of compressive strain before leveling off at the final strain value.

The strain-time curves of the component gages obtained from Tests 33--39 are presented in Figs. 21--85. All strain traces are plotted such that the strain at zero time is the initial test load strain.

The second peak occurring in the component gage traces (and principal strain traces) in Figs. 43, 45, 47, and 50 was attributed to electrical effects associated with the recording equipment (although there is still some question regarding this matter), and not the double fracture of the plate specimen in Test 36.

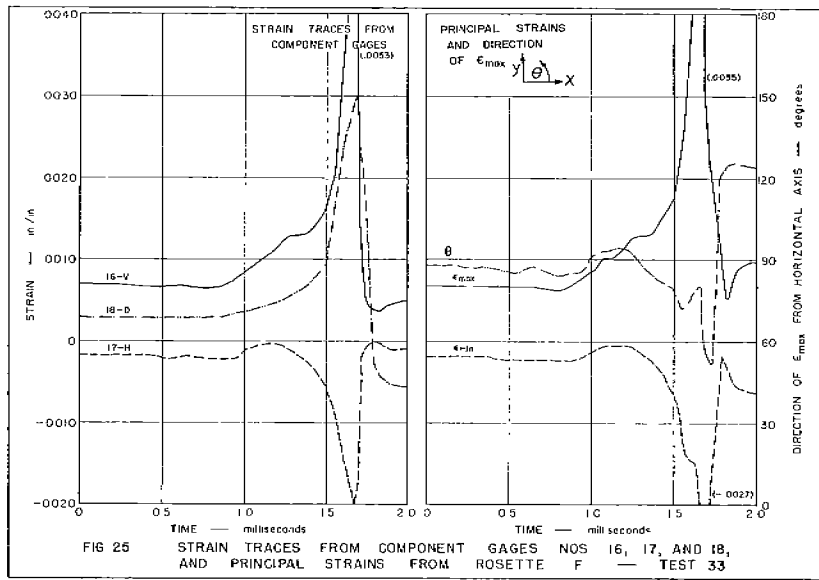
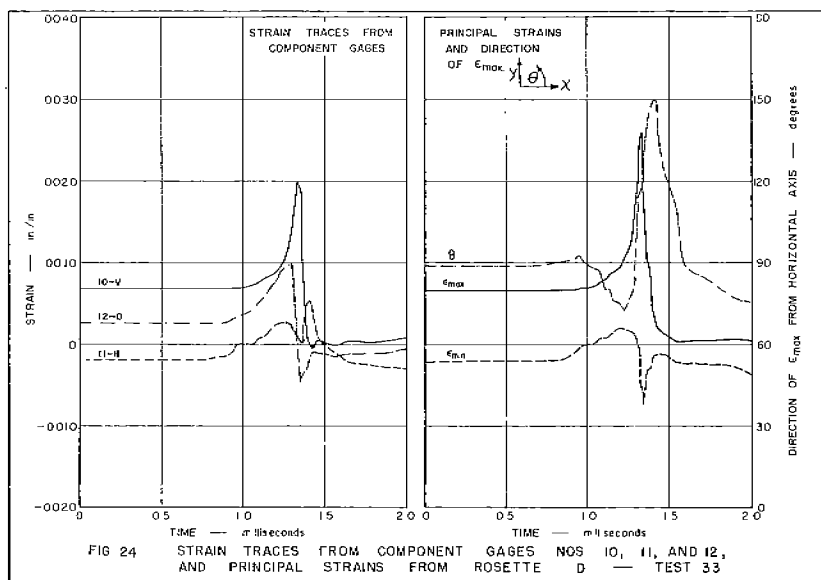
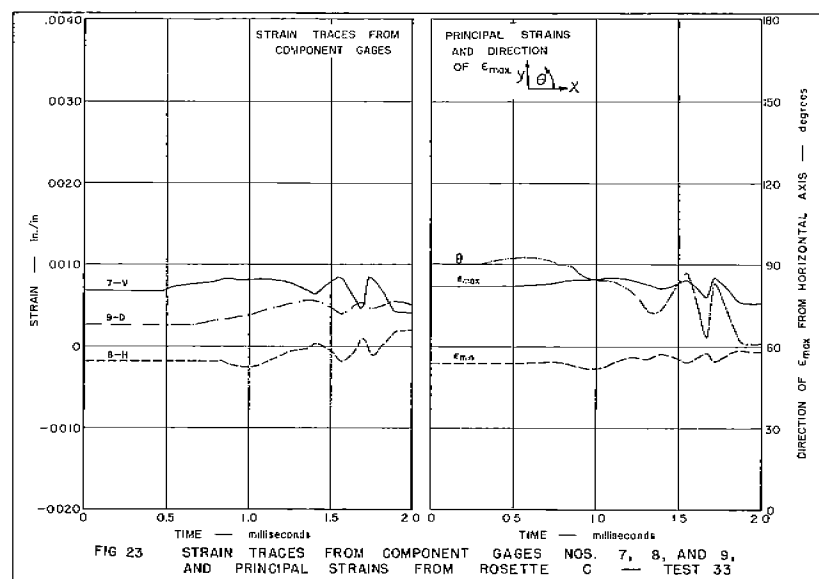
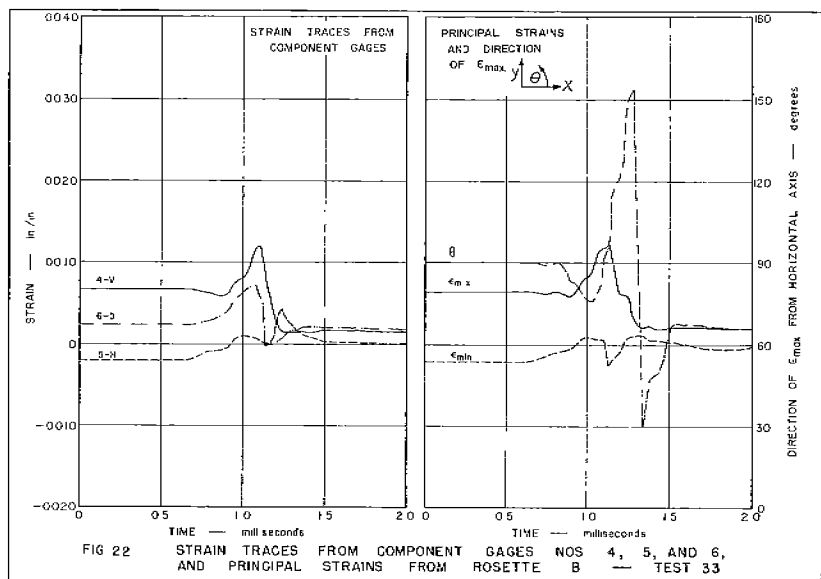
The crack speed detectors were used to measure the approximate surface fracture speed and to aid in determining the location of the surface fracture at any time during the brittle fracture test. The average surface speeds of propagation of the brittle fracture for Tests 33--39 are presented in Table 4. It will

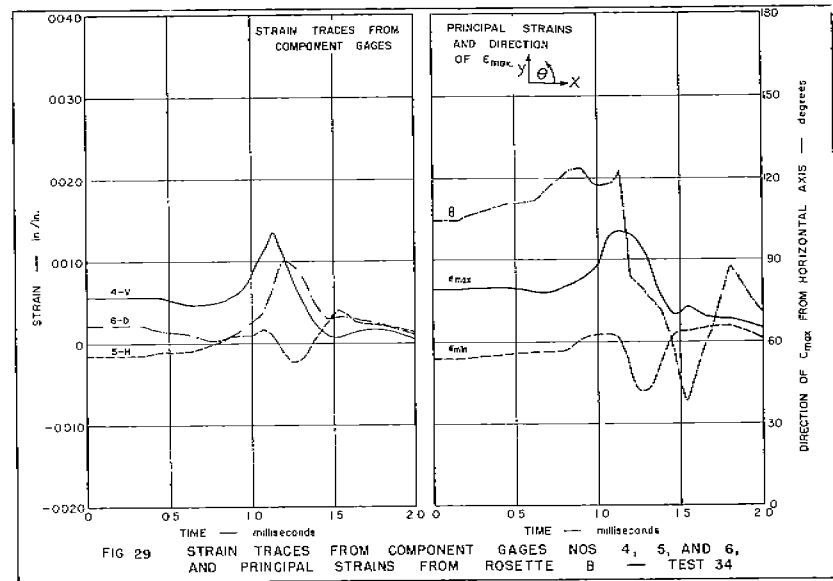
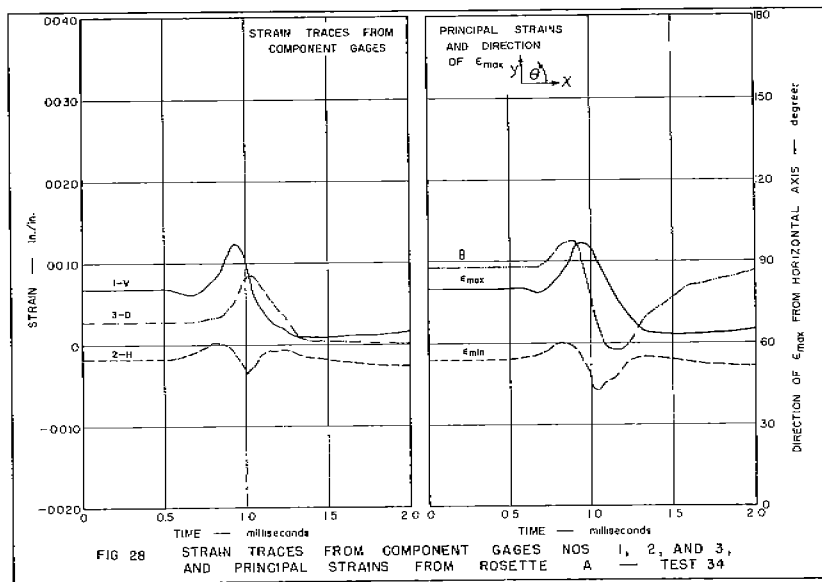
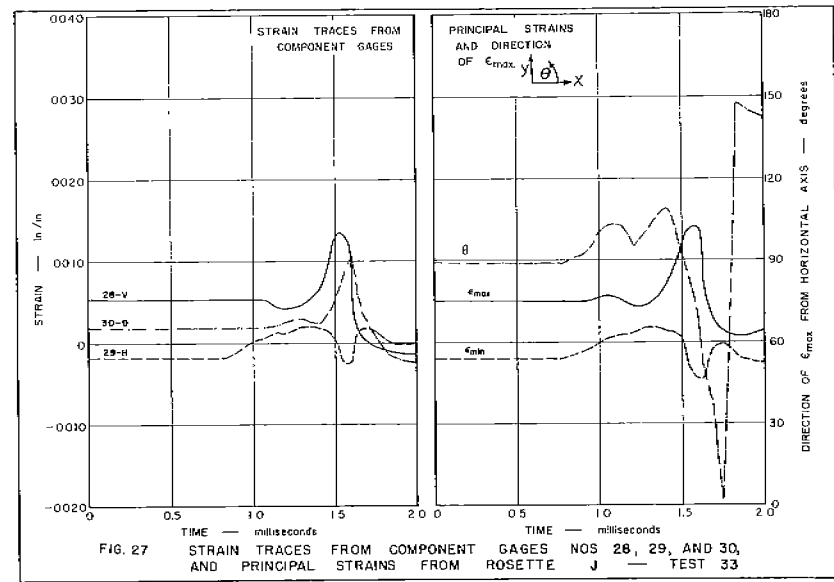
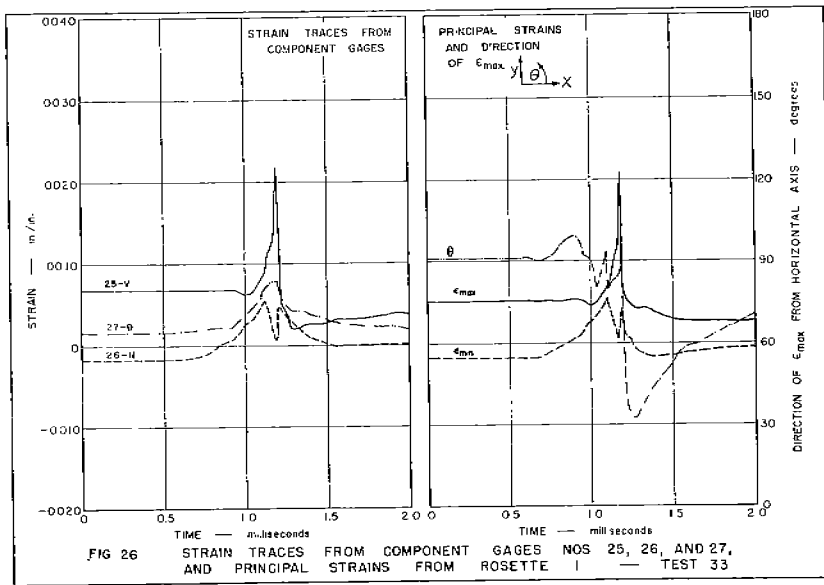
(Text continued on page 39)

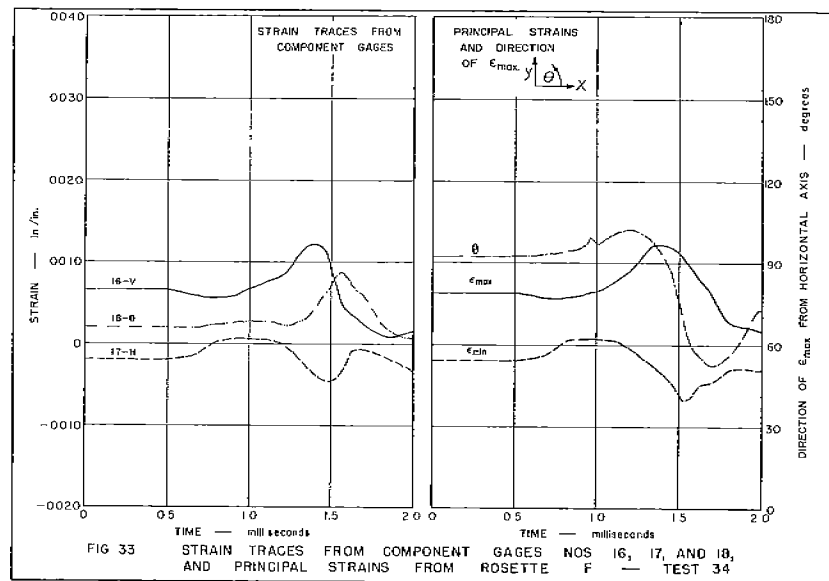
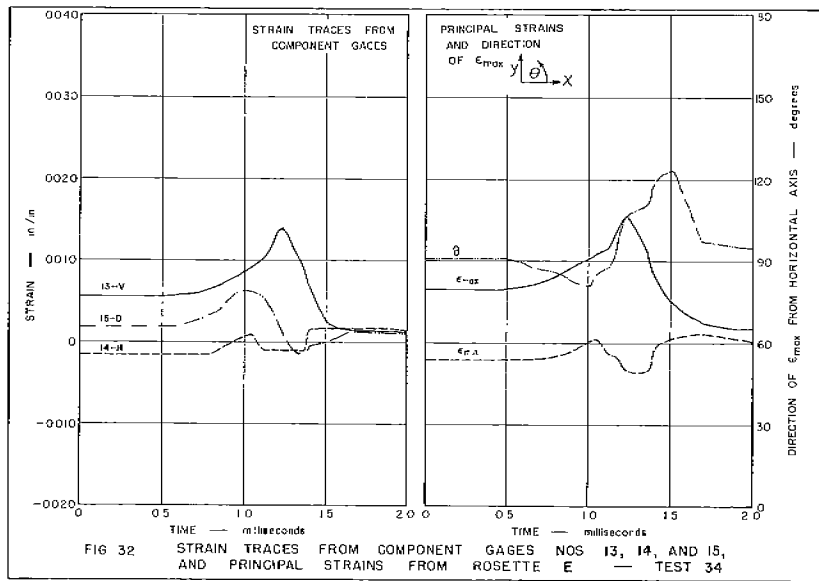
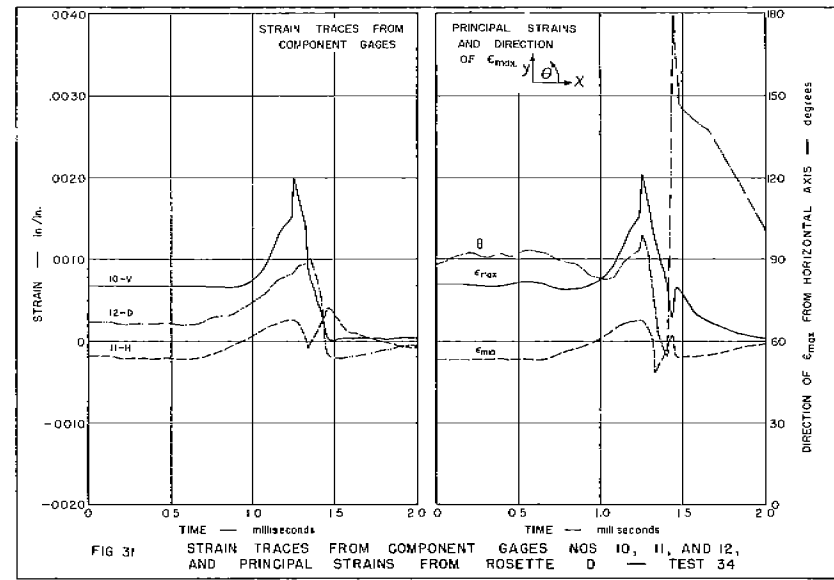
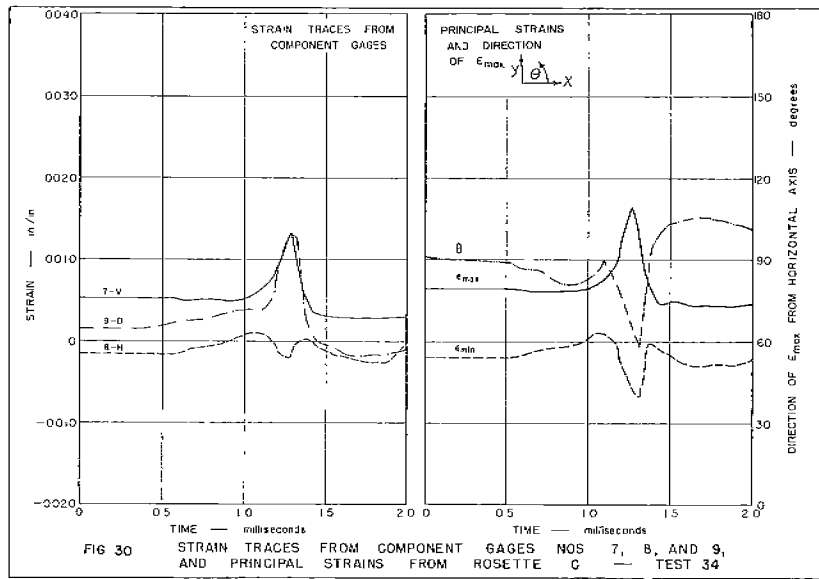
TABLE 4. FRACTURE SPEEDS

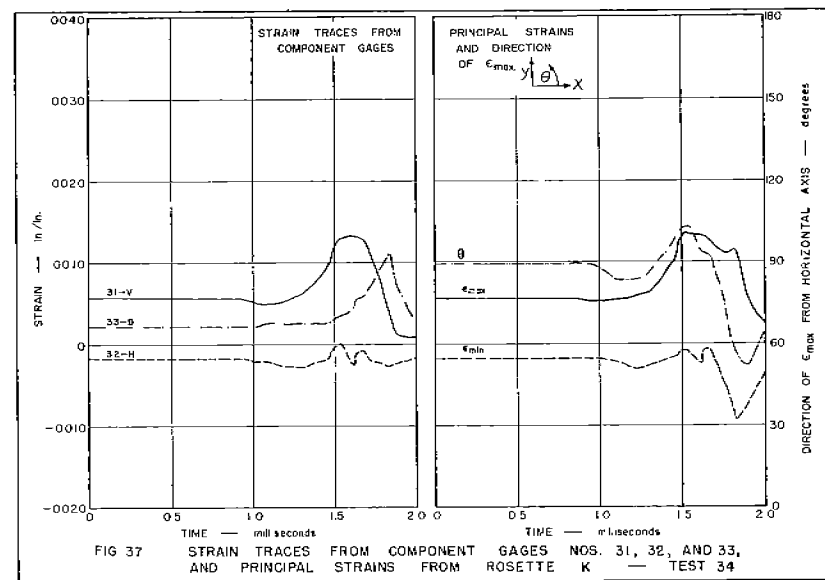
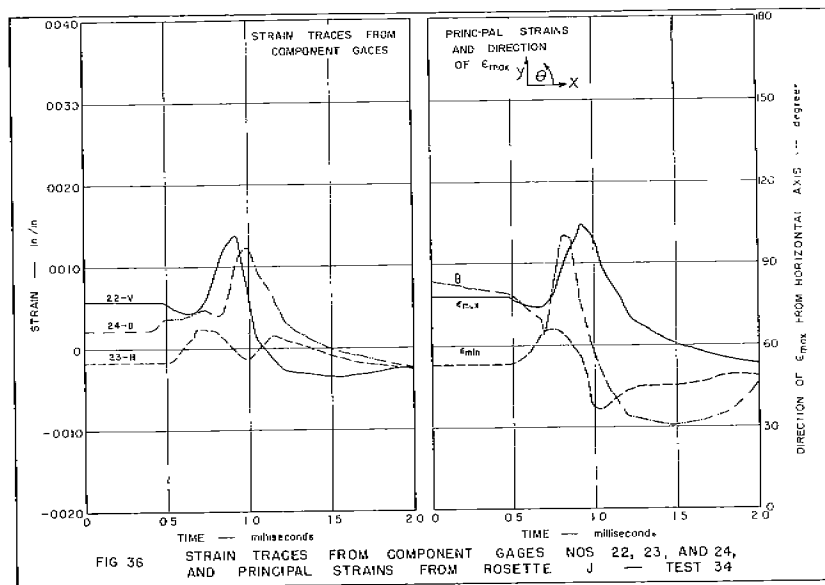
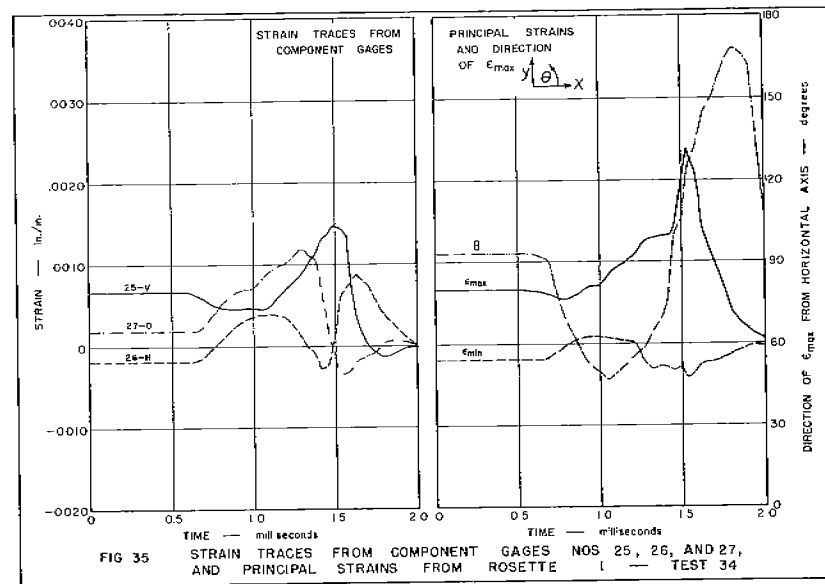
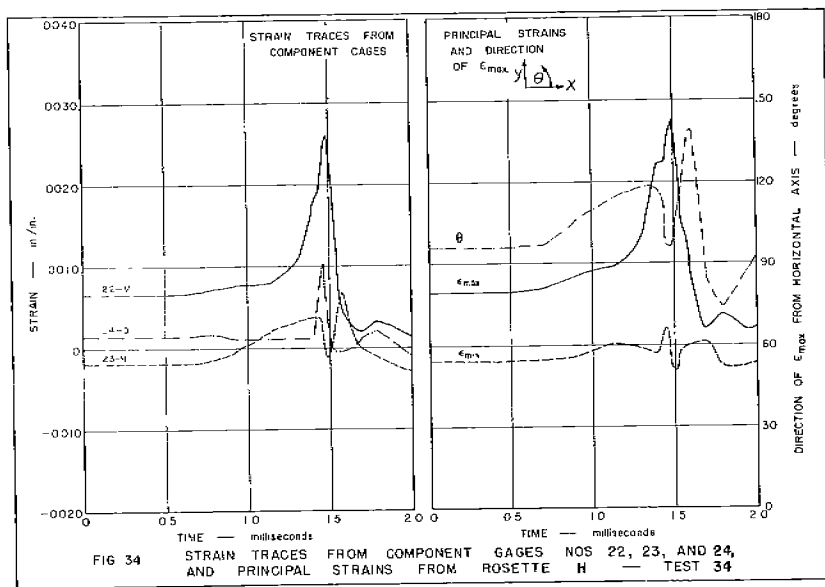
All distances are measured along the crack path.  
Speeds are rounded off to nearest 50 fps.

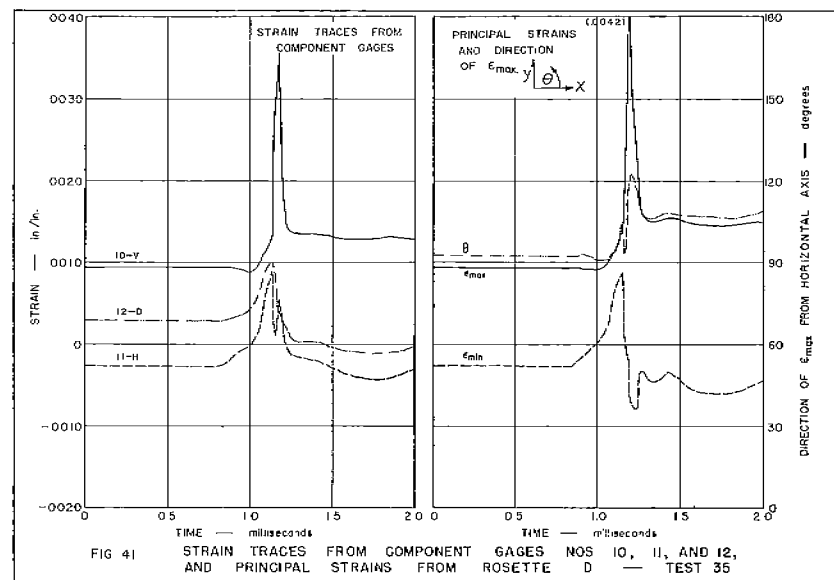
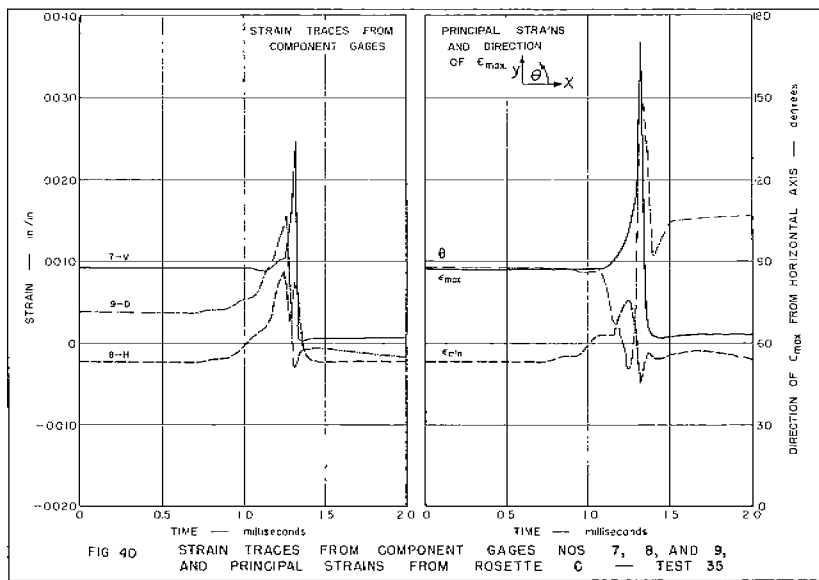
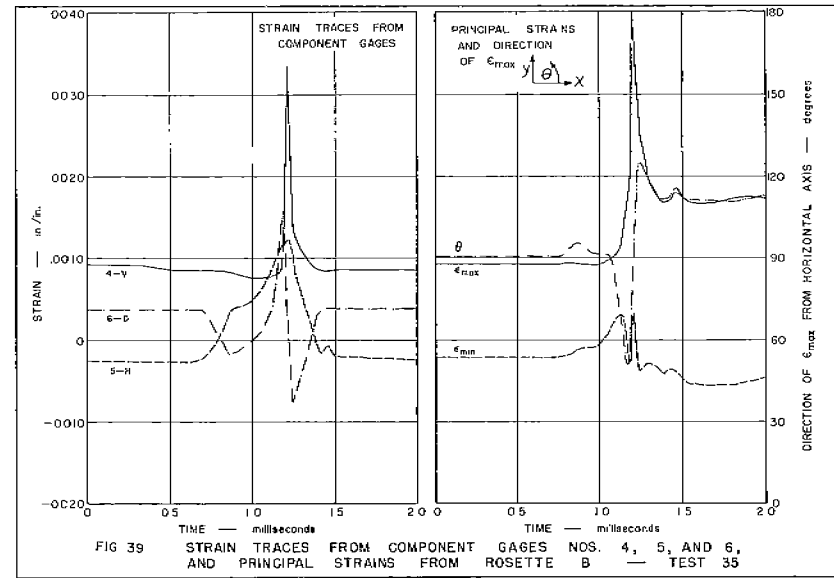
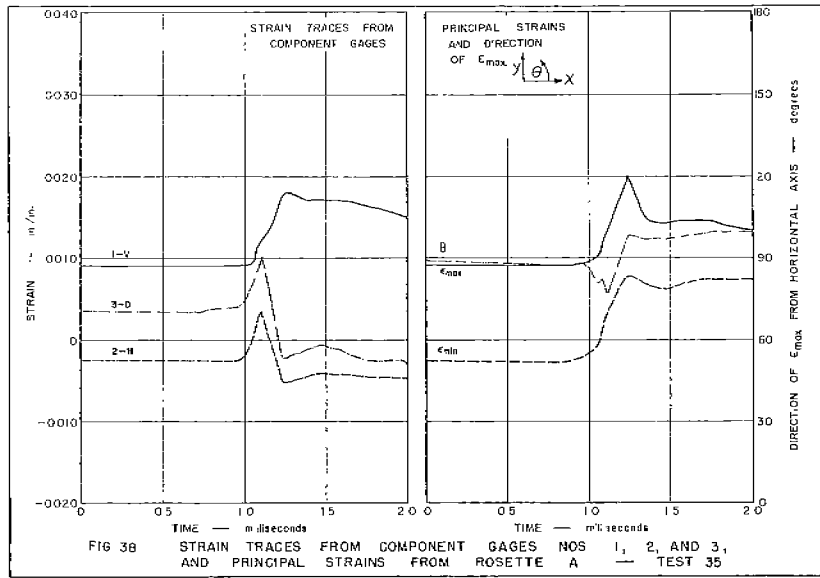
Detector	Distance between Detectors (in.)	Breaking Time (milliseconds)	Time Interval	Speed (fps)	Detector	Distance between Detectors (in.)	Breaking Time (milliseconds)	Time Interval	Speed (fps)
<u>TEST 33</u>					<u>TEST 37</u>				
A	12.02	0.76	0.36	2800	A	7.02	0.96	0.14	4200
B	13.16	1.12	0.37	2950	B	7.10	1.10	0.18	3300
C	6.02	1.49	0.22	2300	C	6.50	1.28	0.22	2450
D	6.05	1.71	0.25	2000	D	6.97	1.50	0.28	2100
E		1.96			E	13.60	1.78	0.62	1850
<u>TEST 34. Fracture Passed above Crack Detectors</u>					F		2.40		
<u>TEST 35</u>					<u>TEST 38</u>				
A	8.00	0.77	0.23	2900	A	7.14	0.34	0.15	3950
B	8.00	1.00	0.14	4750	B	7.16	0.49	0.16	3750
C	8.00	1.14	0.24	2800	C	6.71	0.65	0.20	2800
D	8.00	1.38	0.20	3350	D	6.94	0.85	0.22	2650
E		1.58			E	13.84	1.07	--	--
<u>TEST 36</u>					F		--		
A	7.10	0.31	0.13	3500	<u>TEST 39</u>				
B	6.64	0.44	0.15	4150	A	6.73	0.06	0.19	2950
C	7.32	0.59	0.23	3050	B	7.18	0.25	0.44	2700
D	7.15	0.82	0.20	3000	C	7.18	--	--	--
E	14.47	1.02	0.52	2800	D	7.24	0.69	0.26	2300
F		1.54			E	14.0	0.95	0.46	2550
					F		1.41		

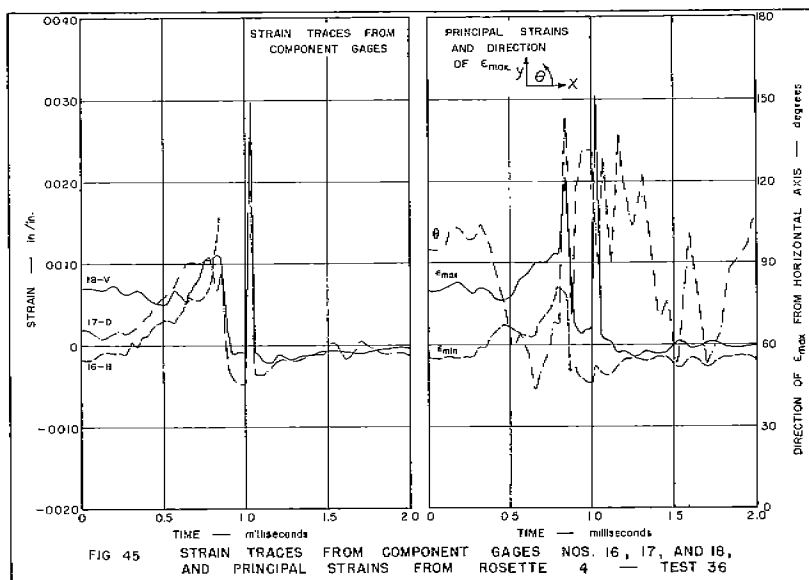
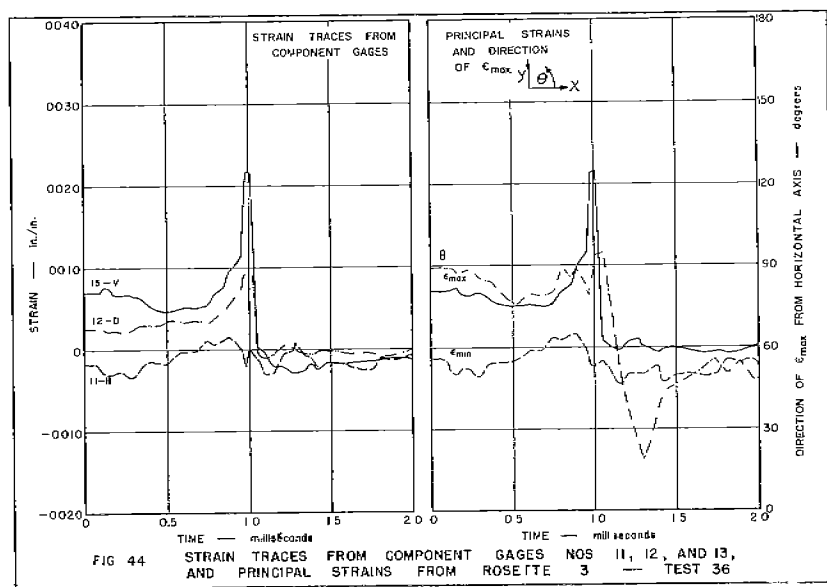
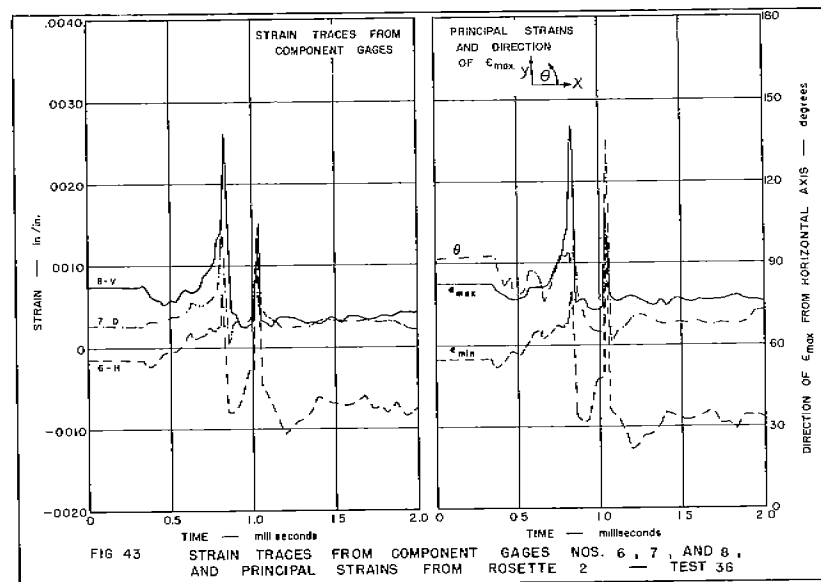
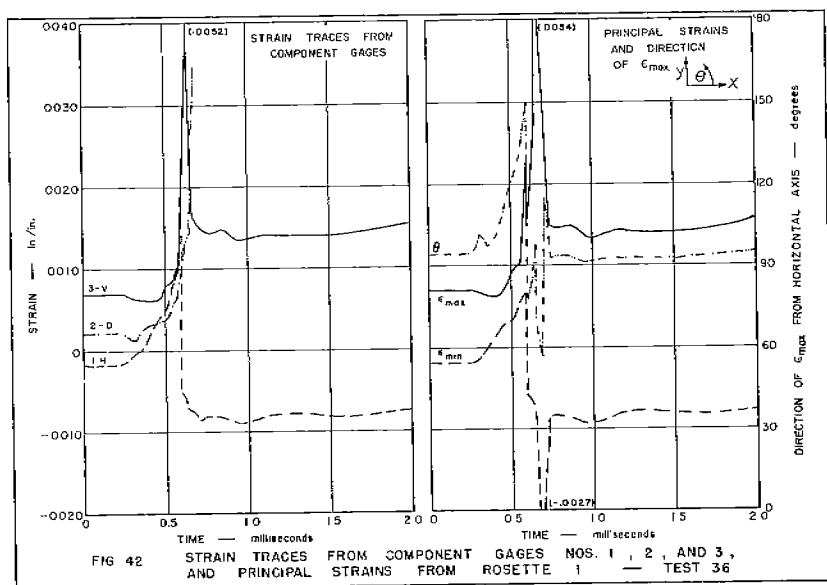


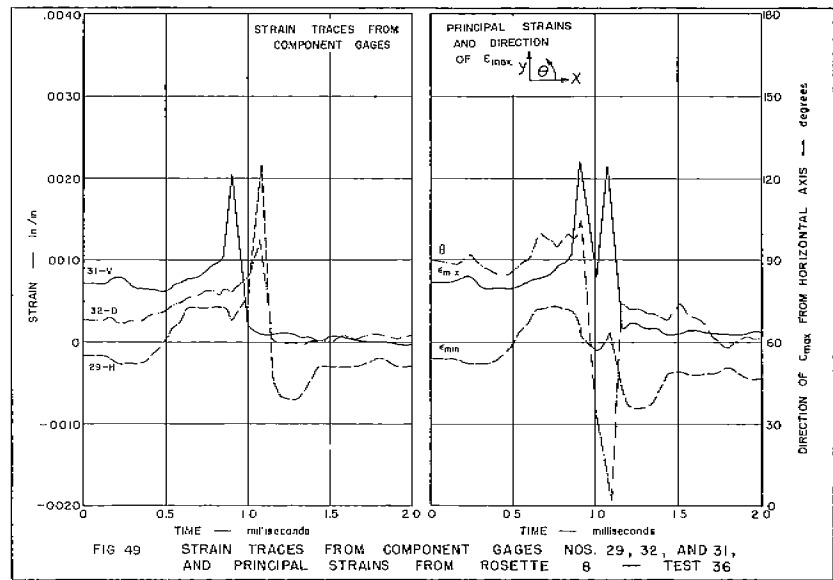
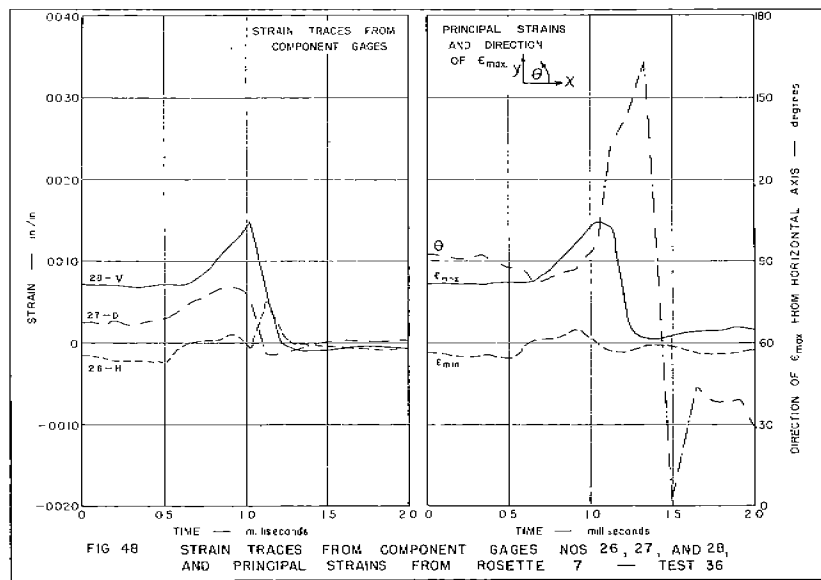
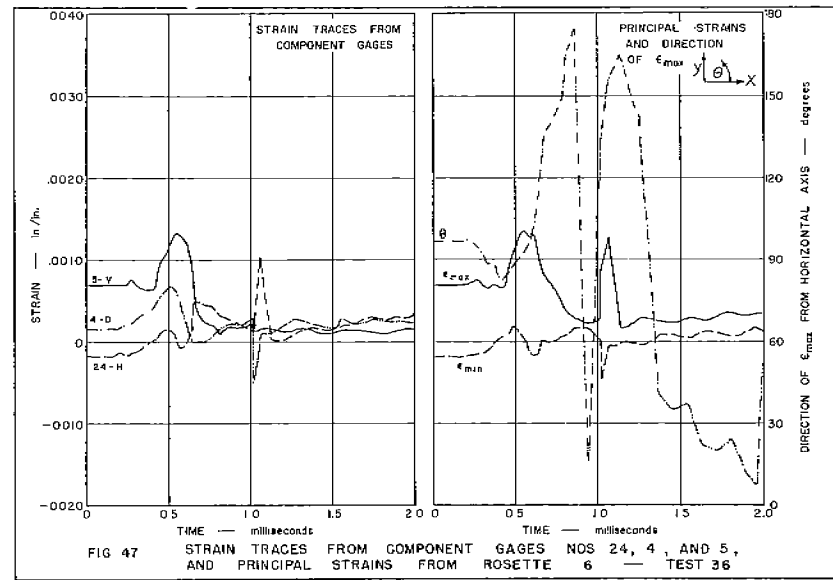
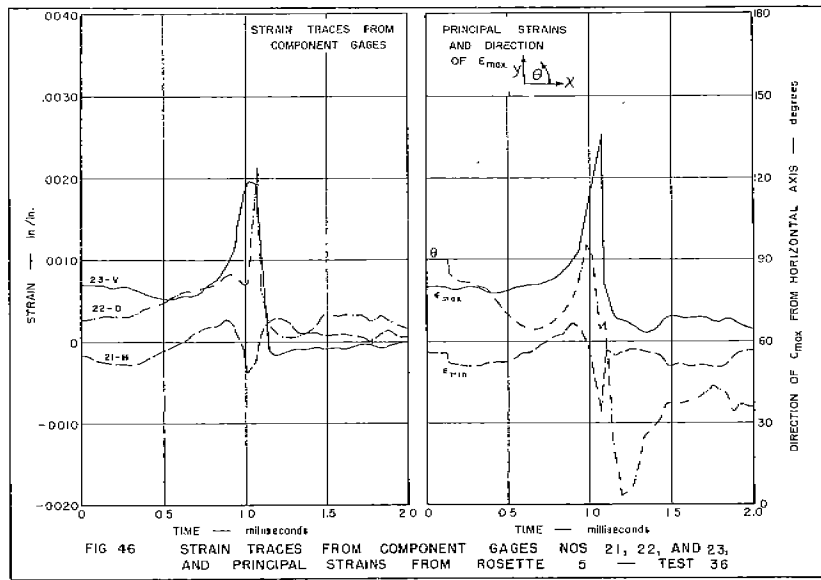


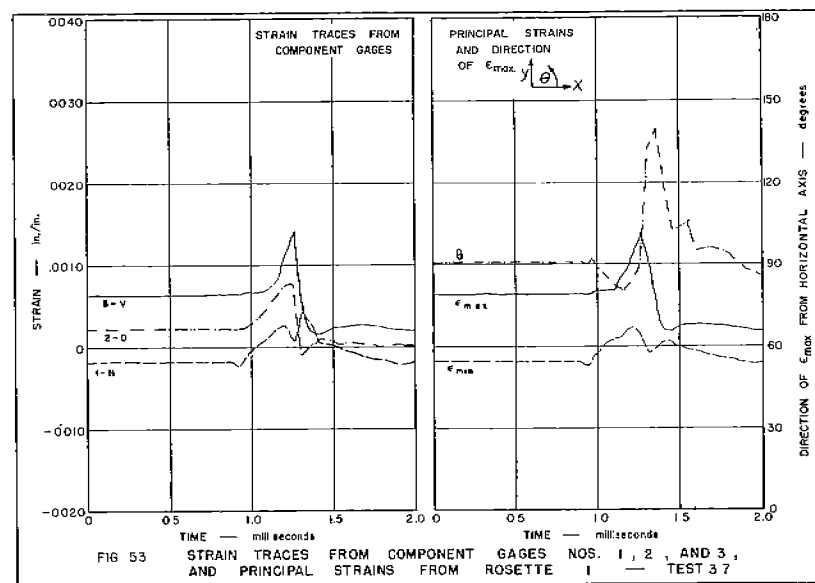
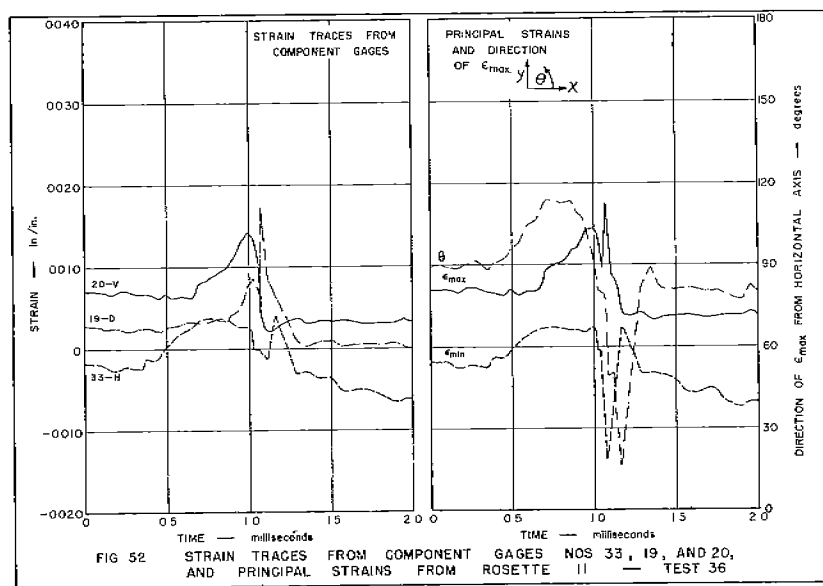
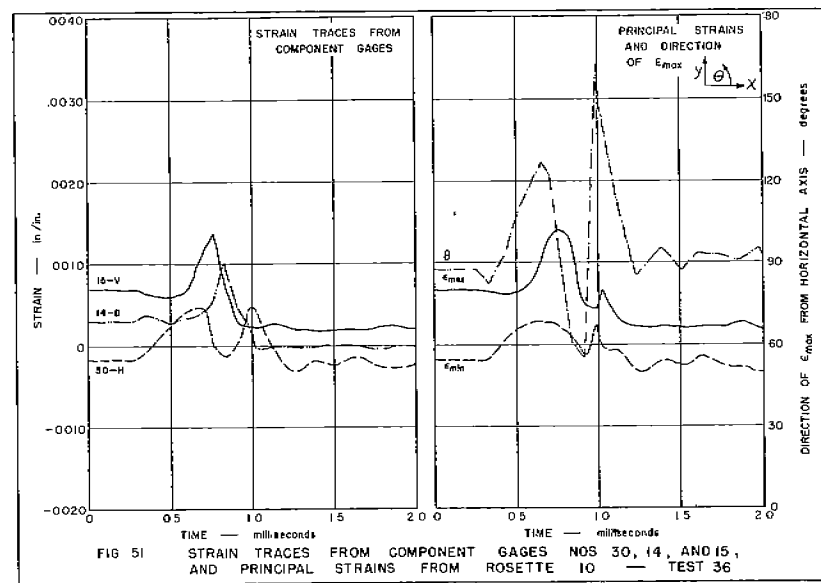
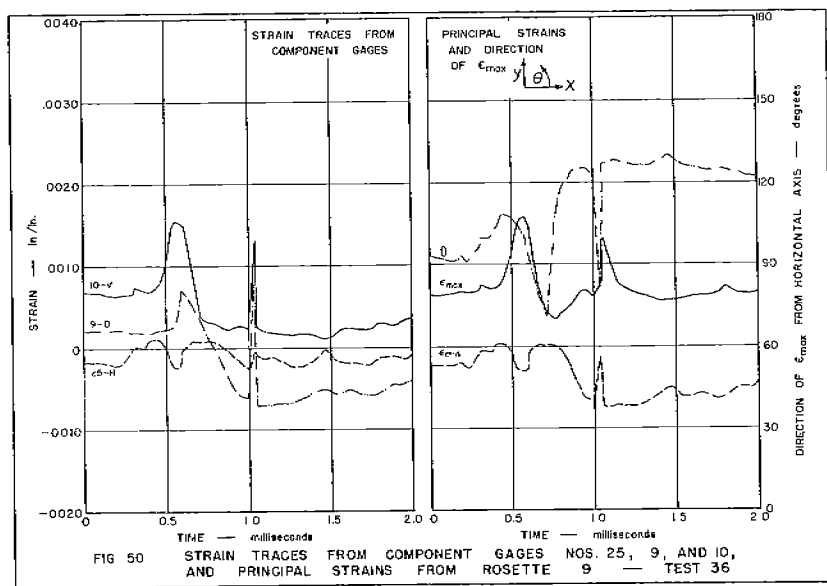


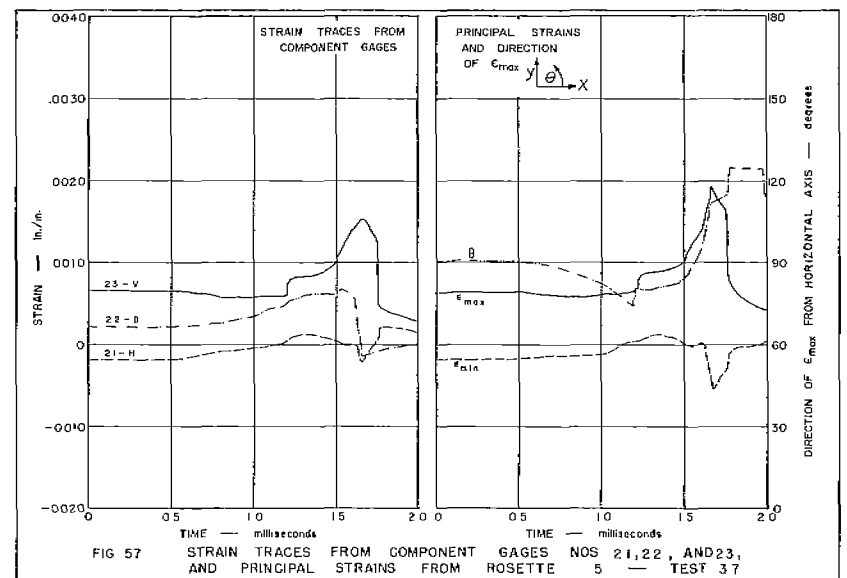
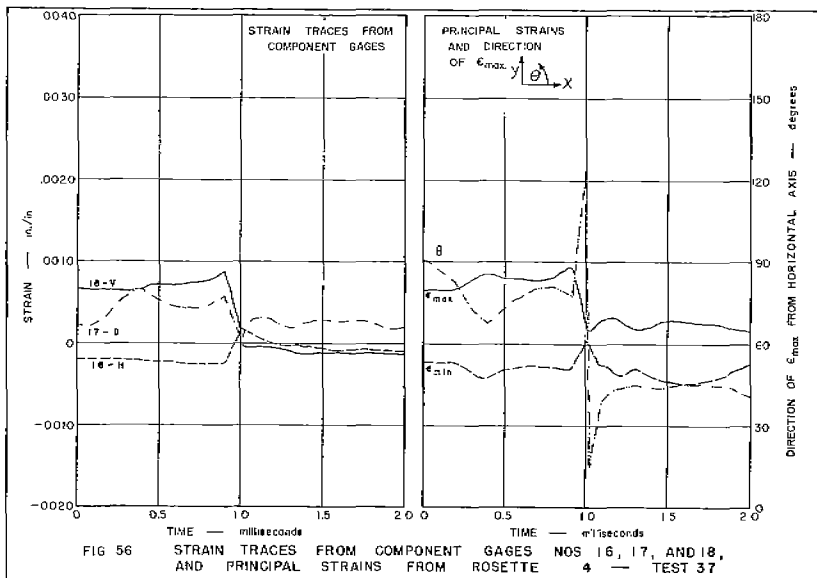
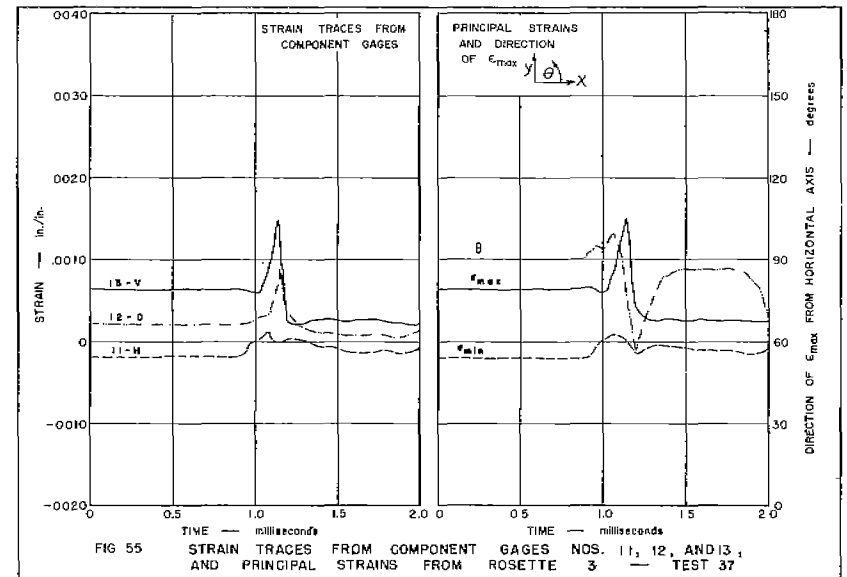
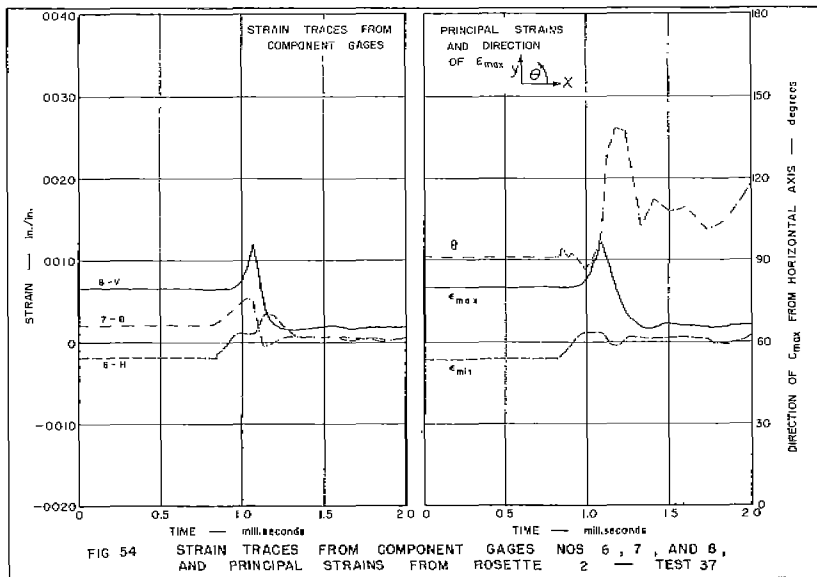


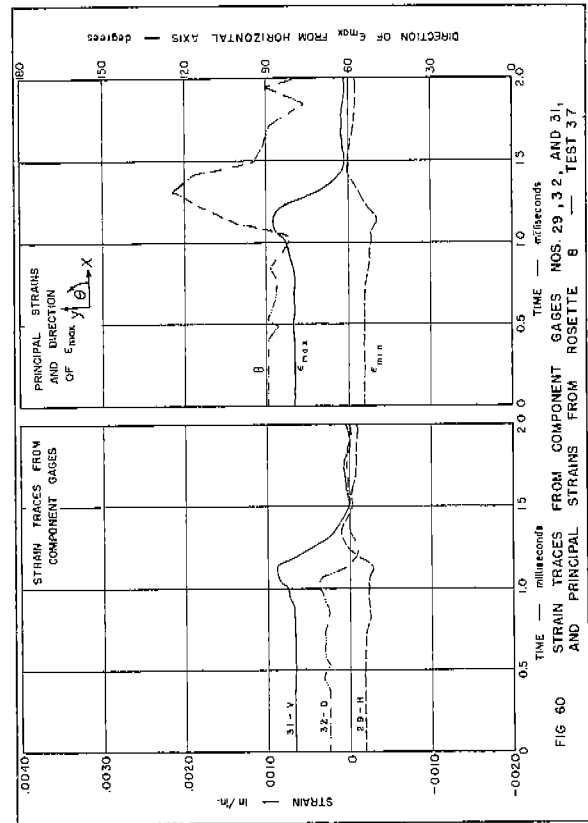
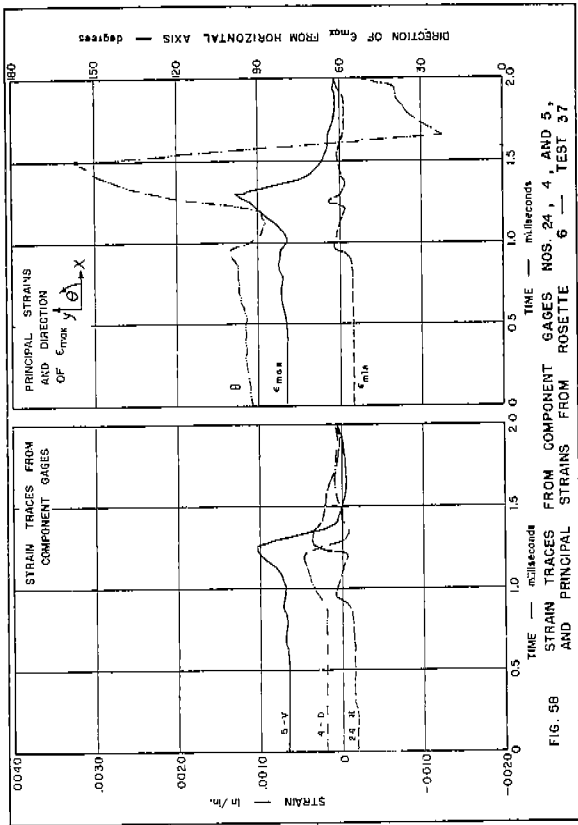
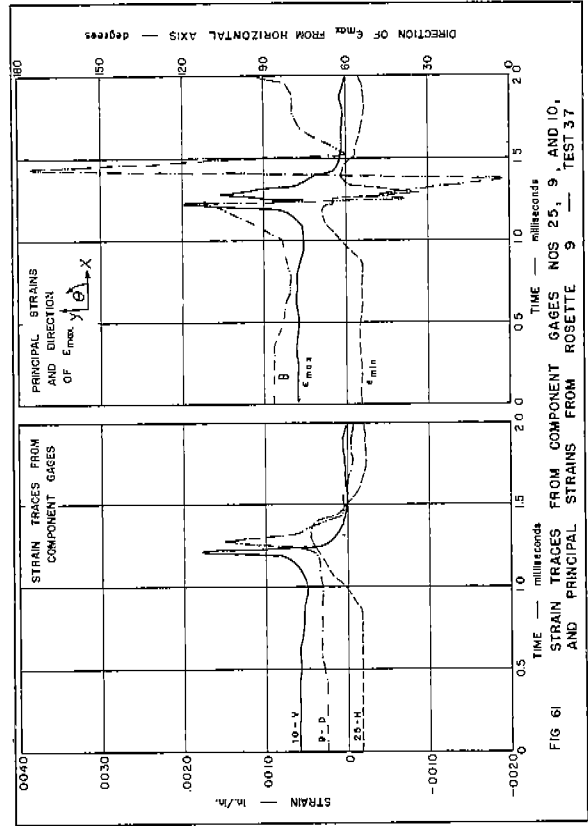
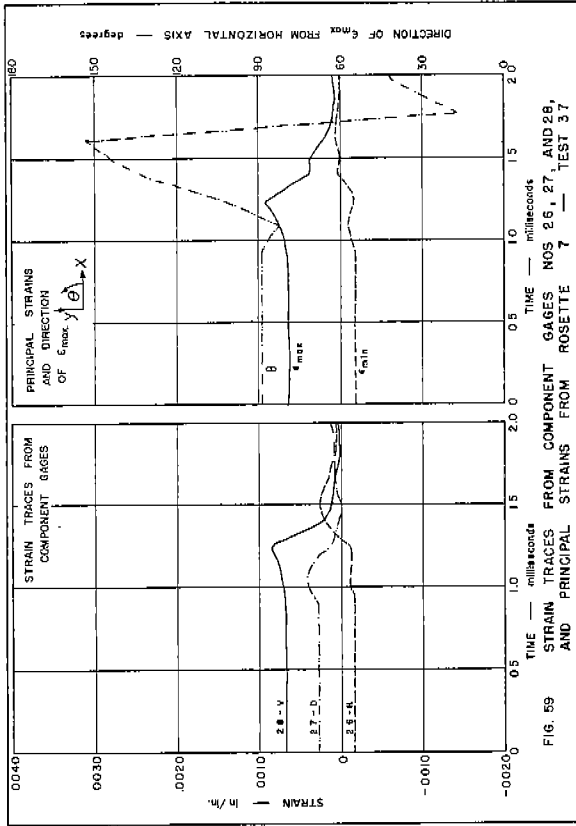


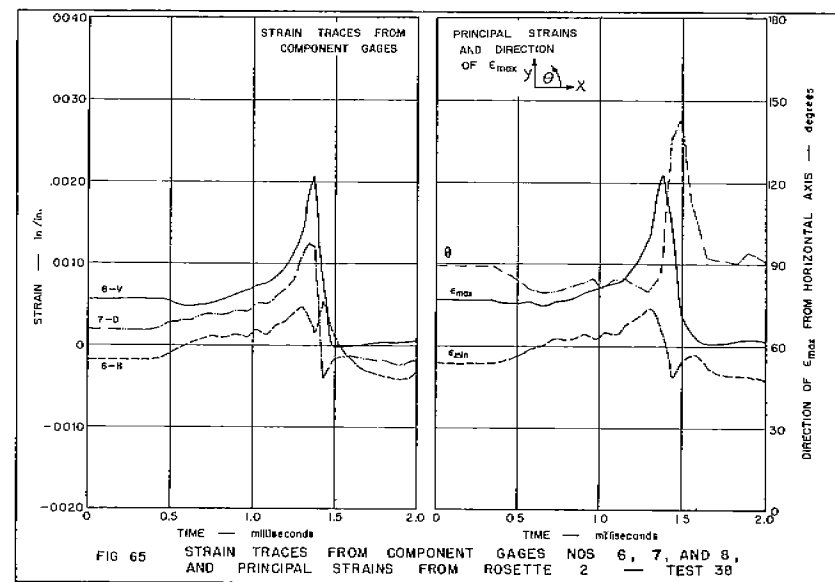
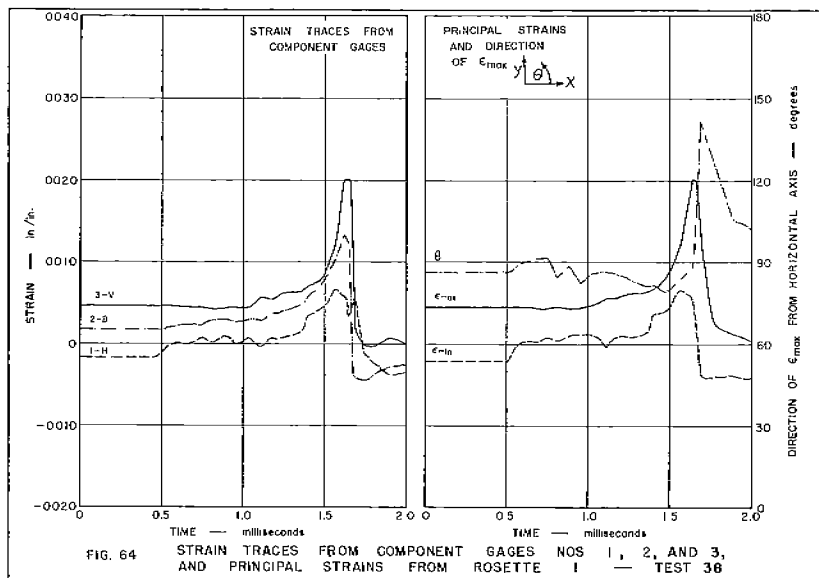
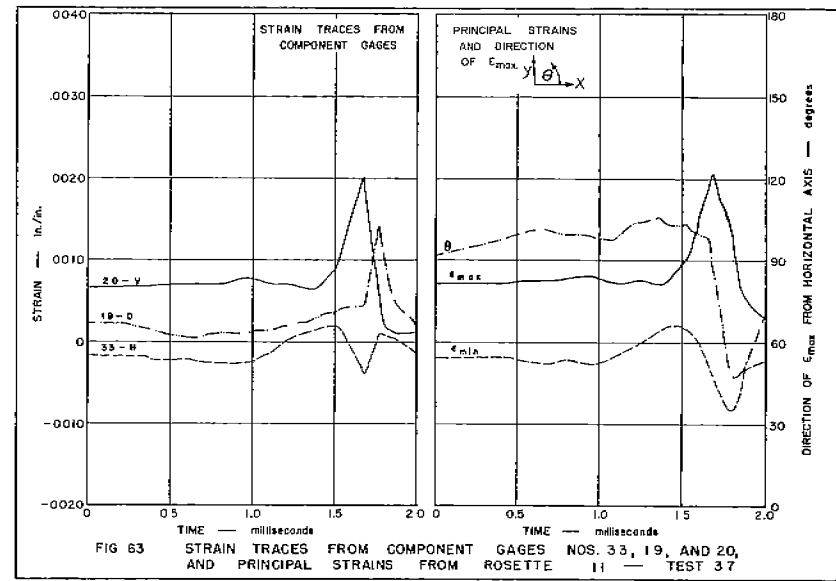
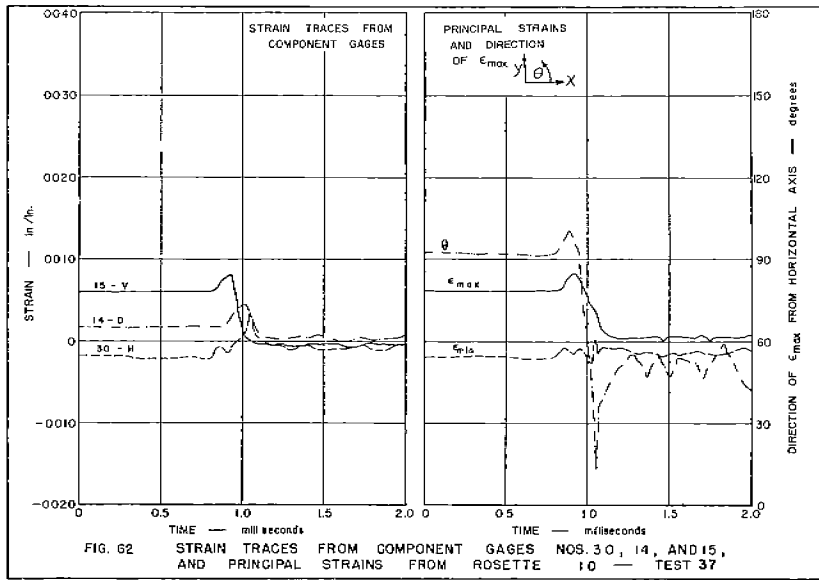


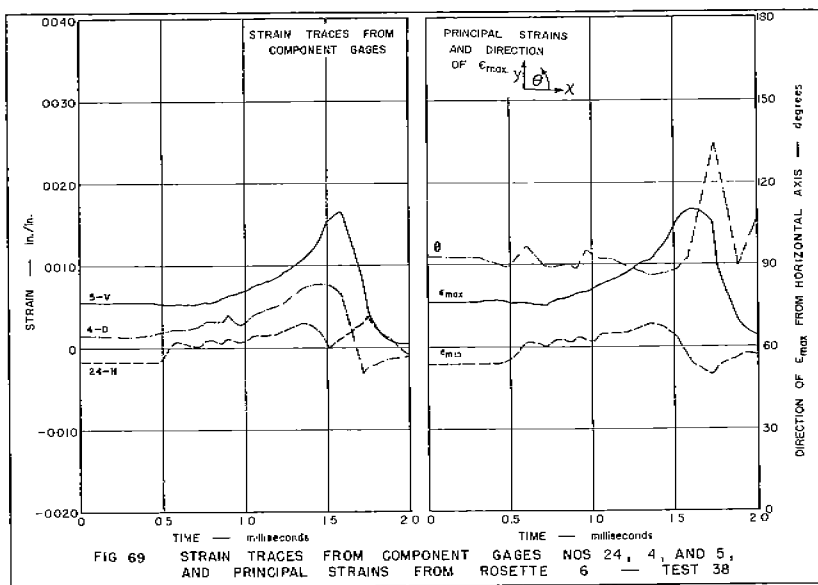
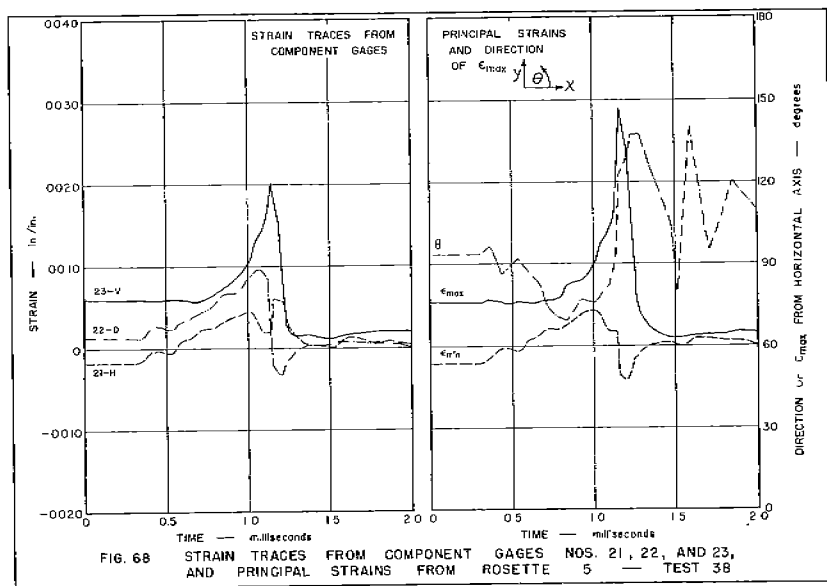
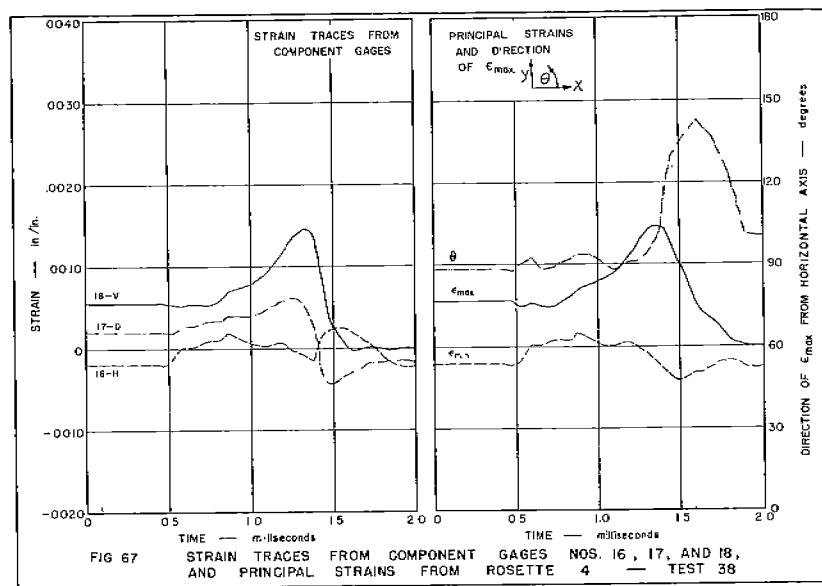
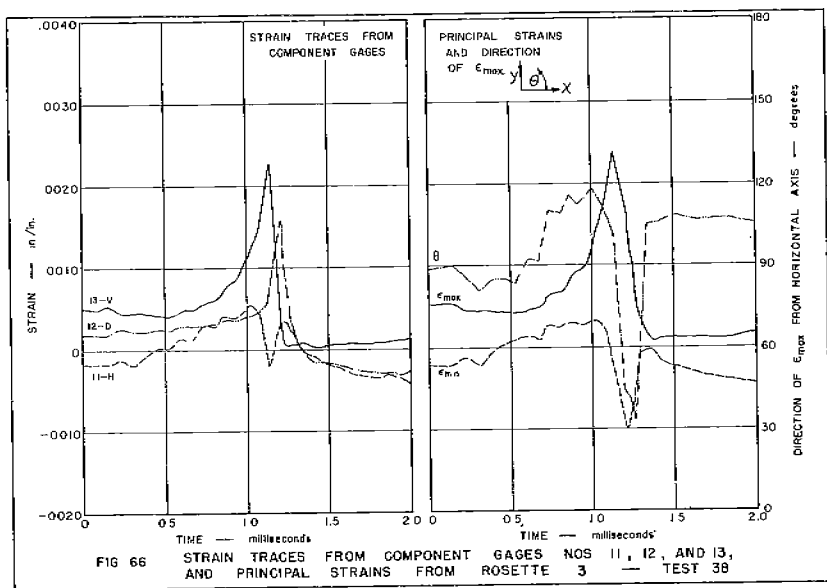


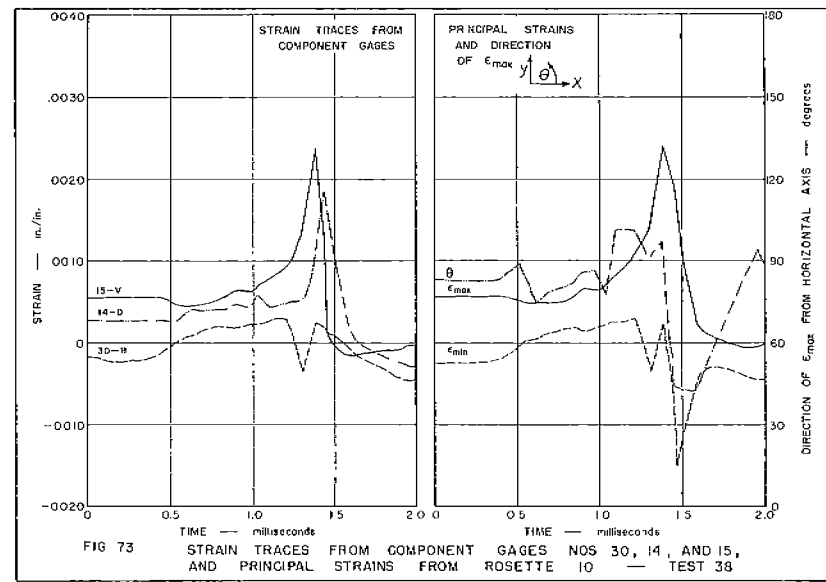
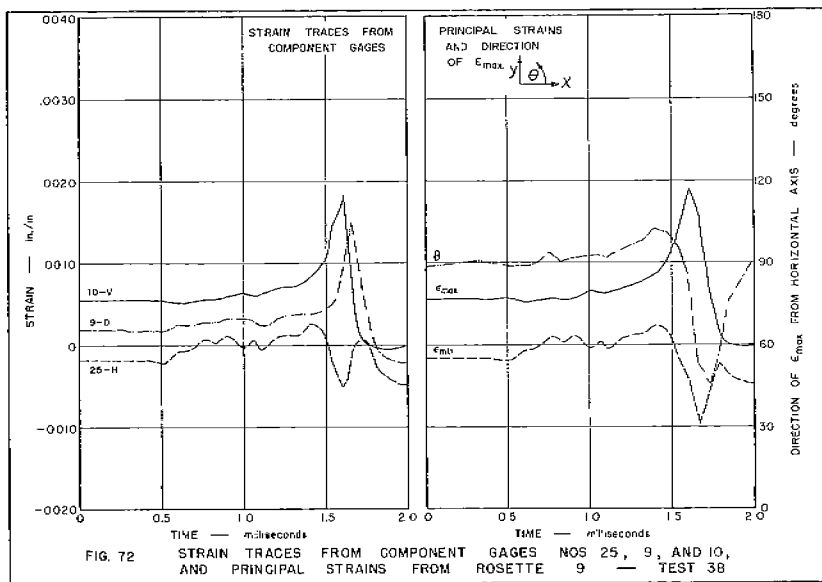
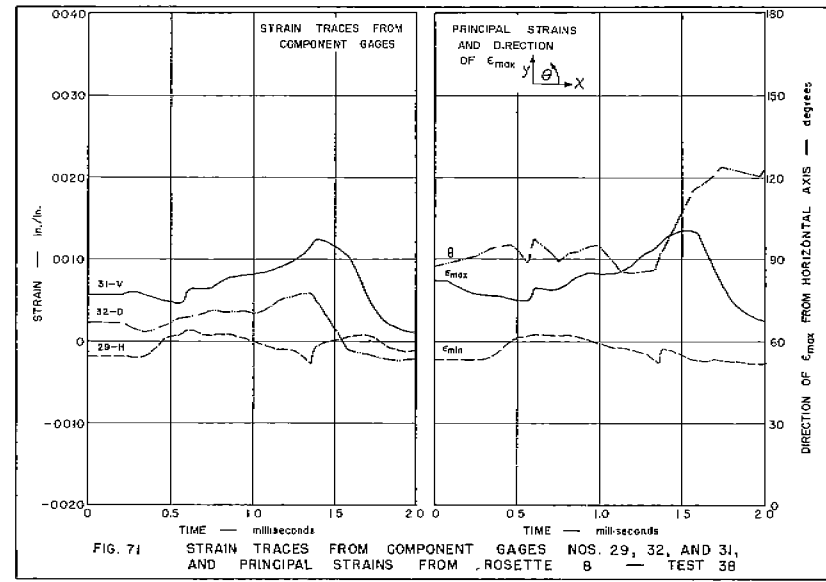
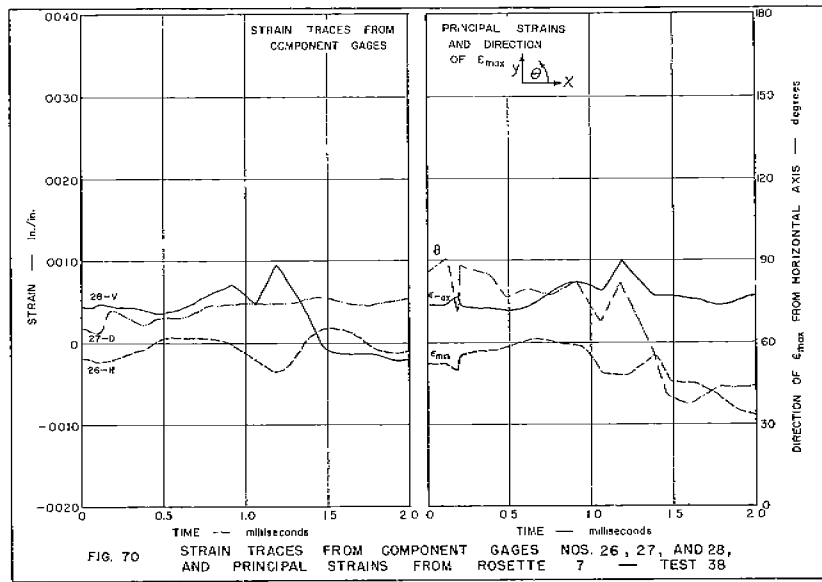












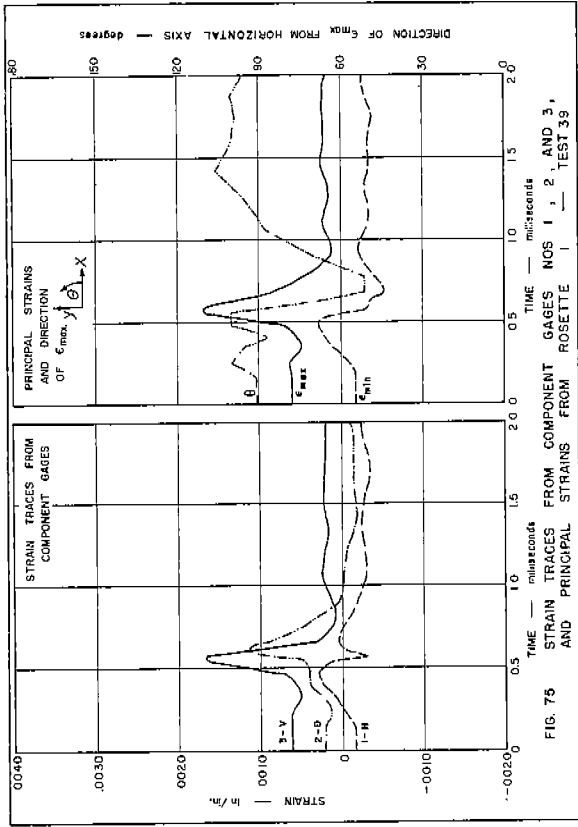


FIG. 75 STRAIN TRACES FROM COMPONENT GAGES NOS. 1, 2, AND 3, AND PRINCIPAL STRAINS FROM ROSETTE 1 - TEST 39.

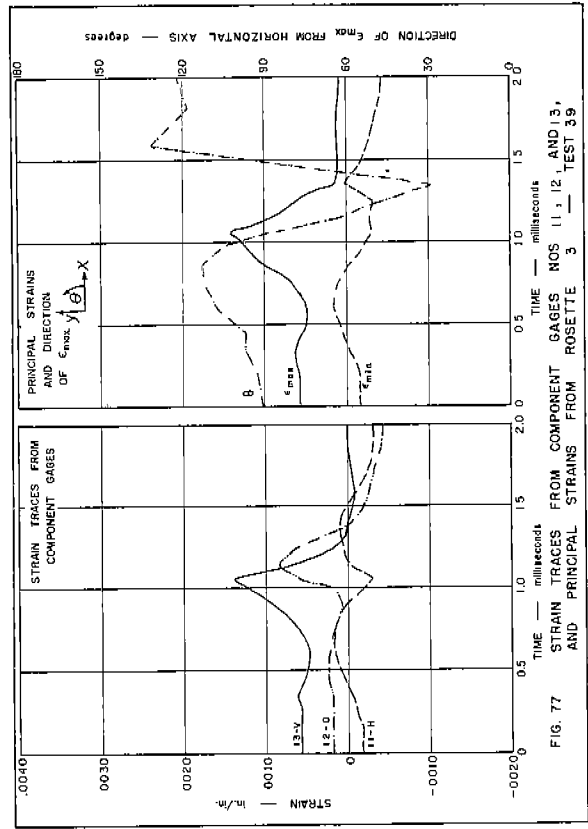


FIG. 77 STRAIN TRACES FROM COMPONENT GAGES NOS. 11, 12, AND 13, AND PRINCIPAL STRAINS FROM ROSETTE 3 - TEST 39.

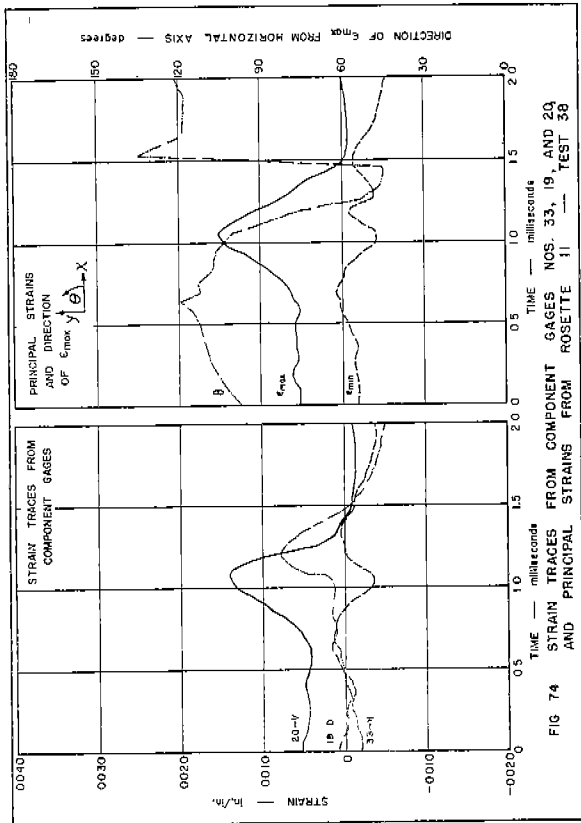


FIG. 74 STRAIN TRACES FROM COMPONENT GAGES NOS. 33, 19, AND 20, AND PRINCIPAL STRAINS FROM ROSETTE 1 - TEST 38.

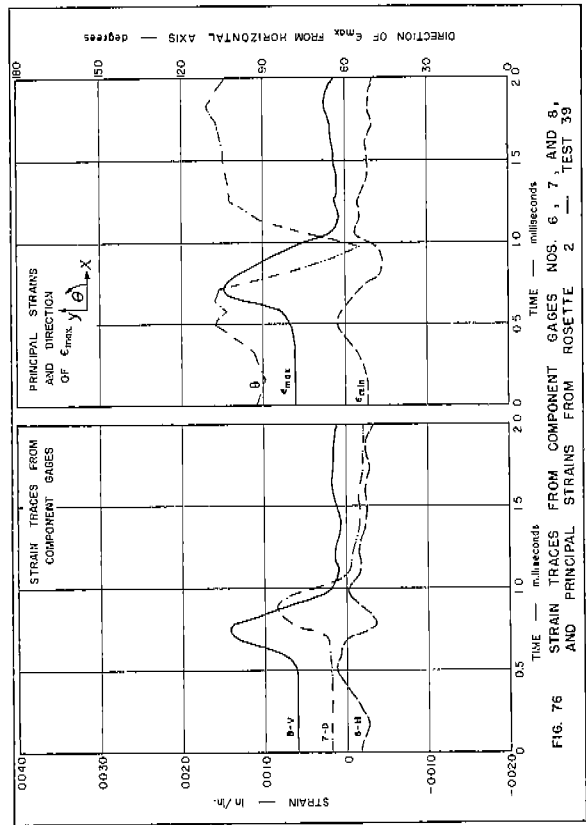
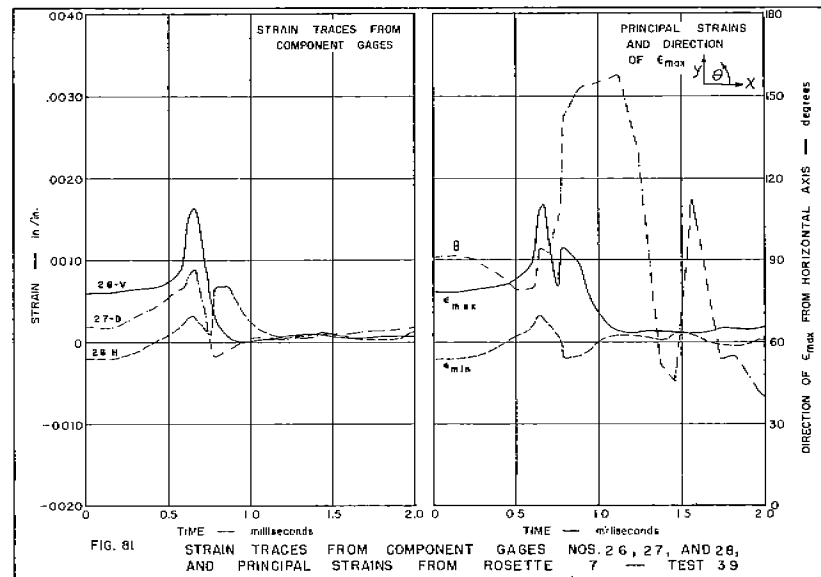
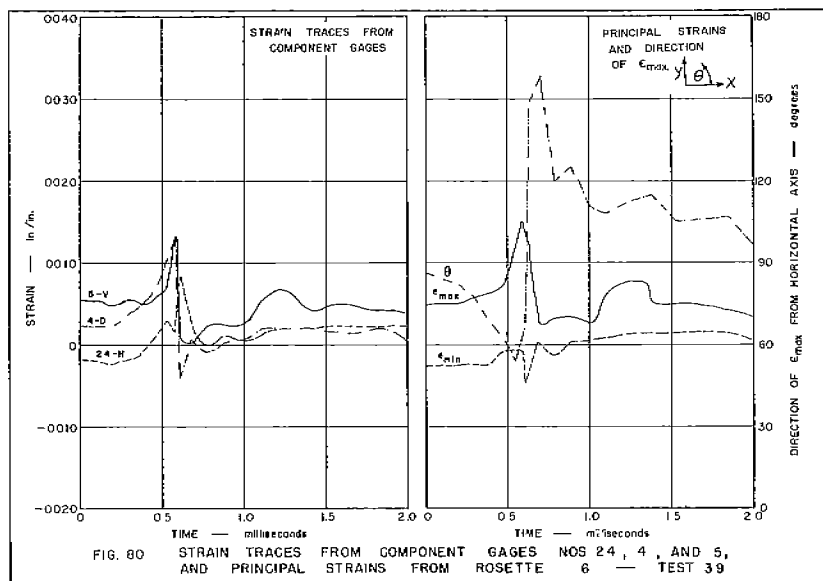
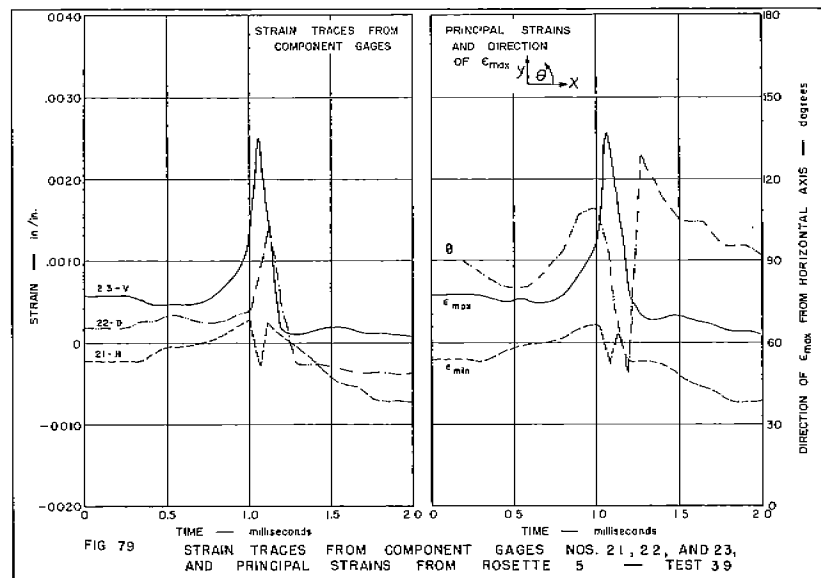
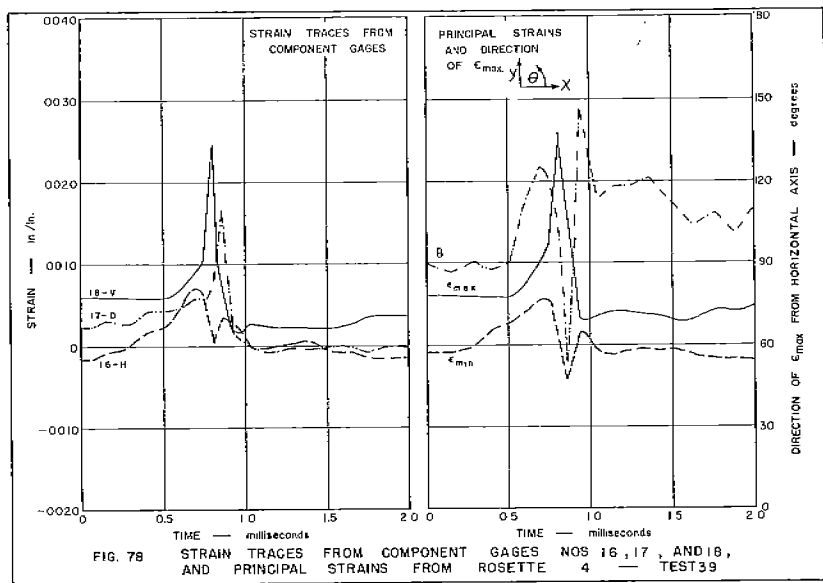
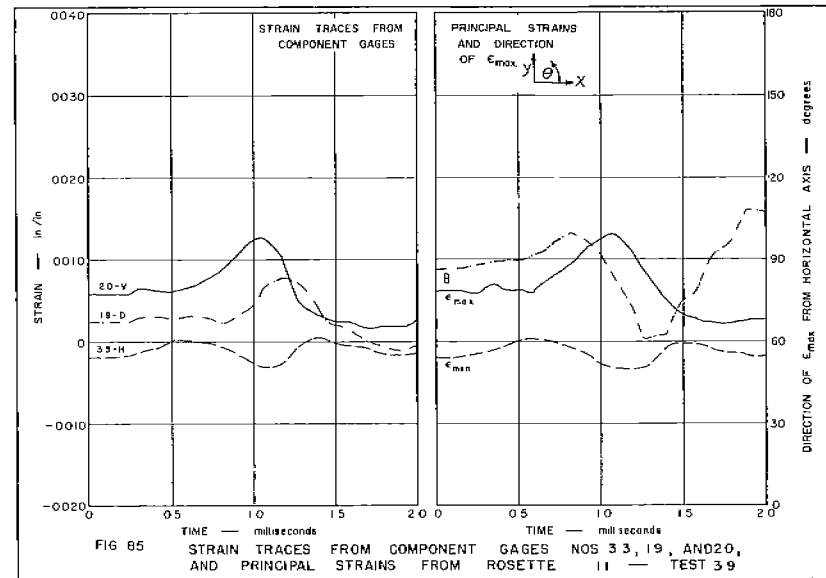
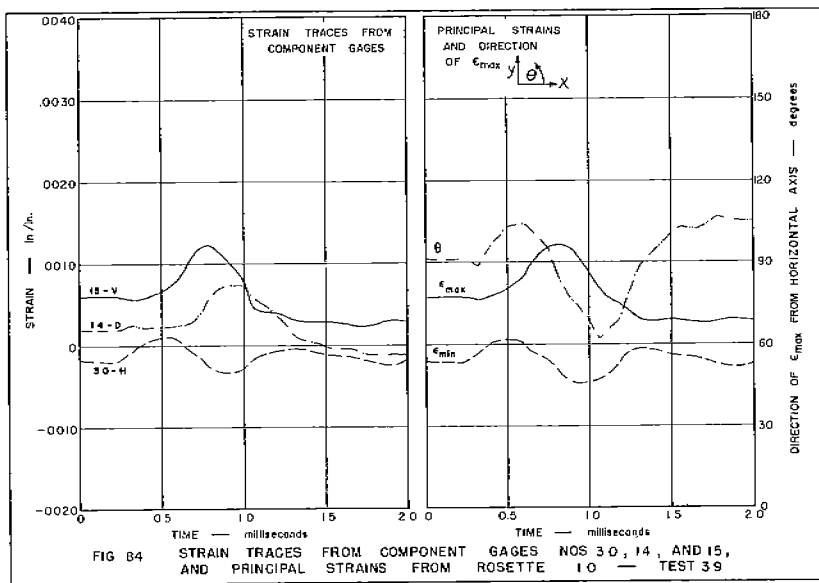
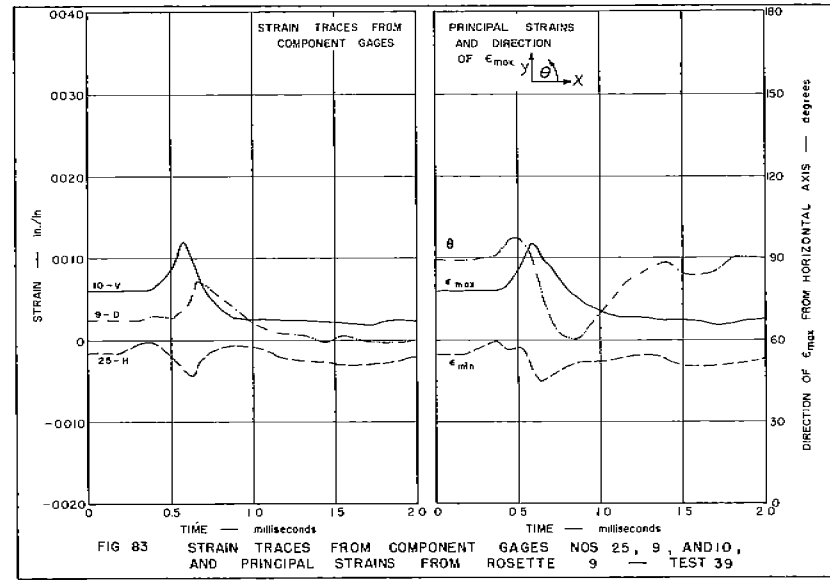
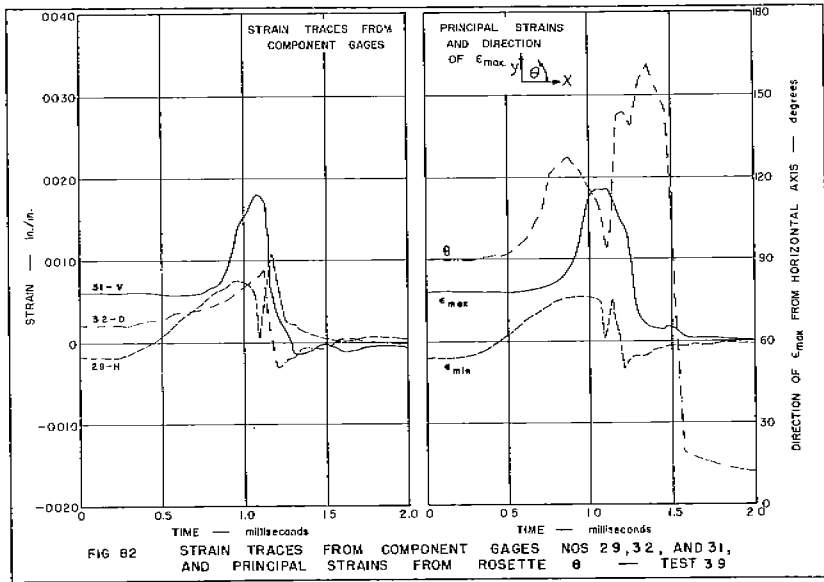


FIG. 76 STRAIN TRACES FROM COMPONENT GAGES NOS. 6, 7, AND 8, AND PRINCIPAL STRAINS FROM ROSETTE 2 - TEST 38.





be noted that these speeds ranged from 1850 to 4750 fps, and are thus in the same range as those reported for earlier tests.<sup>1, 2</sup>

### Computed Principal Strains

To compute the principal strains from the rectangular strain rosette equations, it was necessary to determine strain values from the three component gage traces at selected times; the times were selected arbitrarily at points corresponding to changes in strain in the component gage traces.

The rectangular strain rosette equations used in computing the principal strains and the direction of the maximum principal strain are as follows:

$$\epsilon_{\max} = \frac{1}{2} \left[ \epsilon_v + \epsilon_h + \sqrt{2(\epsilon_h - \epsilon_d)^2 + 2(\epsilon_d - \epsilon_v)^2} \right]$$

$$\epsilon_{\min} = \frac{1}{2} \left[ \epsilon_v + \epsilon_h - \sqrt{2(\epsilon_h - \epsilon_d)^2 + 2(\epsilon_d - \epsilon_v)^2} \right]$$

$$\theta = \frac{1}{2} \tan^{-1} \frac{2\epsilon_d - \epsilon_h - \epsilon_v}{\epsilon_h - \epsilon_v}$$

where:

$\epsilon_{\max}$  = maximum principal strain

$\epsilon_{\min}$  = minimum principal strain

$\theta$  = angle between  $\epsilon_{\max}$  and the positive X-axis

$\epsilon_v$  = vertical (Y) component gage strain

$\epsilon_d$  = diagonal component gage strain

$\epsilon_h$  = horizontal (X) component gage strain

The resulting curves of the principal strains ( $\epsilon_{\max}$  and  $\epsilon_{\min}$ ) and the direction of  $\epsilon_{\max}$  with respect to the positive X-axis ( $\theta$ ) for Tests 33--39 are presented in Figs. 21--85.

There are several important details that should be noted with respect to the time--alignment of the component strain traces for any particular rosette gage. In the case of strain records obtained with gage layout A (Fig. 12), the vertical gage peaked before or at the same time as the horizontal and diagonal gages for about 80 per cent of the rosettes. A detailed study of the component gage traces and the principal strain computations indicated that changes in the vertical and horizontal strain values have the greatest effect on the principal strain magnitudes; thus in Tests 36--39 it was decided to center the vertical and horizontal gages above one another in the manner shown in layout B (Fig. 12). For records obtained with gage layout B, the vertical and horizontal gages peaked before or at the same time as the diagonal gages in the case of about 85 per cent of the rosettes. Typical component gage traces from both layouts are shown in Fig. 86; the offset in peaking times may be noted clearly.

It was believed initially that a refinement in the results could be obtained by shifting the recorded component gage traces to a position where the maximum strain values would occur at the same time. However, later studies showed that there was only a small change in the principal strains as a result of this shifting of the component gage traces. This is illustrated in Fig. 87, which shows the principal strain traces for a typical rosette computed 1) for the component strain traces as-recorded and 2) for the component strain traces shifted to make the peaks occur at the same time. It will be noted that shifting the trace does not change the shape or magnitude of the maximum principal strain trace markedly. For most rosettes it would be necessary to shift the trace by less than 0.1 milliseconds to make the maximum strain values occur at the same time. This time difference is of the same order of magnitude as the inherent time error that accompanies matching of the trace times during a reduction of the original 35-mm strip-film record. It should be noted that many other factors also tend to affect the strain traces, such as the discontinuous nature of the fracture, the deviation of the crack path from the notch line, and inherent variations in instrumentation. All of these factors and studies tend to justify the decision not

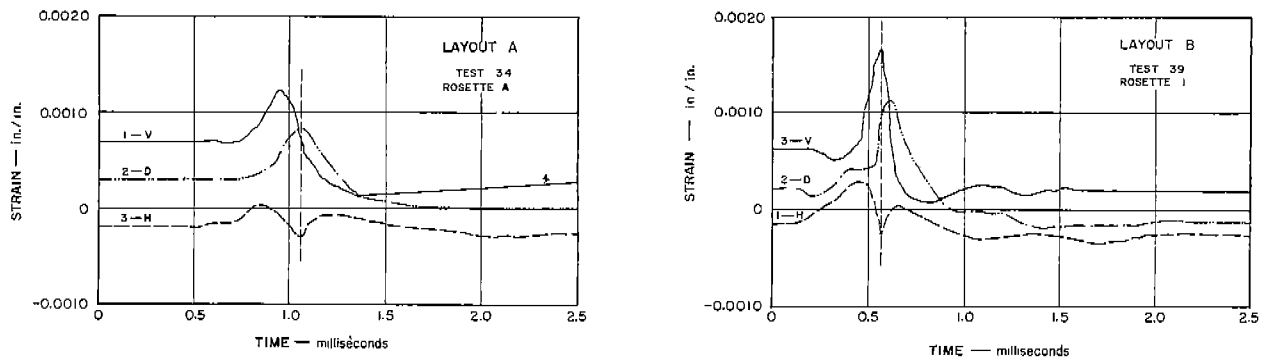


Fig. 86. Typical Strain Traces from Component Gage Layouts A and B.

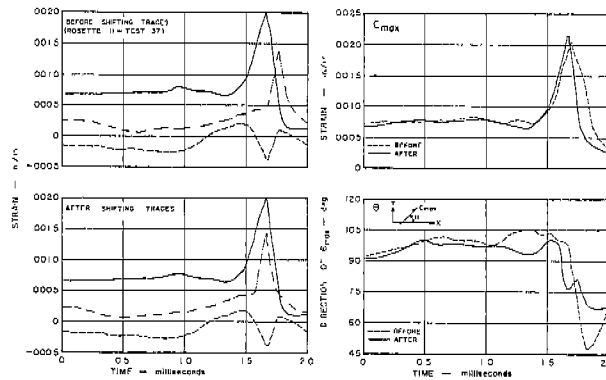


Fig. 87. Effect of Shifting Component Gage Traces on Principal Strains.

to shift the traces; therefore, all of the principal strains have been computed from the as-recorded component gage traces.

### Discussion of Strain Traces

In general, the maximum principal strain trace for each rosette is of essentially the same shape as the vertical component gage trace. The magnitudes of the peak strain for the vertical gage trace and for the principal strain trace are also nearly equal for any rosette. This is shown in Fig. 88, in which a comparison is given of the maximum principal and vertical peak strain magnitudes; it will be noted that there is nearly a one-to-one correspondence in strain values, irrespective of the distance from the fracture path. Almost all peak strain values fall into a range between 0.0008 in./in. and 0.0030 in./in.

The minimum principal strain traces are characterized by a shape that

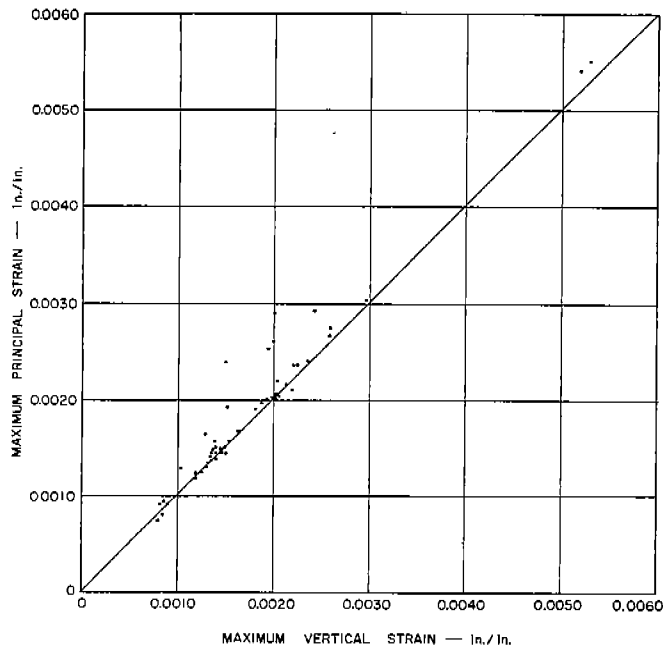
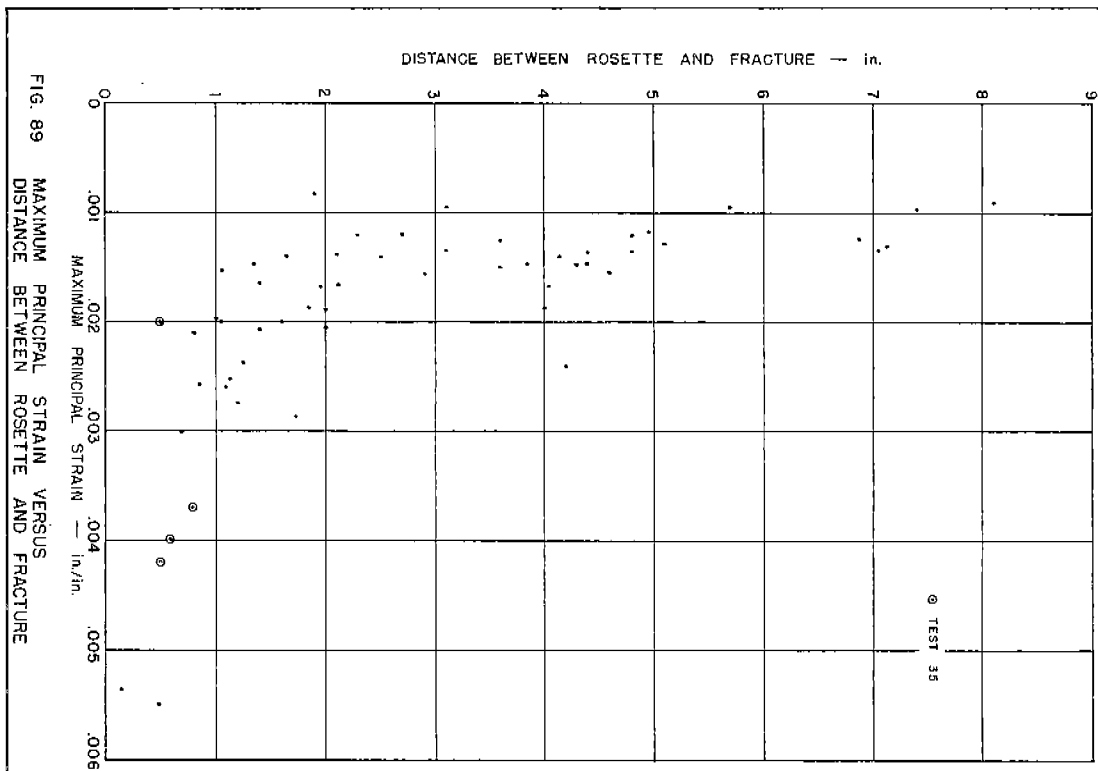
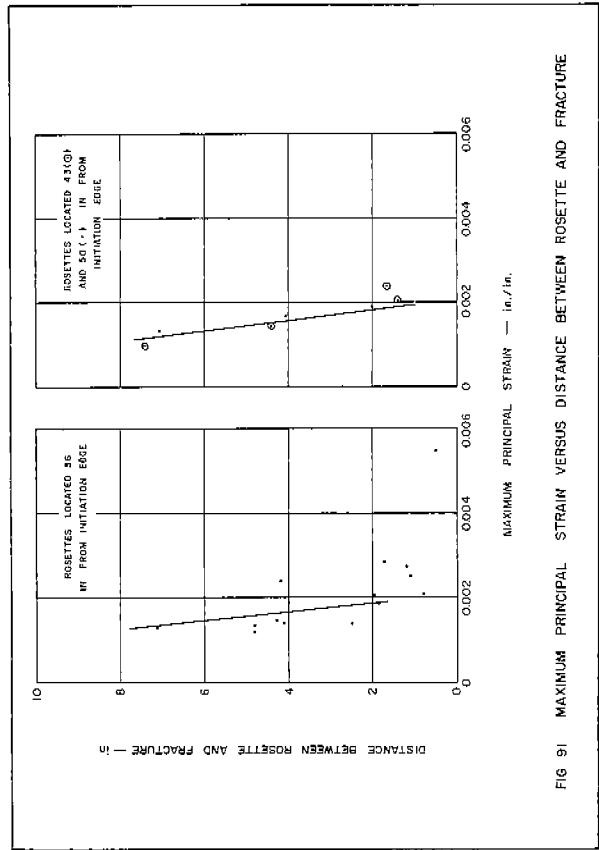
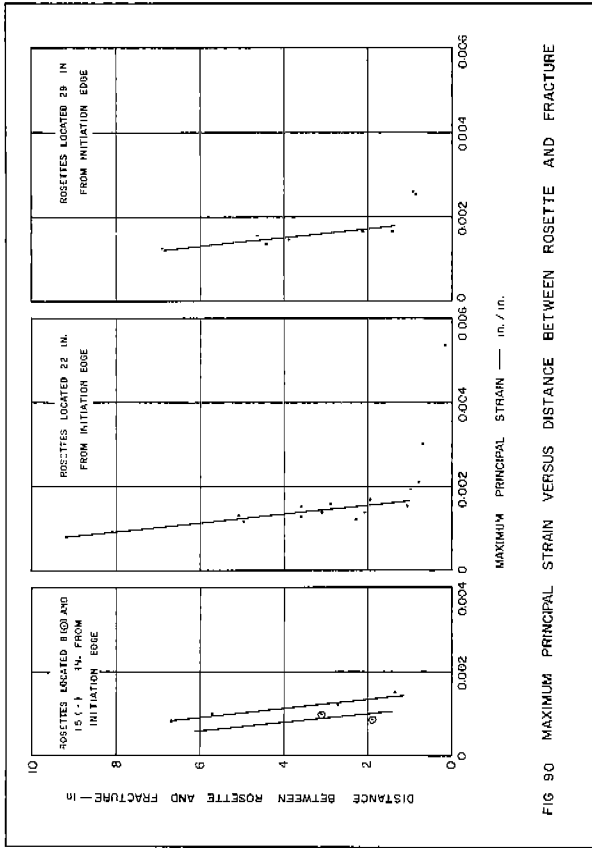


Fig. 88. Comparison of Maximum Principal and Vertical Strain Magnitudes.

exhibits a slight peak in tension, followed by a fairly sharp compressive pulse occurring as the fracture propagates past the rosette; this compressive pulse corresponds to the tension peak of the maximum principal strain. The traces then return to the final strain level of the rosette.

In the case of rosettes located close to the fracture path, the magnitude of the strain peak is relatively large. As the distance between a rosette and fracture increases, the peak principal strain magnitude decreases rapidly. This may be seen clearly in Fig. 20, in which typical principal strain traces for rosettes located at various distances from the fracture are presented. When the distance between the rosette and the fracture exceeds about 2 in., the rate of decrease of the peak strain magnitudes is somewhat less. Figure 89 is a plot of all the peak maximum principal strains versus distance between the rosette and the fracture. This figure gives the impression that there is a wide scatter; however, if the curves are plotted for rosettes located at varying distances from the initiation edge (8 in., 15 in., etc.), the individual curves move to the right with increasing distance, as may be seen in Figs. 90 and 91. Thus, there is an increase in the peak maximum principal strain with increasing distance from the initiation edge; this increase is noticeable to a distance from 22 to 29 in. from the initiation edge, after which there is no apparent change. Thus, the strain field associated with the propagating fracture appears to reach a "steady state" condition at about 22 to 29 in. from the initiation edge.

The variation of the maximum strain rate with vertical distance of the



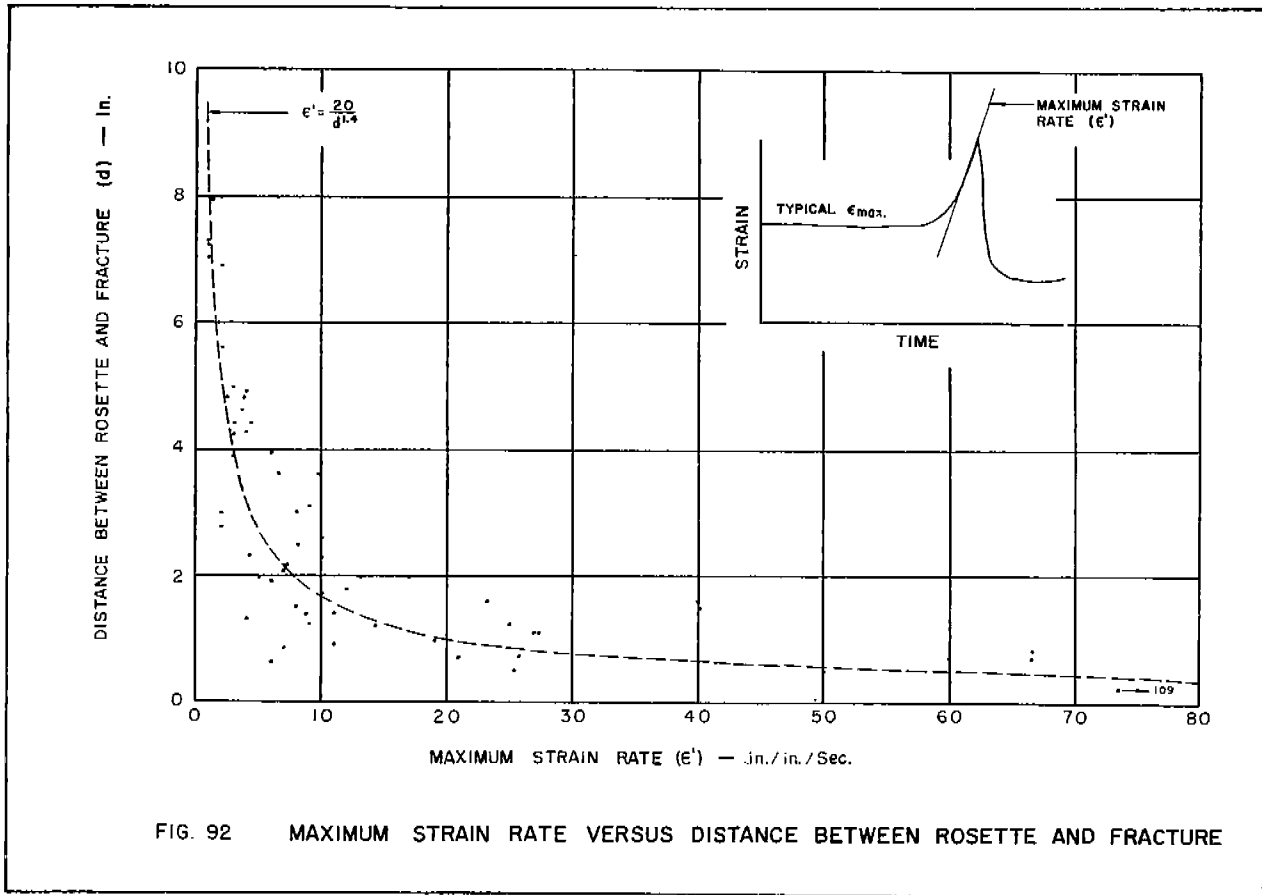


FIG. 92 MAXIMUM STRAIN RATE VERSUS DISTANCE BETWEEN ROSETTE AND FRACTURE

rosette from the fracture surface was also studied. The strain rate (in./in./sec) is difficult to determine accurately because of the very nature of the strain traces (Fig. 4); the computed strain rates presented in Fig. 92 should be considered as only a qualitative picture. However, it is apparent that a general trend of strain rate versus distance between rosette and fracture does exist, as might be expected. The sketch in the upper right corner of Fig. 91 illustrates the procedure by which the strain rates were determined. A "best fit" curve of all points is also shown on the plot. Strain rates ranging from 1 to 109 in./in./sec were computed; however the majority of the values fall in the range of 1 to 30 in./in./sec for gages located at 1/2 in. to 3 in. from the fracture.

Figures 38--41 present strain-time curves of the component gages, as well as the computed principal strains of the four rosettes for which records

were secured, as taken from Test 35. This test was conducted at a higher stress (28,000 psi) and a lower temperature (-15 F) to determine the effect of a higher stress level on the strain pattern. The traces are essentially the same shape as those found in the plates tested at lower stresses, although the peak maximum strains are slightly higher. However, the rosettes were located quite close to the fracture path and in view of the earlier discussion it is to be expected that the strain magnitudes might be fairly high. The maximum principal peak strain magnitudes of rosettes obtained in Test 35 are plotted in Fig. 89. These exhibit the same trend as peak strain magnitudes from the other tests. Thus, on the basis of one test only, it appears that there was no marked change in the strain behavior for a propagating crack at this somewhat higher stress level.

#### Maximum Principal and Vertical Strain Contours

In order to depict the strain distribution in a plate during the time a fracture is propagating, it was decided to plot contours of certain strain components for various crack lengths. The available data consist of strain-time traces for horizontal, diagonal, and vertical gages obtained from this series of tests, as well as from earlier tests, and computed principal strain values for the rectangular rosettes formed with the component gages of this test series. The maximum principal strains are of particular interest since they provide both the magnitude and direction of the maximum tensile strain.

Strain contours were obtained by superimposing the results from a number of tests. The data were superimposed only from plates tested under similar conditions of stress, temperature, and impact; the only major variable among the individual tests was the location of the fracture path with respect to the notch line. In general, the fractures sloped upward from the point of initiation and then leveled off as they traveled across the plate. The excursions from the notch line were of the order of 2 to 8 in.; precise locations of the fracture paths are tabulated in Figs. 5--11. However, since these distances are small in relation to the plate width, the actual crack length was never more than a few per cent greater than the net plate width. The horizontal projection of the fracture was used as the common fracture path on the strain contour plots.

The procedure used in plotting the strain contours may be summarized as follows. It was first necessary to establish from the original strain-time curves the time relative to various selected crack lengths. Also it was necessary to establish the position of the gage with respect to the fracture path. Then, at any particular time corresponding to a given crack length, the strain values were obtained from the test data, and these strain data were used in plotting the contours. The contour lines were drawn in regions where data were available by joining points of equal strain. No contours were drawn in regions where there were no data, although it is obvious that strain contours do exist in these regions.

Before strain values could be determined for any particular crack location, it was necessary to establish the respective times that corresponded to the desired crack positions in every test. These times were determined by a knowledge of the breaking times of the crack detectors and the peaking times of the vertical strain gages located closest to the fracture surface; they are tabulated in Table 5 for various crack lengths. It was assumed that the peak strain of a rosette occurs when the surface fracture is directly above or below the rosette, although the exact position of the tip of the fracture cannot be determined at any precise time. At points where there was disagreement between detector breaking times and gage peaking times, the peaking times of the strain gages were selected as the more reliable indication of the surface fracture location because of the more sensitive response of the strain gage. As a general rule, the detector breaking times were used only as a guide in the selection of times corresponding to selected crack lengths. At fracture positions where there were no strain gages or detectors, the corresponding time was approximated by a linear interpolation between any two known points.

Since the horizontal projection on the notch line of the actual fracture path was used as the common fracture path in all tests for purposes of superposition, it was important to locate accurately each gage or rosette with respect to this common fracture. Three different methods of determining the gage and rosette locations on the plate layout using the common fracture path were investigated. The first method consisted of measuring the vertical distance between the rosette and the actual fracture for particular tests and locating the rosettes on the plate layout ac-

TABLE 5. TIMES CORRESPONDING TO VARIOUS CRACK LENGTHS

All times are in milliseconds and refer to the time base of the strain-time curves presented in Figs. 21--85

Crack Length (in.)	Test No.				
	33	34	37	38	39
8	0.22	0.03	0.92	0.35	0.10
15	0.94	0.50	1.11	0.52	0.31
18.5	1.05	0.72	1.18	0.61	0.45
22	1.16	0.95	1.24	0.70	0.59
25.5	1.24	1.10	1.35	0.81	0.67
29	1.32	1.25	1.45	0.92	0.75
32.5	1.57	1.37	1.56	1.03	0.91
36	1.62	1.50	1.66	1.14	1.07
39.5	1.74	1.63	1.82	1.26	1.18
43	1.86	1.77	1.97	1.37	1.30

Note: These times, corresponding to various crack lengths, were used in determining both the maximum principal strain contours (Figs. 93--102) and the vertical strain contours (Figs. 103--112).

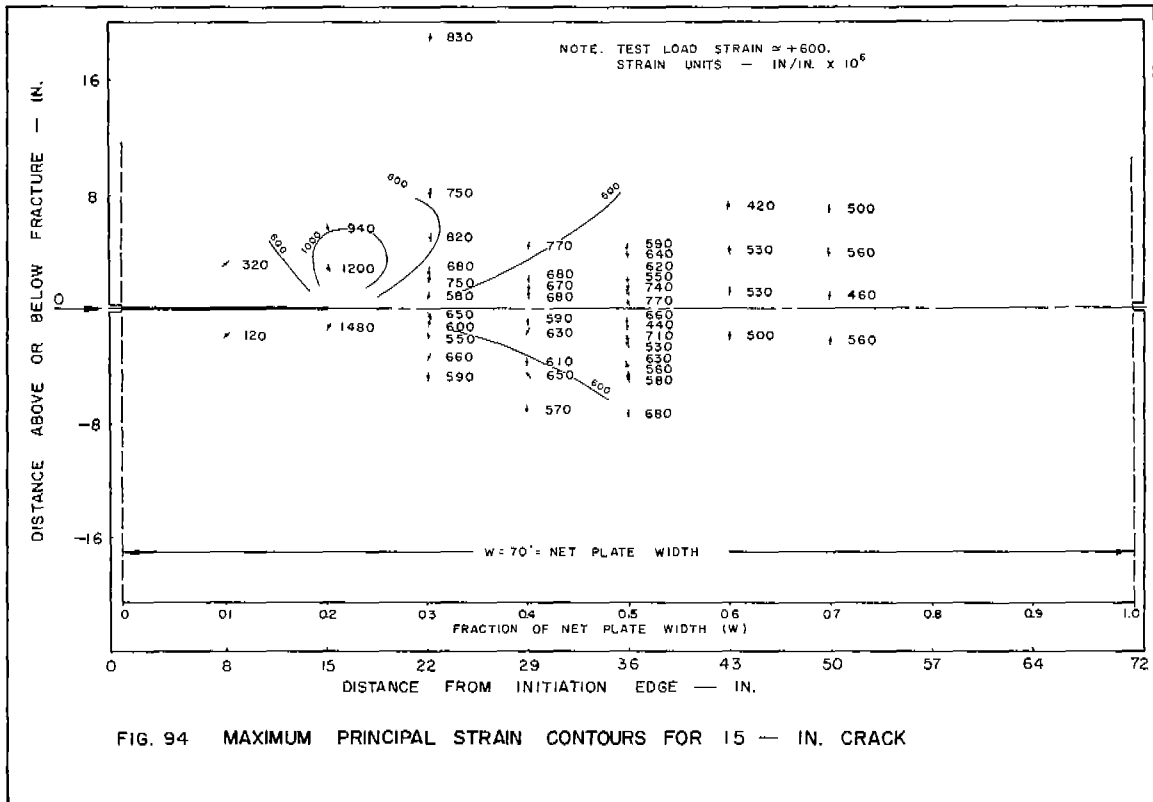
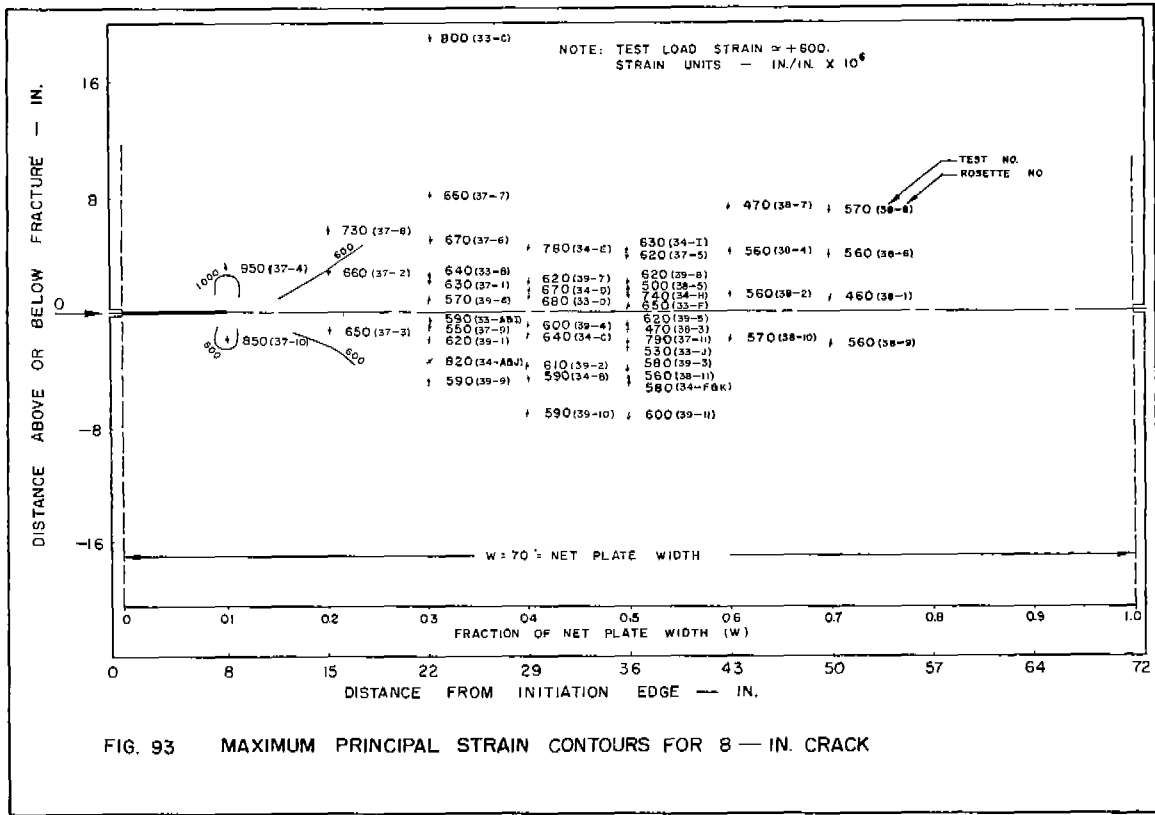
cordingly; the second method consisted of measuring the perpendicular distance of each rosette or gage from a horizontal line projected across the plate from the tip of the surface fracture for the particular crack length under investigation; and the third method consisted of 1) measuring either the perpendicular distance between a rosette and the fracture or the extension of the fracture in the direction in which it was traveling at that particular instant, and 2) locating the rosette above or below the common fracture path by this amount. A study of the three methods of locating the gages and rosettes on the strain contour plots indicated that regardless of the method used, the final strain contours were essentially unchanged. Since, in general, the fracture followed a horizontal path as it passed through the region where rosettes were placed, it was obvious that in the majority of cases there would be no significant difference in

the final rosette locations as determined by any of the three methods investigated. In tests where the fracture was not horizontal, there would be a change in rosette locations; however, the changes in strain at some distance in front of the tip of the fracture were usually so small that the strain contours were still not altered markedly. Therefore it was decided to use the actual fracture path as the common reference line for location of the strain gages and rosettes.

The maximum principal strain contours are presented in Figs. 93--102, and are based on the data from Tests 33, 34, 37, 38, and 39. The data from Tests 35 and 36 were not used in the contour plots because Test 35 was conducted on an arrestor specimen at a higher applied stress level and Test 36 resulted in a double fracture. However, careful examination of the strain-time records (Figs. 38--52) from gages and rosettes of Tests 35 and 36 will show that the data from these two tests are similar to those of the other tests reported. In the contour plots, the magnitudes and directions of the maximum principal strain are shown at the respective locations on the plate layout; the directions of the maximum principal strain are shown as short straight lines. For ease in interpretation of the contours, all strain units are in./in. times  $10^6$ . Since all of the tests were made at about the same stress level, it appeared desirable to plot the contours in terms of absolute strain, i.e., with respect to the as-rolled condition.

In the majority of cases, as the fracture approaches the rosette, the direction of the maximum principal strain rotates slightly, so that it points toward the approaching fracture, and then returns to a more or less vertical position as the peak value of the strain occurs. After the maximum strain value is reached, the direction of the maximum principal strain continues to rotate and, in general, continues to point toward the surface fracture tip. Values of  $\theta$ , plotted as short straight lines in the direction of  $\epsilon_{\max}$  on the principal strain contours, show this behavior quite clearly.

For an 8-in. crack (Fig. 93), the shortest crack length for which contours have been plotted, it will be noted that the increase in strain directly above and below the surface fracture tip is small in comparison with strain changes for longer crack lengths. At points in front of the 8-in. crack, the strain changes are negligible and the plotted strains correspond to the test load principal strains. The varia-



tion in test load principal strains for the rosettes and for the various tests accounts for the differences noted in the plotted strain values. The numbers in parentheses following the strain values refer to the test number and corresponding rosette from which the plotted strain values were obtained. These two numbers are shown only on Fig. 93 but refer also to Figs. 94--102 as well.

For an 8-in. crack length, the small changes in strain exhibited by the rosettes located only 8 in. from the initiation edge attest to the fact that the notch-wedge-impact method of fracture initiation has little effect on the strain distribution in a wide plate at some distance from the source of initiation.

The change in strain distribution as the crack length increases may be seen clearly by comparing Figs. 93, 94, and 95, in which the maximum principal strain contours are presented for crack lengths of 8 in., 15 in., and 18.5 in. As the crack length increases it is noted that the magnitude and extent of the strain field associated with the crack tip also increase. At a crack length of 22 in. (Fig. 96), the strain pattern surrounding the moving crack tip ceases to change, and for crack lengths in excess of 22 in. (Figs. 97--102), the strain field surrounding the advancing crack tip remains essentially unchanged. This general effect was noted earlier in connection with Figs. 90 and 91, which show the results of a study of the peak strain magnitude versus distance of the rosette from the fracture for rosettes located at various distances from the initiation edge. The extent of the strain contours directly in front of the fracture increases only slightly with increasing crack length. Thus, for this particular specimen geometry, the propagating brittle fracture apparently does not reach a "steady state" condition until it has traversed a distance of about 22 in. This length is somewhat longer than that suggested by earlier studies.

As may be seen in Fig. 96, the major portion of the strain field associated with the propagating brittle fracture extends only about 8--10 in. in front of the fracture. In the region directly in front of the cracks, the strains decrease slightly as the fracture approaches. It is likely that some of the strain variation observed directly in front of the fracture is associated with the formation of fracture nuclei in front of the main fracture, or with transmitted strain changes resulting from the fracture and strain energy relaxation.

The main changes in strain occur above and below the fracture tip and

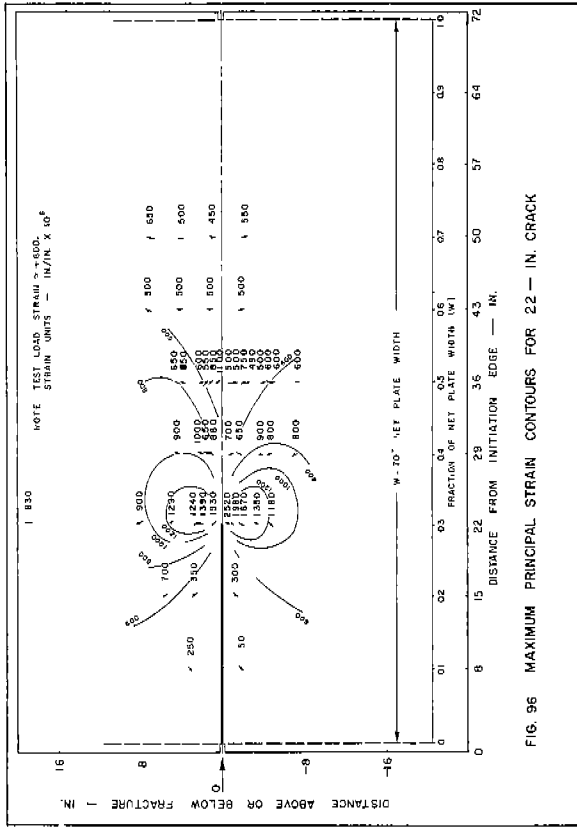


FIG. 96 MAXIMUM PRINCIPAL STRAIN CONTOURS FOR 22 — IN. CRACK

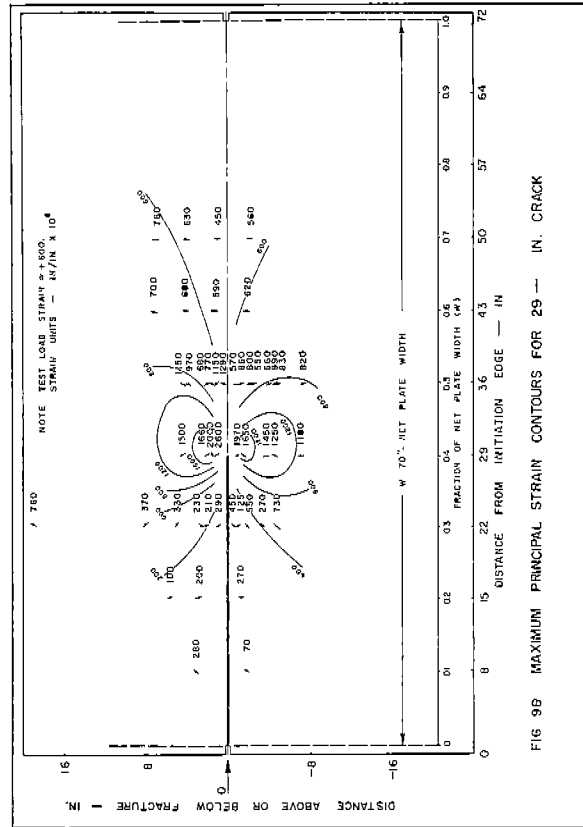


FIG. 97 MAXIMUM PRINCIPAL STRAIN CONTOURS FOR 25.5 — IN. CRACK

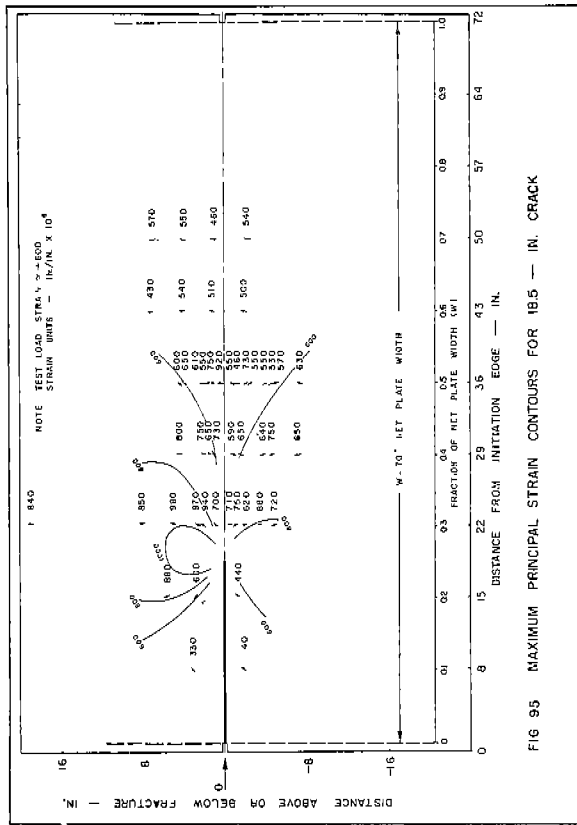


FIG. 98 MAXIMUM PRINCIPAL STRAIN CONTOURS FOR 22 — IN. CRACK

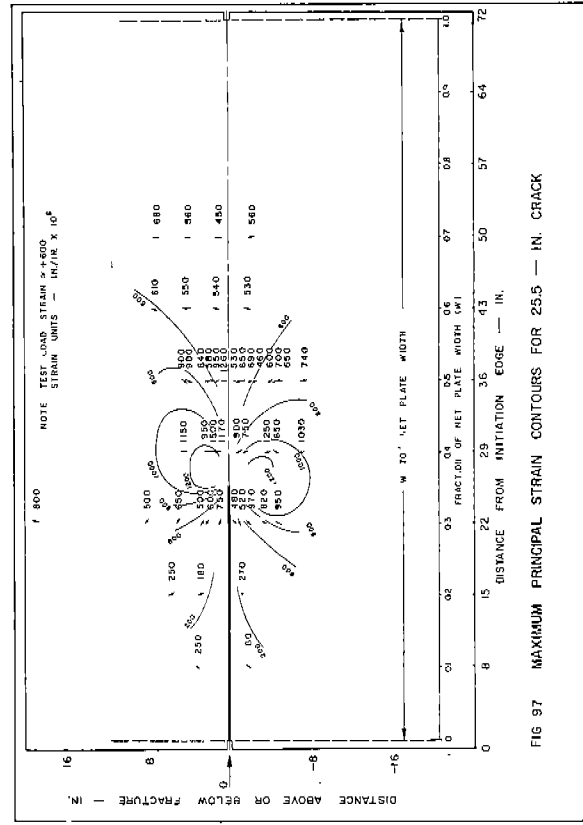
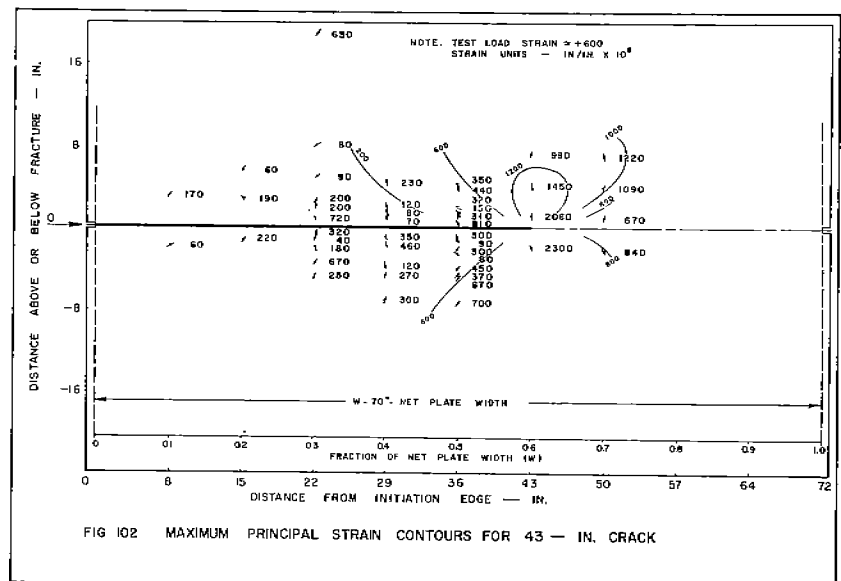
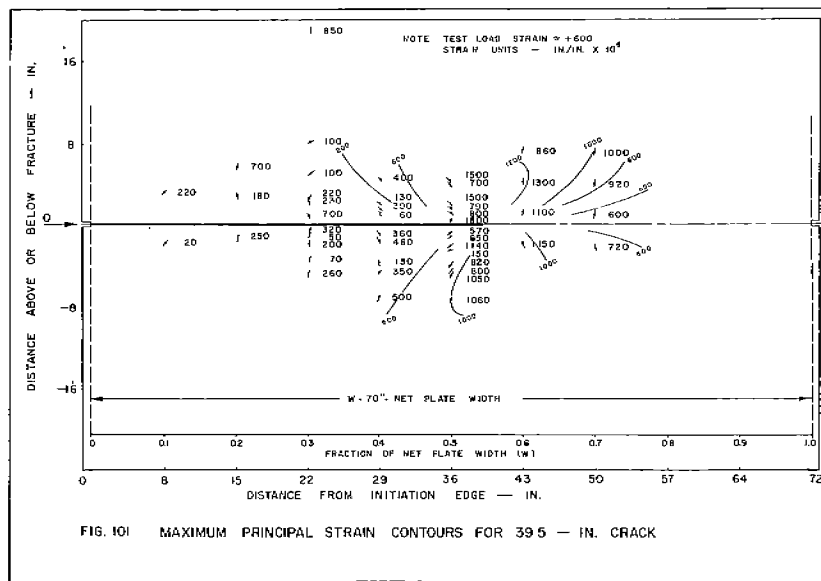
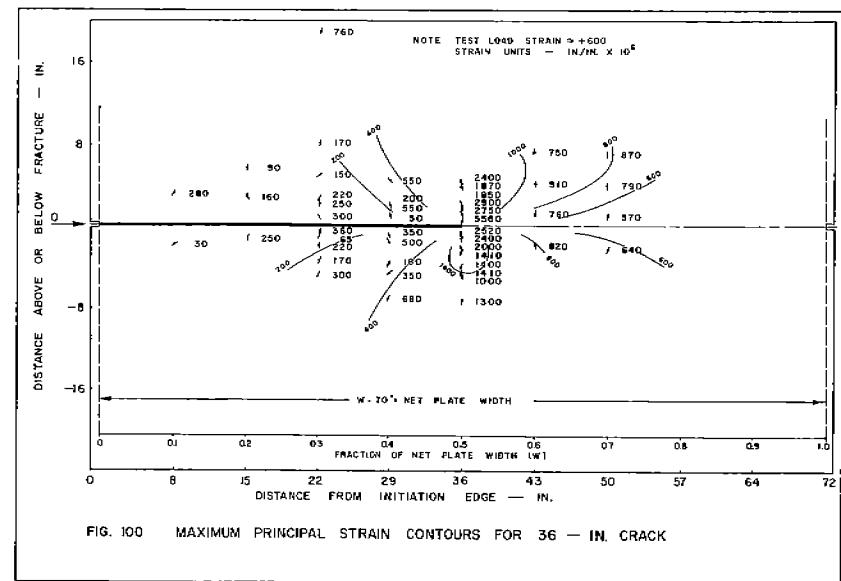
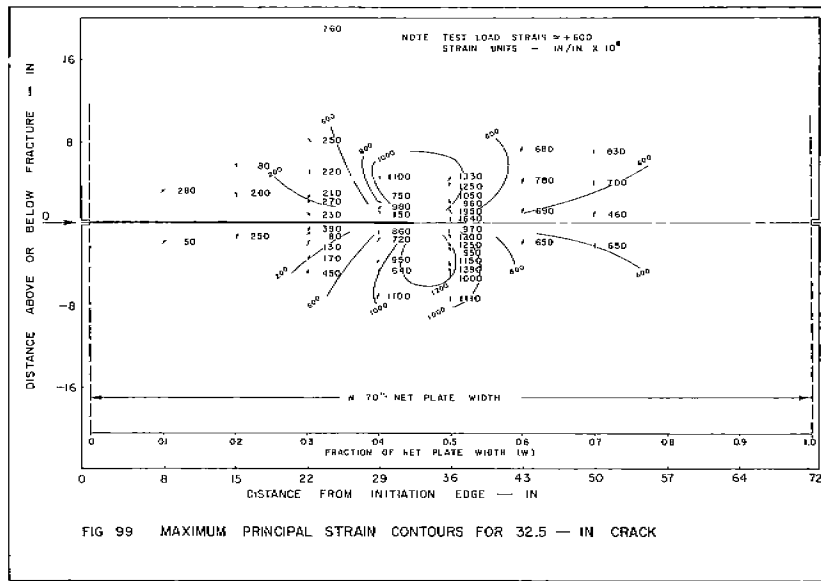


FIG. 99 MAXIMUM PRINCIPAL STRAIN CONTOURS FOR 25.5 — IN. CRACK



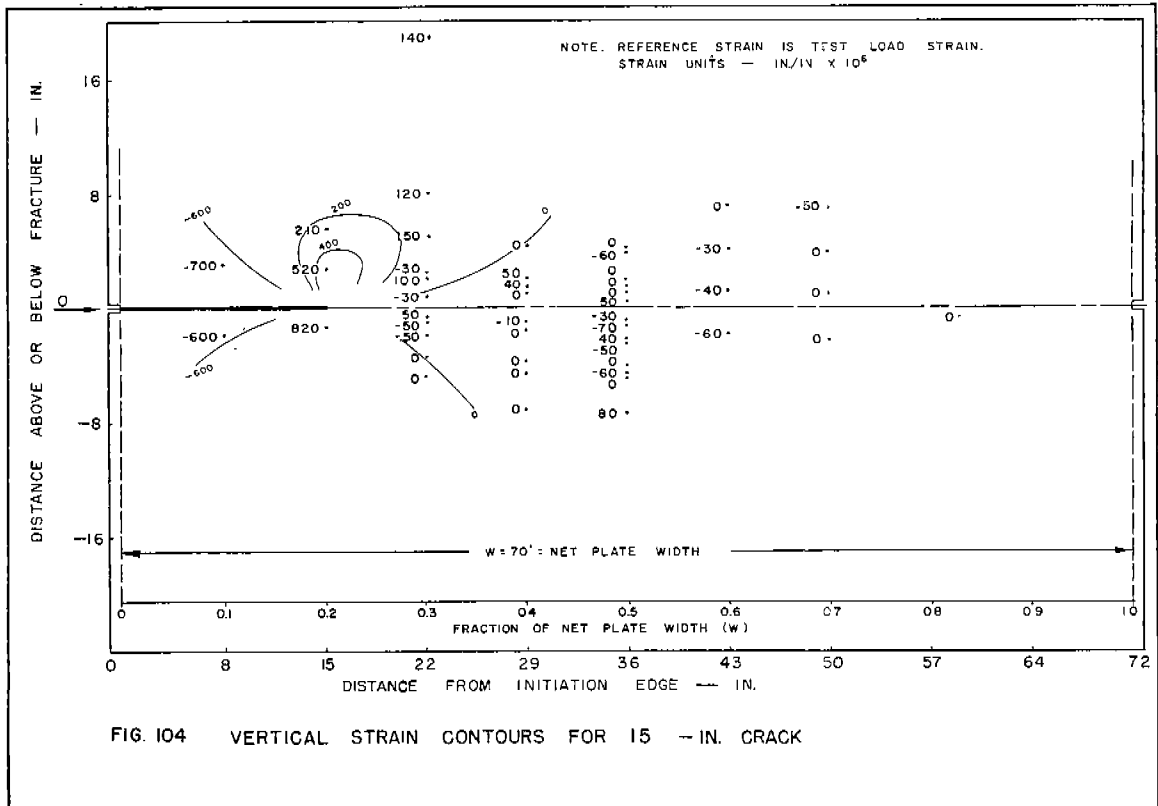
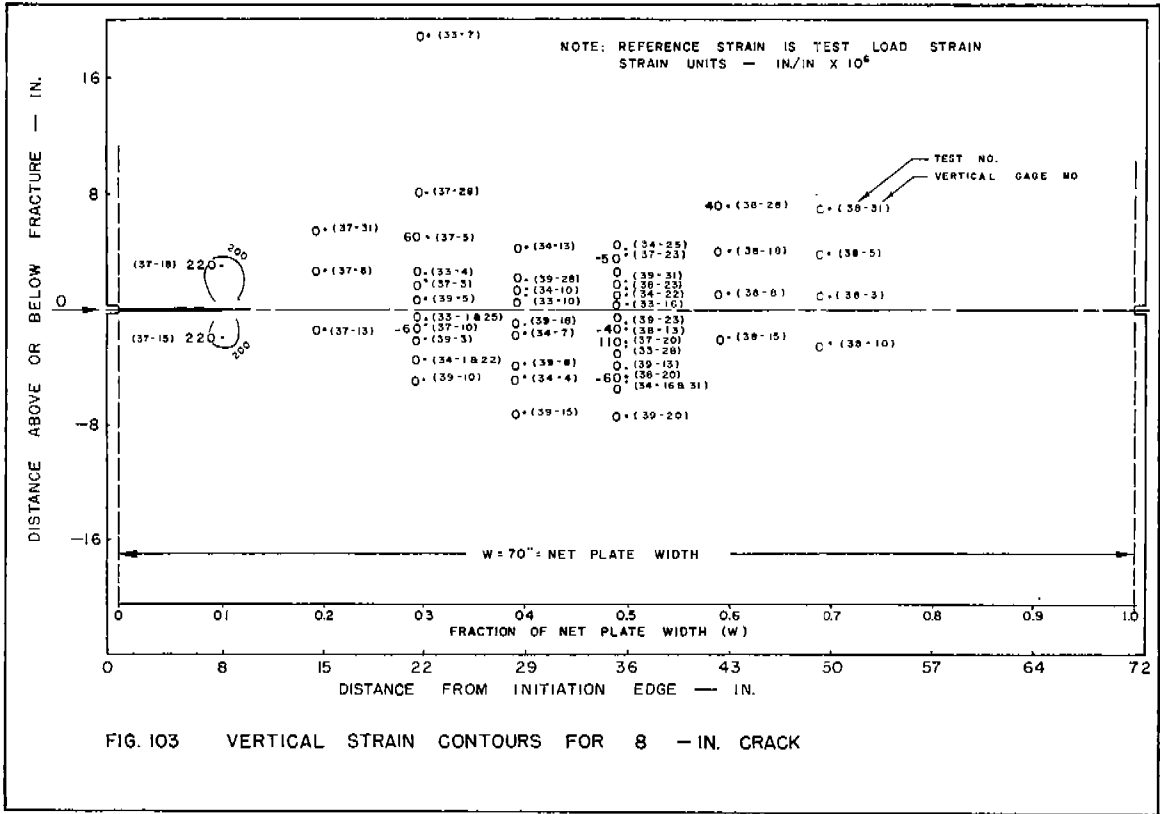
slightly in front of it. Behind the fracture front the strains decrease rapidly. Actually all strain contours appear to converge at the fracture front. Although extensive strain measurements were not obtained at distances far above and below the fracture, the recorded strain data indicate that the contours are symmetrical around the fracture path.

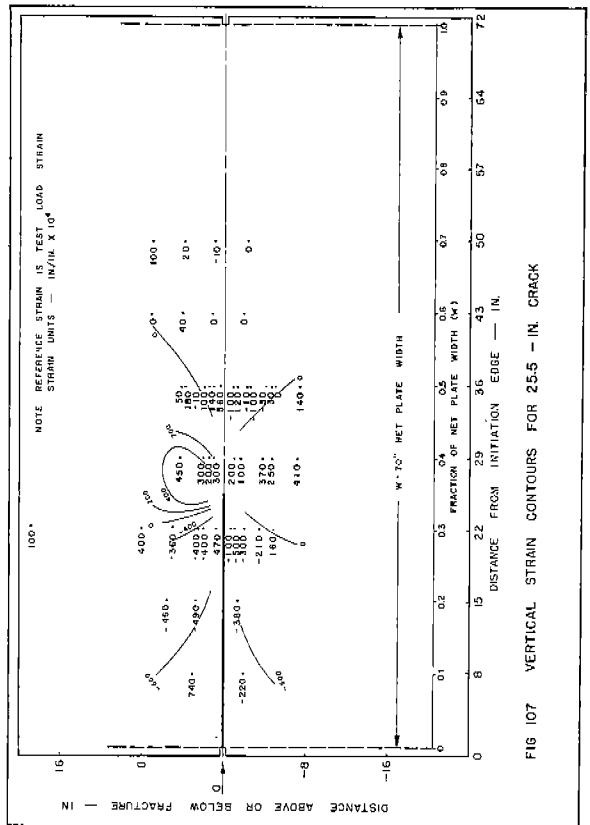
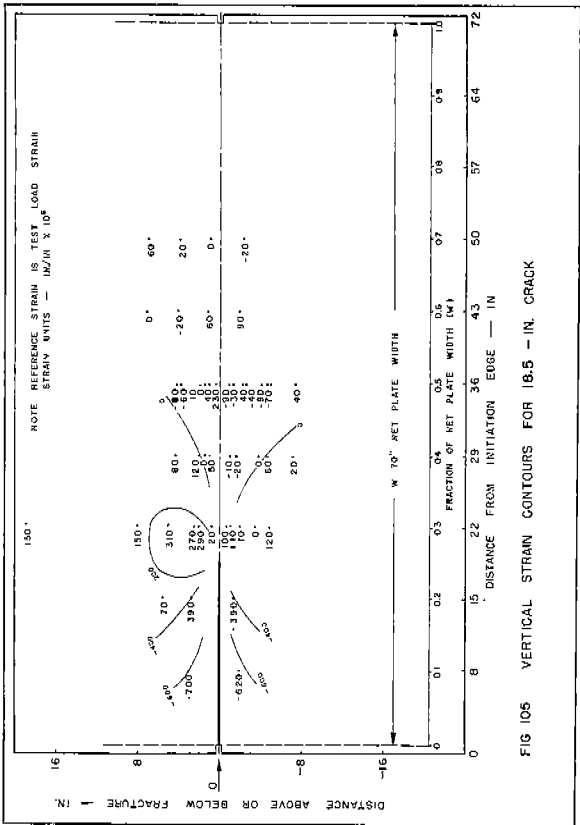
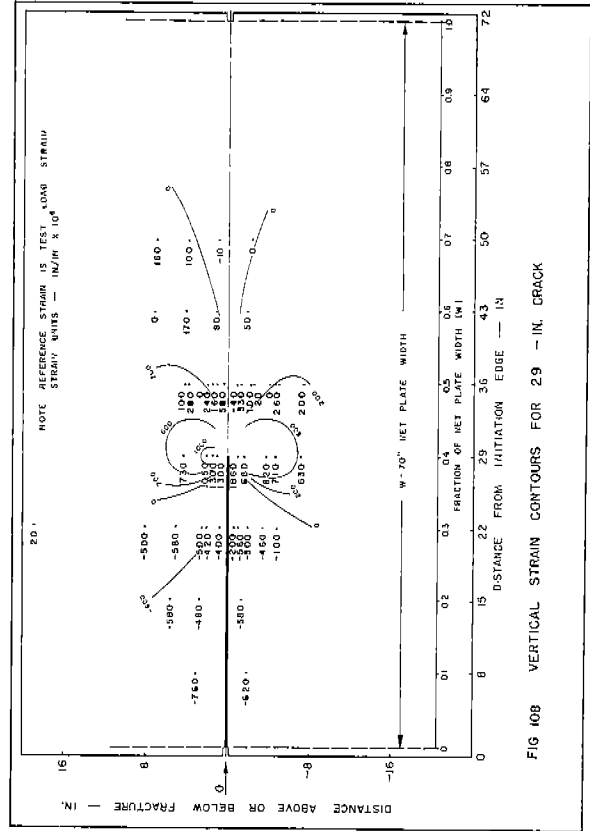
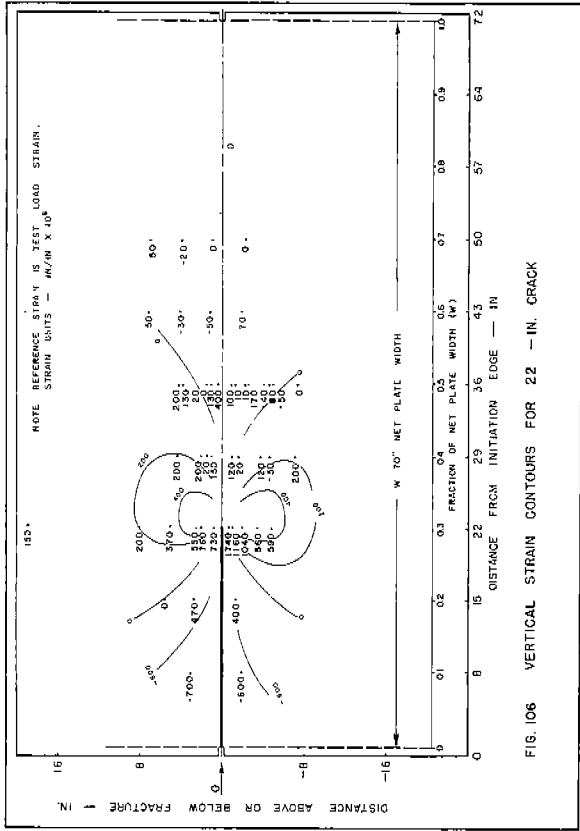
Further information on the extent of the strain field associated with a propagating brittle fracture may be obtained by studying the strain traces presented in Figs. 44 and 46. These strain traces are for two rosettes (Numbers 3 and 5) located between the double fracture occurring in Test 36 (Fig. 8). Each rosette was located approximately 2 in. from one of the fractures and the strain traces of the rosettes are typical of strain curves for rosettes so located. A study of the strain data would seem to indicate that the strain field associated with either of the advancing fractures was affected little, if any, by the strain field associated with the other advancing fracture.

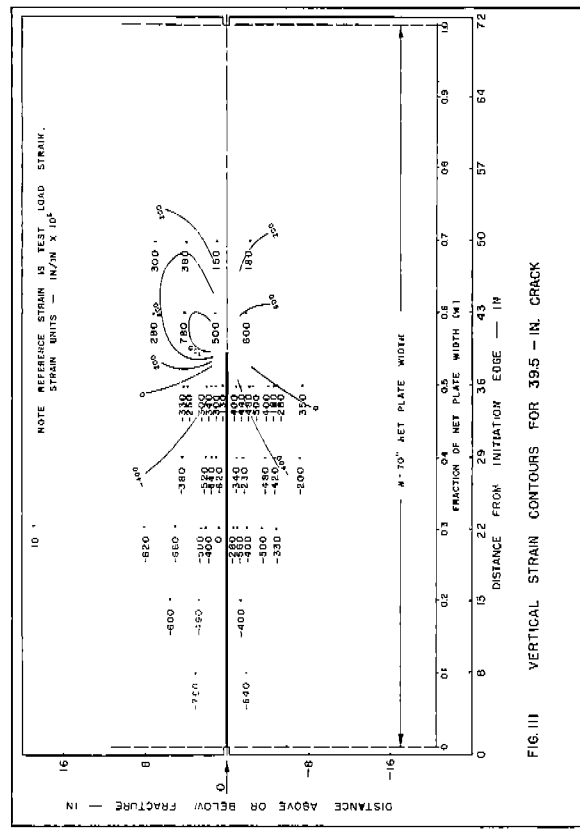
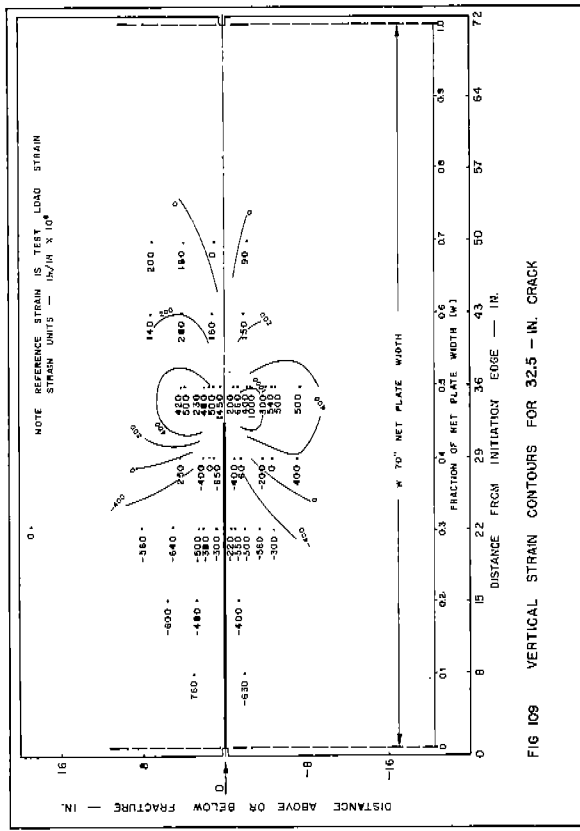
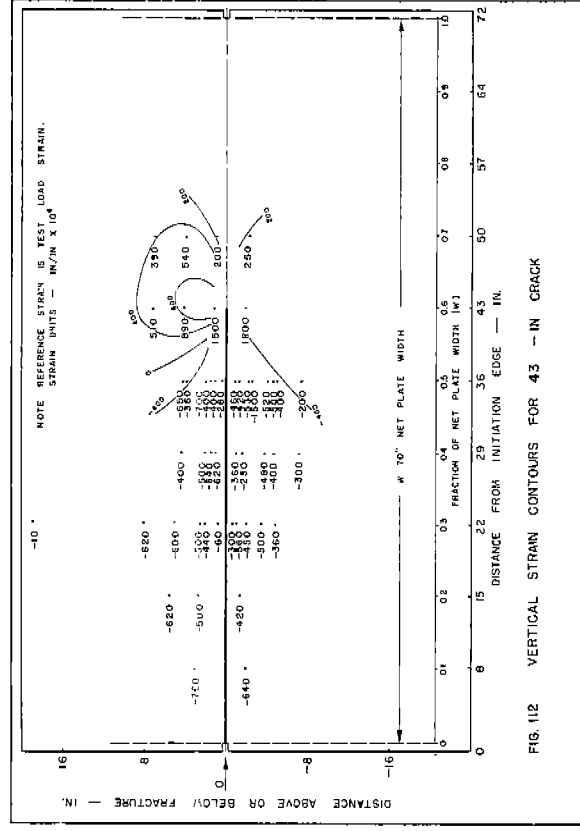
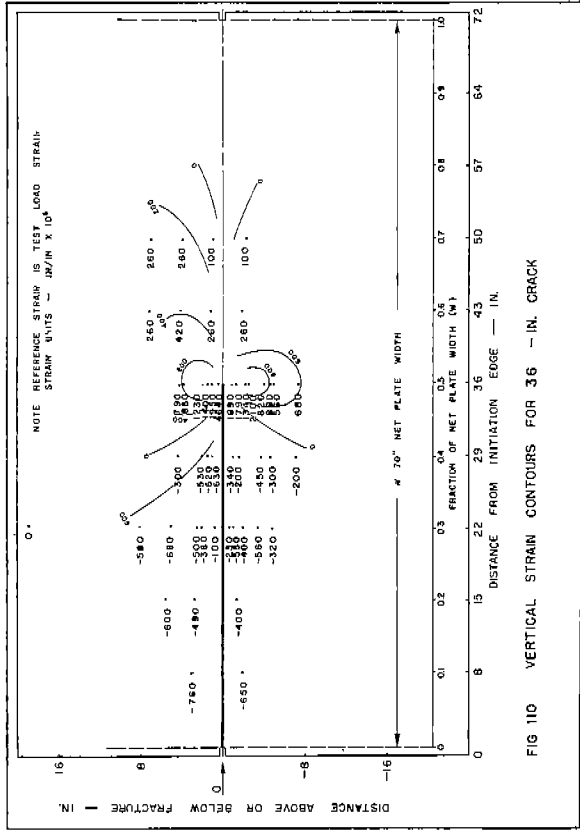
As has been noted earlier, the magnitude of the maximum principal strain is essentially equal to that of the maximum vertical strain; one reason for this is that the principal strain direction does not rotate much from the vertical. Thus, as a matter of comparison and because a plot of the vertical strain allows an incorporation of data from the earlier tests, it was decided to present contours for the vertical strains as well; these are presented as Figs. 103--112. It is to be noted that in these figures the reference strain is the test load strain.

The vertical strain contours could have been plotted in terms of absolute strain as was done for the principal strain contours. However, in order to incorporate the data from earlier tests in which the test load stress varied from 15,000 psi to 20,000 psi, it was decided to subtract the test load strain from the absolute vertical strain and plot the relative strain values. In Fig. 103 the numbers in parentheses following the strain values refer to the original test number and corresponding vertical gage number respectively from which the plotted strain values were obtained. In general, the vertical strain contours are similar in shape and magnitude (if the test load strain were added) to the maximum principal strain contours discussed previously.

With regard to the strain data, which are plotted at any particular time for purposes of establishing the strain contours, there are several additional factors of







importance that should be noted. Because of the nature of the recording equipment, the component gage strain and the computed principal strains are accurate only to about the nearest 0.0001 in./in., and the recorded times are accurate only to about 0.05 milliseconds. For an average fracture speed of 2500 fps, this time error of 0.05 milliseconds would correspond to a fracture length of about 1-1/2 in. The value of the test load strains varied somewhat for the tests because of the slight bending of the plates which was caused by the welding of the specimens to the pull-plates, and by changes of the residual strains in the plates. Consideration of such variables led to the decision to not plot contours at intervals of less than 0.0002 to 0.0004 in./in.

A set of typical maximum principal strain contours is presented in Fig. 113; these contours are based on the results presented in Figs. 96--102, and, for the geometry and test conditions reported here, are considered to be representative of the strain field associated with the crack tip for a crack length in excess of 22 in.

A typical set of vertical strain contours based on the results of Figs. 106--112 and for a crack length in excess of 22 in., is presented as Fig. 114.

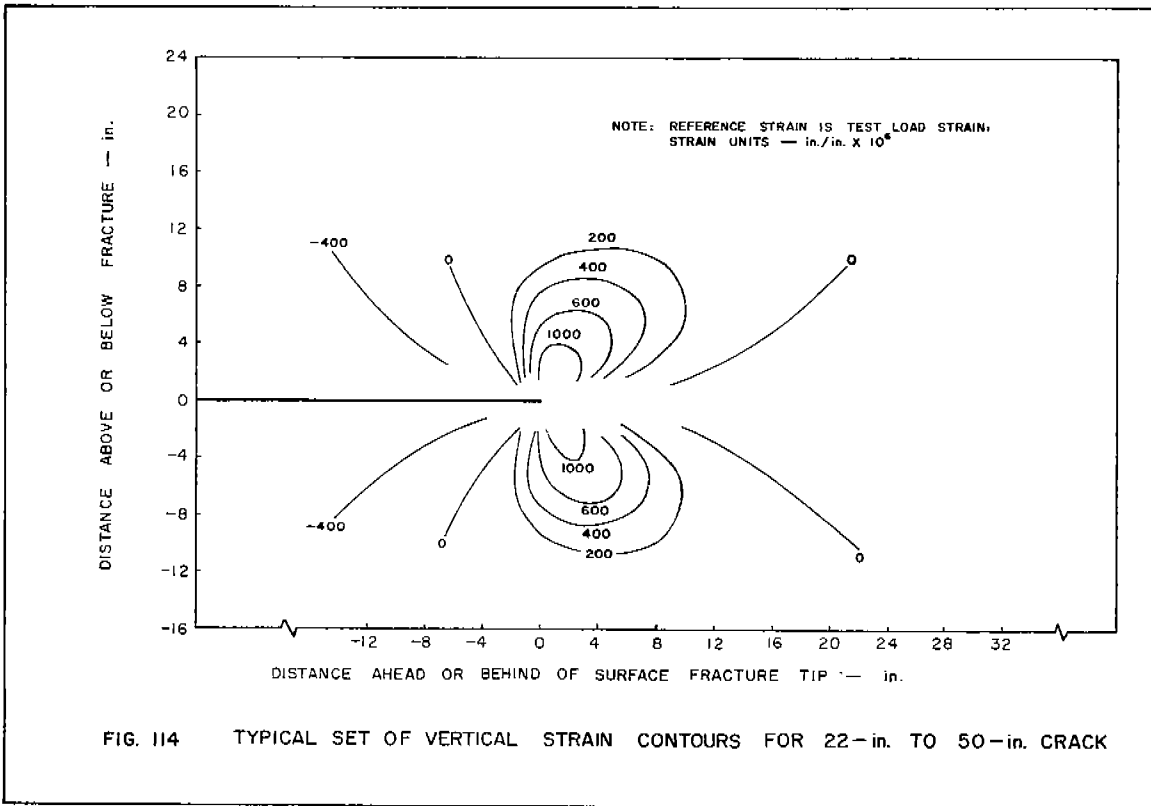
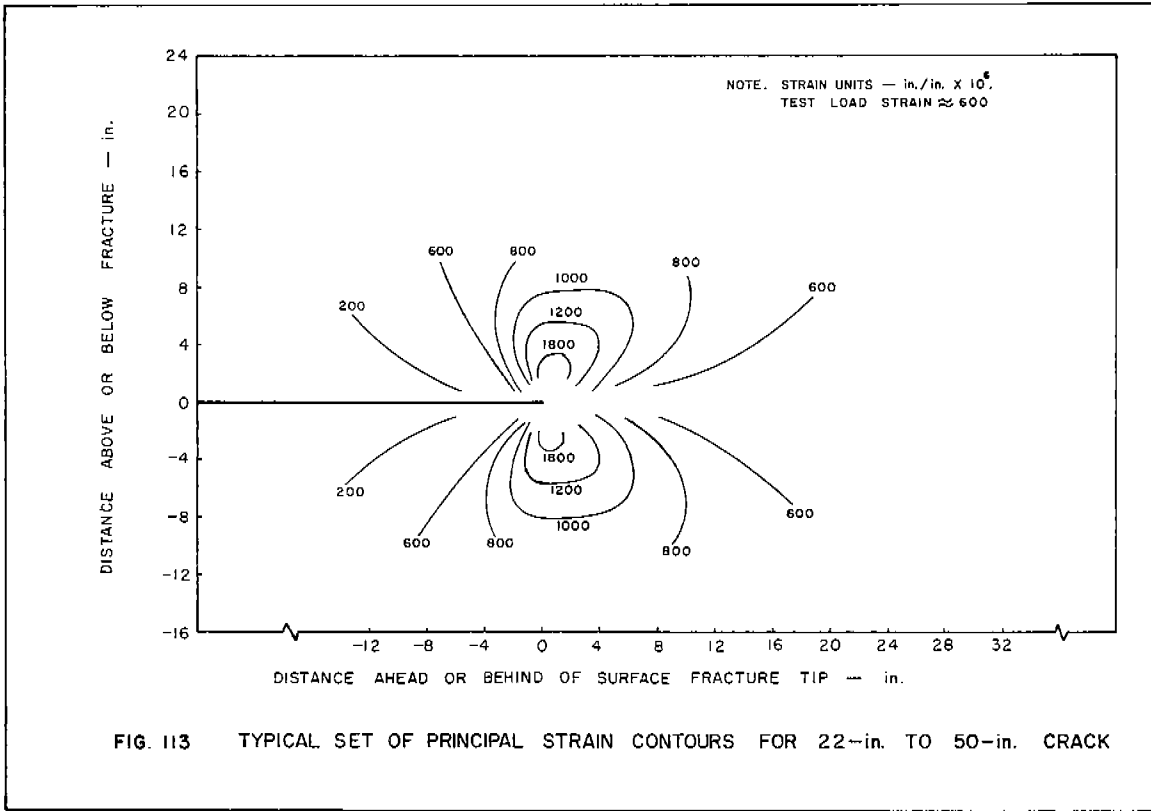
Vertical strain contours for a crack length of 29 in., based on results from all earlier 6-ft wide plate tests are presented in Fig. 115. A tabulation of the data used to plot the contours in Fig. 115 is presented in Table 6. These values are typical for the crack lengths in excess of 22 in. investigated for Tests 13--32. The strain values were superimposed in a manner described earlier; although a few exceptions may be noted, the strain values exhibit the same general pattern as shown in Fig. 114.

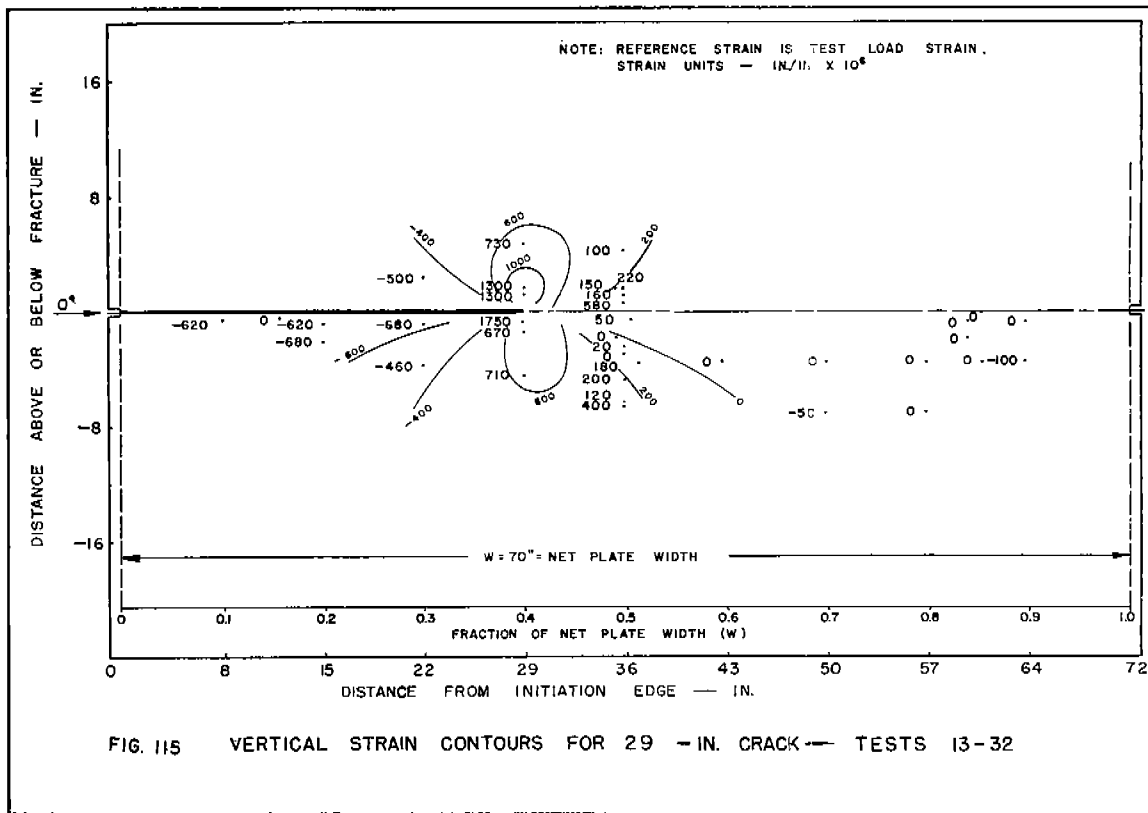
Although contours of only the maximum principal strain and vertical strains are presented in this report, contours of the other strain components, namely the diagonal strain, horizontal strain, minimum principal strain, and shear strain, could be prepared from the strain data presented in Figs. 21--85.

The contours of maximum principal strain and vertical strain are based on data obtained from all the 6-ft wide plates tested as a part of this investigation, and are considered to be representative of the strain distribution recorded on the surface of the plates during brittle fracture propagation. In spite of the

TABLE 6. DATA OBTAINED FROM PREVIOUS TESTS 13-32  
(See Fig. 115)

Test No.	Vertical Gage No.	Distance of Gage from Init. Edge (in.)	Distance of Gage from Fracture (in.)	Time Corres. to 29-in. Crack (milliseconds)	Total Strain (in./in.)	Test Load Strain (in./in.)	Strain Referenced to Test Load Strain (in./in.)
13	1	12.0	-0.3	0.66	.00063	.00063	0
	2	35.5	-1.7	0.66	.00072	.00072	0
	3	60.0	-2.0	0.66	.00066	.00066	0
15	1	35.0	1.6	0.81	.00079	.00064	.00015
	2	36.0	1.6	0.81	.00071	.00049	.00022
	3	36.0	-3.4	0.81	.00090	.00078	.00012
19	2	36.5	-0.6	0.56	.00052	.00047	.00005
	4	61.0	0	0.56	.00055	.00055	0
22	1	37.0	-3.5	0.32	.00082	.00064	.00018
	4	61.0	-3.5	0.32	.00062	.00062	0
23	5	36.0	-3.0	0.82	.00067	.00067	0
	6	43.0	-3.4	0.82	.00067	.00067	0
	7	50.0	-3.5	0.82	.00064	.00064	0
	8	57.0	-3.5	0.82	.00063	.00063	0
	9	64.0	-3.5	0.82	.00052	.00062	-.00010
25	1	8.0	=0.5	0.92	-.00003	.00059	-.00062
	2	15.0	-0.8	0.92	-.00001	.00061	-.00062
	3	22.0	-0.7	0.92	-.00007	.00061	-.00068
	4	29.0	-0.7	0.92	.00231	.00056	.00175
	9	64.0	-0.8	0.92	.00061	.00061	0
32	1	15.0	-2.0	0.60	-.00011	.00057	-.00068
	2	36.0	-6.6	0.60	.00095	.00055	.00040
	3	50.0	-7.2	0.60	.00050	.00055	-.00005
	4	57.0	-7.1	0.60	.00054	.00054	0



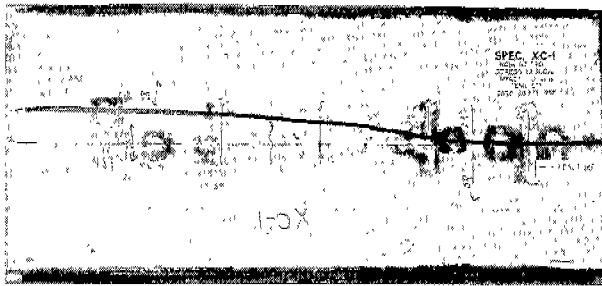


limitations discussed in this section, it is felt that the strain contours presented give a very representative picture of the effect of a propagating brittle crack on the strain distribution in a wide steel plate.

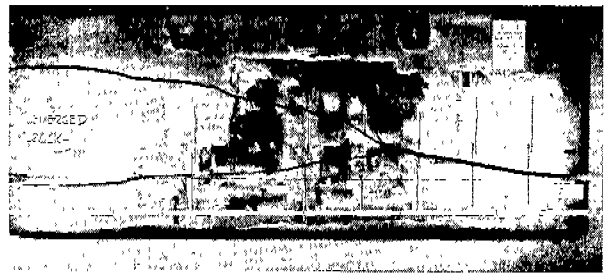
#### Crack Path and Surface Texture

Photographs of the fractured plate specimens are presented in Fig. 116. In general, the fractures slope upward from the point of initiation and then level off. A black string is stretched along the notch line in these figures. In most tests a secondary crack started from the notch cut at the far edge, propagated toward the approaching fracture, and ended in a submerged crack before reaching the main fracture. These secondary cracks may be seen in the figures. The fracture in Test 36 branched into two complete fractures near the center of the plate.

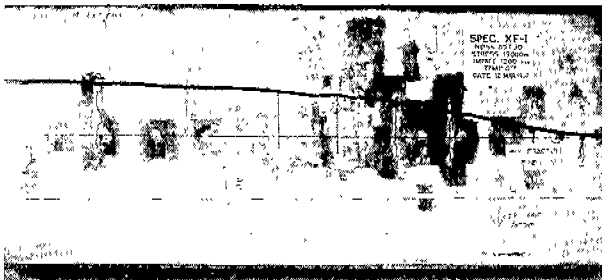
Views of a typical fracture surface are presented in Fig. 117. The shear lip associated with the fractures was very small and almost imperceptible. Por-



Test 33



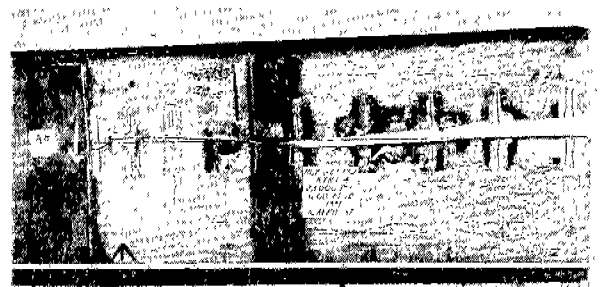
Test 36



Test 34



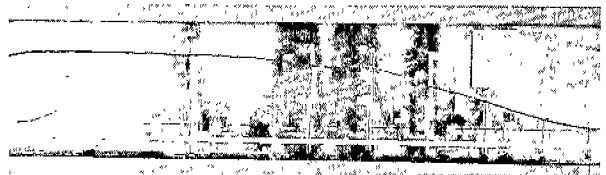
Test 37



Test 35



Test 38



Test 39

Fig. 116. Fracture Paths--Tests 33--39

tions of the surface exhibit a coarse texture with the usual herringbone pattern, while in other regions, usually near the initiation edge, the texture is quite smooth. Enlarged views of typical smooth and coarse fracture texture are presented in Fig. 118.

The reduction in plate thickness in the region of the fracture surface was one to two per cent; this reduction in thickness is of the same order of magnitude as that found in earlier fracture tests conducted as a part of this program.

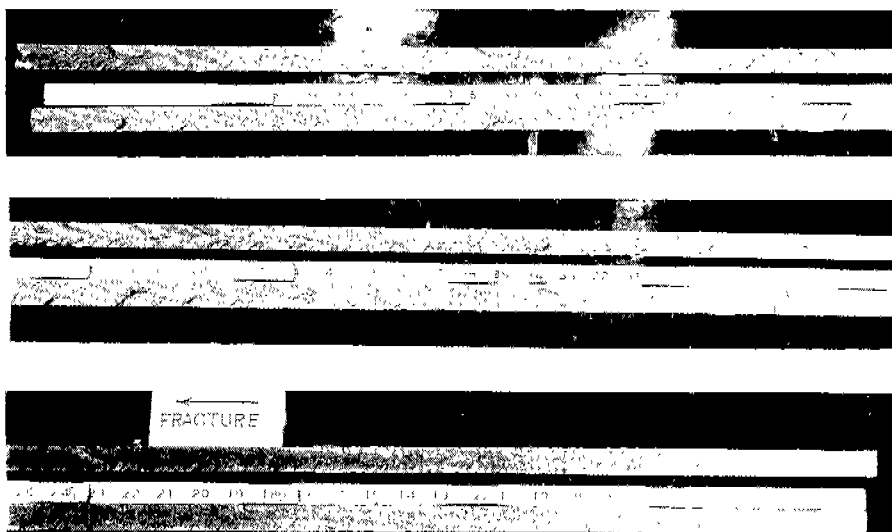


Fig. 117. Typical Fracture Surface--Test 38

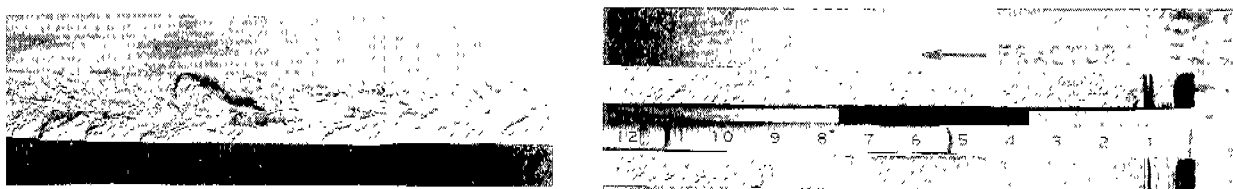


Fig. 118. View of Portions of Typical Fracture Surfaces from Test 34 Showing a Coarse Surface on the Left and a Smooth Surface on the Right.

### SUMMARY

This research report contains a summary and preliminary analysis of data primarily from Tests 33--39, conducted as a part of the current brittle fracture propagation study. More complete studies of these data, as well as data obtained subsequently, are being made as a part of the program.

The specimens were tested with a net stress of about 19,000 psi, at a temperature of about -10 F and with a nominal impact of 1200 ft-lb for fracture initiation. Thirty-four channels of instrumentation were used for each test; this is more than three times as many channels as had previously been available for any one test. The strain-time traces from the component gages, as well as the computed principal strains, are presented. Since the tests were

conducted under similar conditions of stress, temperature, and impact, it was possible to superimpose the strain data to obtain a more complete picture of the strain distribution on the surface of the plate associated with the moving fracture.

The behavior exhibited by the component gages was similar to that observed in earlier tests. For example, in the case of a vertically oriented strain gage, as the distance between the gage and the fracture path decreased, the strain pulse became sharper and had a greater magnitude; as the distance between the gage and fracture increased, the strain pulse extended over a longer period of time, but the precise shape of the pulse depended on the distance from the fracture path. For gages oriented in the diagonal and horizontal directions, this same general trend was noted, but the shape of the strain trace, particularly in the case of the horizontal gage, was markedly different.

In the case of the principal strains computed from the component strain traces, the maximum principal strain was found to exhibit the same type of behavior as observed for a vertically oriented gage, with the exception that the direction of the maximum principal strain was found to rotate slightly to either side of the vertical axis depending upon the location of the fracture.

Although the nature of the strain traces are such that only a rough picture of the strain rates may be obtained, the trend is of some interest. As would be expected, the maximum strain rate occurs for gages located quite close to the fracture. Strain rates ranging from 1 to 109 in./in./sec have been computed; the majority of the values fall in the range 1--30 in./in./sec for gages located 1/2--3 in. from the fracture.

Contours of maximum principal strain and vertical strain for various crack lengths are presented. The major portion of the strain field associated with the front of the propagating brittle fracture extends only about 8--10 in. in front of the fracture; the regions most affected are above and below the fracture tip and slightly in front of it. Although extensive strain measurements were not obtained at distances far above and below the fracture, the recorded strain data indicate that the contours are symmetrical around the fracture path.

A study of the data reveals that for crack lengths in excess of about

22 in., the extent, magnitude, and nature of the strain field associated with the advancing tip of the fracture remains essentially unchanged. Typical maximum principal strain contours and vertical strain contours based on all of the available data are presented for fractures propagating in the central one-third of the plate width.

#### REFERENCES

1. Hall, W. J., Godden, W. G., and Fettahtlioglu, O. A., Preliminary Studies of Brittle Fracture Propagation in Structural Steel (Ship Structure Committee Report Serial No. SSC-111), Washington: National Academy of Sciences-National Research Council, May 15, 1958.
2. Lazar, R., and Hall, W. J., Studies of Brittle Fracture Propagation in Six-Foot Wide Structural Steel Plates (Ship Structure Committee Report Serial No. SSC-112), Washington: National Academy of Sciences-National Research Council, September 17, 1959.
3. Lynam, T. M., Strain Patterns During the Propagation of a Brittle Fracture in Steel Plates (M. S. Thesis submitted to the Graduate College, University of Illinois), 1957.
4. Rolfe, S. T., Studies of the Strain Distribution in Wide Plates During Brittle Fracture Propagation (M. S. Thesis submitted to the Graduate College, University of Illinois), 1958.
5. Hall, W. J., Mosborg, R. J., and McDonald, V. J., "Brittle Fracture Propagation in Wide Steel Plates," The Welding Journal, 36:1, Research Supplement, pp. 1s-8s (January 1957).

COMMITTEE ON SHIP STRUCTURAL DESIGN  
Division of Engineering & Industrial Research  
National Academy of Sciences-National Research Council

Chairman:

N. J. Hoff  
Head of Department of Aeronautical Engineering  
Stanford University

Vice Chairman:

M. G. Forrest  
Vice President-Naval Architecture  
Gibbs and Cox, Inc.

Members:

George F. Carrier  
Gordon MacKay Professor of  
Mechanical Engineering  
Harvard University

C. O. Dohrenwend  
Dean of Graduate School  
Rensselaer Polytechnic Institute

J. M. Frankland  
Consultant, Mechanics Division  
National Bureau of Standards

Dana Young  
Dean, School of Engineering  
Yale University